Detection of forest water stress under future climate change in drought prone ecosystems of the Southwestern United States

Maria Magdalena Warter

School of Earth and Environmental Sciences

Cardiff University

Submitted in partial fulfillment of the requirements for the

Degree of

Doctor of Philosophy

September 2022

An understanding of the natural world

is a source of not only great curiosity,

but great fulfilment.

David Attenborough

ABSTRACT

Terrestrial ecosystems are becoming increasingly vulnerable to climate changes that negatively affect the spatial and temporal water availability, especially in water-limited regions of the Southwestern USA, which may yield potentially irreversible consequences to biodiversity and species distribution across this dryland region. Substantial uncertainties remain regarding future climate variability and the associated vegetation responses to extreme climatic events, especially droughts that produce prolonged water deficits. Projected climate scenarios are still quite variable across this region, ranging from hotter/drier, to hotter/wetter/stormier. These variations pose potentially compounding challenges for terrestrial vegetation ecosystem functioning. Therefore, an improved understanding of the key climate drivers of vegetation functioning is needed which is capable of quantifying potential vegetation responses to future climate change and variability. This new capability would provide land managers with a modeling tool to explore climatological and hydrological scenarios and ecological responses. Such models would inform sustainable, adaptive management strategies of vulnerable habitats in response to the "new normal" climate conditions, thus increasing the future resilience of ecosystems to such altered climate conditions.

In this thesis, climate-vegetation interactions are analyzed through data and models across different biomes and spatio-temporal scales. Using multi-decadal climate records, remote sensing information and several new numerical models that characterize ecohydrology, past and potential future vegetation responses to varying moisture availability were quantified. First, by using local climate and in-situ soil moisture records, as well as a simple soil moisture balance model, I quantified vegetation responses of two contrasting Southern California grassland ecosystems to prolonged moisture deficits that occurred under the recent period of extreme drought and more extreme droughts that might be expected in the future. I show that shifting climate conditions towards warmer and drier will arguably increase vegetation water stress, affecting vegetation phenology and threatening the integrity of grassland and forest ecosystems. Next, to address current limitations to dynamically model plant phenology in response to changing climate conditions, I developed a dynamic vegetation module (DYNA-VEG) that improves the quantification of climate-

vegetation interactions in dryland ecosystems within the existing dryland water partitioning model DRYP. The functionality of the module was evaluated through synthetic experiments to test its effectiveness in capturing climate-soil-vegetation interactions under different future scenarios of climate change. The results from these model simulations highlighted the diverging sensitivities between shallow rooted soil moisture and groundwater dependent riparian species to alterations in recharge and groundwater levels and precipitation, respectively. Most significantly, simulations showed the compound effects of altered climate conditions and hydrological changes on riparian forest responses, where declines in water tables of several meters resulted in peak physiological stress. Simulations highlighted that climate induced changes to recharge and water table dynamics are the key drivers of future vegetation responses, which has broader implications for exploring adaptive management strategies. Indeed, for sensitive riparian habitats future ecologically sustainable groundwater thresholds and managed aquifer recharge can be explored through ecohydrological modeling framework and translated into future management approaches.

DECLARATIONS

This work has not been submitted in substance for any other degree or award at this or any other university or place of learning, nor is being submitted concurrently in candidature for any degree or other award.

STATEMENT 1

This thesis is being submitted in partial fulfillment of the requirements for the degree of PhD.

STATEMENT 2

This thesis is the result of my own independent work/investigation, except where otherwise stated, and the thesis has not been edited by a third party beyond what is permitted by Cardiff University's Policy on the Use of Third-Party Editor by Research Degree Students. Other sources are acknowledged by explicit references. The views expressed are my own.

STATEMENT 3

I hereby give consent for my thesis, if accepted, to be available online in the University's Open Acesss repository and for inter-library loan, and for the title and summary to be made available to outside organizations.

Signed _____ (candidate) Date _____

AUTHOR CONTRIBUTIONS

Chapter 2 has been published as:

Warter, M.M., Singer, M.B., Cuthbert, M.O., Roberts, D., Caylor, K.K., Sabathier, R. and Stella, J., 2021. Drought onset and propagation into soil moisture and grassland vegetation responses during the 2012–2019 major drought in Southern California. *Hydrology and Earth System Sciences*, *25*(6), pp.3713-3729. doi: 10.5194/hess-2020-479

Chapter 3 has been published as:

Warter, M.M., Singer, M.B., Cuthbert, M.O., Roberts, D., Caylor, K.K., Sabathier, R. and Stella, J., 2022. Modeling seasonal vegetation phenology from hydroclimatic drivers for contrasting plant functional groups within drylands of the Southwestern USA. *Environmental Research: Ecology. In Press.* doi: 10.1088/2752-664X/abc9a0

While both papers have multiple co-authors, model development, investigation and writing of the manuscript was entirely my own work. The other co-authors offered recommendations and feedback on the manuscript and on emergent issues during the analysis, which did not exceed the usual assistance given from supervisors.

The original dryland water partitioning model (DRYP) used for analysis in Chapter 5 was developed by Quichimbo et al. (2022) and is published as:

Quichimbo, E.A, Singer, M.B. Michaelides K., Hobley D., Rosolem, R. Cuthbert M.O. 2021. DRYP 1.0. A parsimonious hydrological model of DRYland Partitioning of the water balance. *Geosci. Model Dev. Discuss.* 2021, 1-34. doi: 10.5194/gmd-2021-137

While the design and conceptualization of DYNAamic VEGetation module (DYNA-VEG) developed in Chapter 3 is my own work, the module was coded into DRYP by EAQ. Any references or use of original DRYP material are clearly cited in the thesis.

ACKNOWLEDGEMENTS

First off, I must thank my former professor at Wageningen University, Roel Dijksma, for bringing the advertisement of this PhD to my attention and encouraging me to apply.

I am grateful to have been part of this great project, led by Prof. Michael Singer, which provided me with so many amazing opportunities to travel, present my work at conferences and work with other PhD students and professors.

As a PhD student you are essentially lost unless you have someone to show you the way, occasionally redirect you and even push you off the beaten path. I was lucky enough to have a supervisor like that, and so my biggest thanks goes to Michael, for being such a sensible, supportive, and kind supervisor who believed in me and forced me to grow outside my comfort zone, academically and personally. His unwavering support and understanding were key to finishing this work and learning so much in the process.

I would also like to thank the collaborators from UCSB and SUNY, Dar Roberts, Kelly Caylor, and John Stella for providing valuable feedback and comments on paper drafts and research methods over the years.

From Cardiff, I need to thank Dr. Mark Cuthbert for his countless comments and edits on papers, methods, and this thesis. His eye for detail pushed me to produce the best research I could.

I also would like to express my gratitude to Andrés Quichimbo, whose support was essential in finishing the modeling experiments. Thank you for answering my many questions and taking the time to meet with me and fix any issues with the model.

To my family, without whose financial and emotional support over the years I would not have come this far. They continuously encouraged me to travel and follow my passions and lent a supportive hand whenever I needed it.

Ultimately, I would not have finished this PhD without my personal cheerleader, my heart, Lorenz, who saw me through good days and bad days. I was lucky enough to find you in a time when the world was in turmoil, and I am grateful to have had you by side ever since. I could not have done it without you cheering me on, making me

laugh, comforting me and encouraging me when I needed it the most. You are my umbrella in the rain.

Lastly, I would also like to acknowledge the Strategic Environmental Research Development Program, who funded this research so generously and provided some amazing opportunities to travel and explore our research areas firsthand.

TABLE OF CONTENTS

LIST OF FIGURES

LIST OF TABLES

CHAPTER 1

1 General Introduction

1.1 The expression of climate change on the global water cycle

Climate change is affecting the terrestrial vegetation as well as global water and carbon cycles, causing severe impacts on natural and human ecosystems (Cook et al. 2014; Bradford et al. 2020; IPCC 2021). With the climate system becoming progressively warmer since the mid-20th century, impacts on natural terrestrial ecosystems have accumulated to unprecedented levels, as decreases in the extent of natural habitat and excessive human water withdrawal and consumption have further aggravated the pressures on vegetation (Gerten 2013). As the atmosphere continues to warm, the risks of pervasive, irreversible impacts to natural ecosystems become more likely, driven by more frequent climate-related extreme events such as heat waves, droughts and wildfires and the increase in atmospheric evaporative demand (Liu et al. 2010; Dai 2011; Cook et al. 2014; Berg and Sheffield 2018). Despite the mounting scientific evidence of vegetation and ecosystem responses to the recent periods of drought during the early 21st century, there are remaining uncertainties about how the projected changes in temperature and precipitation will impact ecological responses and ecosystem functioning of different biomes in the future.

Coupled climate models used in the IPCC assessments revealed a pattern of continued drying throughout the 21st century, which cannot be attributed to natural climate variability alone (IPCC 2021). Drying trends have been observed over most of Africa, southern Europe and the Middle East, large parts of Northern America as well as Australia and Southeast Asia (Dai 2011; Cook et al. 2014). The observed changes in the climate system are largely attributed to the anthropogenic increase in greenhouse gas emissions since the mid-20th century, which has accelerated the warming of the atmosphere, producing changes to potential evapotranspiration (PET) (Cook et al. 2014; Lavers et al. 2015; Allan et al. 2020). Multiple lines of evidence have indicated a strong linear trend between cumulative CO_2 emissions and global temperature changes, which will determine future global surface warming (IPCC,

2014). As a direct response to increased air temperatures, global aridity has increased, impacting soil moisture driven land-atmosphere interactions. This has led to cascading effects that promoted large-scale moisture anomalies, driving the propagation of extreme drought occurrences of recent decades (Jia et al. 2019; Zhou et al. 2019). The effects of drought on water resources and hydrological and ecosystem processes are spatially complex, generating everything from reduced snowpack and widespread tree mortality in higher elevations, to extreme groundwater and surface water depletion, to severe soil drying and declining stream flow in dryland areas (Liu et al. 2012; Berg and Sheffield 2018; Seager et al. 2019; Kibler et al. 2021).

Even though the global water cycle is expected to intensify in response to the warming temperatures, changes will not likely be uniform across all regions, despite the continued global drying trends under increasing greenhouse gas emissions. More specifically, projections point towards diverging responses between humid and dry regions, where wet areas are expected to get wetter, while dry areas continue to get drier (Sheffield and Wood 2008; Dai 2011; Trenberth et al. 2014). A persistent drying of the land surface affects land-atmosphere interaction as evapotranspiration is reduced leading to a reduction of moisture in the atmosphere, and an increasing vapor pressure deficit (VPD) (Samaniego et al. 2018; Zhou et al. 2019). Changes in the atmospheric vapor content are strong indicators of a changing water cycle, as the higher VPD increases the atmospheric evaporative demand, creating negative land-atmosphere feedbacks that exacerbates soil moisture drying and precipitation anomalies (Zhou et al. 2019; Allan et al. 2020). Changes to the water cycle thus strongly affect cloud-radiation interactions, which influences the width of tropical rain belts and the position of storm tracks (Williams et al. 2018; Voigt et al. 2021). Clouds further modulate atmospheric circulation patterns and surface radiation, which drives evaporative demand at the surface. Especially in areas where precipitation is already exceeded by PET (drylands), increases in PET will amplify surface drying, leading to a high probability of concurrent soil moisture droughts that may propagate into groundwater droughts with detrimental effects on vegetation and ecosystem services (Cook et al. 2014; Zhou et al. 2019).

Linear trends between physical changes in the atmospheric and surface processes with global CO_2 emissions, remain strong as global warming will exceed 2°C under higher emission scenarios of RCP 8.5 (Representative Concentration Pathway), unless immediate measures are taken to curb further anthropogenic emissions of greenhouse gases into the atmosphere (Cook et al. 2014; IPCC 2014). Even then, the shift towards more intense and extended heat waves and fewer cold temperature extremes seems virtually certain over most regions on daily and seasonal timescales, affecting urban and natural habitats and altering hydrological systems responses (Troch et al. 2009; Dai 2011; Cook et al. 2014; Berg and Sheffield 2018; Jia et al. 2019). In that context, the rise in temperature extremes may also increase the amount of water in the atmosphere in humid regions, driving a shift towards more extreme precipitation events. Such changes to precipitation are affecting the quality and quantity of water resources, affecting runoff and downstream water resources, which also raises the risk of larger and more frequent flood occurrences in the event of more extreme precipitation events (Lavers et al. 2015; IPCC 2021). While globally more intense, short-lived storms will become more common, regional variations may diverge from global trends (Trenberth 2011; Pal et al. 2013; Aghakouchak et al. 2018). Generally, increases in annual surface evaporation and changes to annual runoff and streamflow regimes follow global precipitation patterns, affecting the seasonal distribution of surface and subsurface moisture to vegetation and associated drought risks. However, the true extent of precipitation changes may vary depending on emission scenarios and changes to ocean-atmosphere teleconnections and will become more certain as the range of climate changes unfold over the coming decades (Troch et al. 2009; Gerten 2013).

1.2 Challenges and implications of climate change for vegetation

Biophysical processes such as plant transpiration and carbon assimilation are tightly coupled to the Earth's energy and water fluxes, which determine the plant-available water in the critical zone (Moore et al. 2015; D'Odorico et al. 2019). Furthermore, soil, topography and other relevant terrestrial characteristics exert considerable influence on the distribution, structure and functioning of ecosystems (Moore et al. 2015). In water limited environments, precipitation is the primary driver

of plant available water, controlling regional hydrological patterns and seasonal moisture availability (Ridolfi et al. 2000; Rodriguez-Iturbe 2000; Daly and Porporato 2005). Generally, ecohydrological process can be either water-limited or energy-limited, depending on the climate region, resulting in different growth-limiting mechanisms, which determine vegetation productivity (Moore et al. 2015).

In water limited environments, the structure and functioning of ecosystems is highly sensitive to the timing and intensity of precipitation events. Consequently, the warmer temperatures and increased surface drying impose substantial pressure on vegetation, especially regions where frequent water limitations create a climate prone to prolonged drought and plant water stress (Cook et al. 2014; Moore et al. 2015; Shellito et al. 2016; Samaniego et al. 2018). Most critically, increases in evaporative demand play a major role in water-limited regions, such as the southwestern USA, where the global temperature increases propagate widespread moisture deficits and water shortages (Wang et al. 2012; Cook et al. 2014; Moore et al. 2015).

Generally, interactions between vegetation and moisture are complex, with large seasonal and interannual as well as spatial variations across the landscape. The role of vegetation in moderating ecohydrological processes is directly related to the spatial redistribution of water and hydrological partitioning processes (Moore et al. 2015). As vegetation occupies different positions in the landscape, individual plant contributions to water, energy and carbon fluxes may differ. However, the spatial heterogeneity of vegetation throughout the landscape can have overall strong impacts on ecohydrological processes and land-atmosphere interactions, creating a range of feedbacks across different spatial and temporal scales (Caylor et al. 2006; Moore et al. 2015; D'Odorico and Porporato 2019). To date, the differential effects of a changing water cycle have raised the potential for more prolonged and frequent plant physiological stress, leading to widespread mortality of terrestrial vegetation and widespread species decline; from lowland grasslands (Gremer et al. 2015; Reynier et al. 2016; Cui et al. 2017; Donovan et al. 2020), upland forests (Mueller et al. 2005; Williams et al. 2013; Fettig et al. 2019), to boreal vegetation (Beier et al., 2012),

The effects of a changing global water cycle on precipitation, stream flow and groundwater recharge are magnified by the immediate hydrologic changes caused by

excessive anthropogenic water abstraction and alterations of natural streamflow conditions, creating increasingly unfavorable and stressed environments for aquatic and riparian plant and animal species (Rodriguez-Iturbe 2000; Snyder and Williams 2000; Troch et al. 2009; Wang et al. 2018). Changes in the seasonal delivery of precipitation and temporal shifts in spring warming disrupt the timing of life cycle events (phenology) in vegetation, shifting the timing of green-up and senescence (Cleland et al. 2007; Körner and Basler 2010; Ma et al. 2015; Munson and Long 2017), and creating a cascade of negative impacts on animal migration patterns and plant-pollinator interactions (Memmott et al. 2007; Burkle et al. 2013; Seebacher and Post 2015). Furthermore, similar to the links between soil moisture and the atmosphere, feedbacks between vegetation and the water cycle drive the amount of moisture in the atmosphere, contributing to the recycling of moisture across the Earth's surface (Villegas et al. 2010; Moore et al. 2015; D'Odorico et al. 2019)

1.3 Vegetation-climate interactions in dryland environments

Changes in the global water cycle are especially impactful in dryland regions, where inherent water deficits and high spatial and temporal variability of precipitation play a critical role in vegetation structure and functioning (Rodriguez-Iturbe 2000; Tamea et al. 2009; D'Odorico and Porporato 2019). Hydrological processes exert considerable control on vegetation in water-limited environments through the soil water content, which is driven by complex interactions between precipitation, infiltration, evaporation, transpiration and soil hydraulic properties (D'Odorico et al. 2019; Rinaldo and Rodriguez-Iturbe 2022). Changes in precipitation and temperature and increasing evaporative demand over arid and semi-arid regions advances dryland expansion and ecosystem degradation, by creating severe hydrological deficits and increasingly unfavorable ecological conditions (Tietjen et al. 2010; Wang et al. 2012; Huang et al. 2016).

Generally, vegetated areas of variable species diversity and density are interspersed with bare soil patches, with variable plant distributions driven by topographic gradients, underlying geology, elevation and geomorphological conditions (Makings 2005; Stromberg et al. 2017; Sabathier et al. 2021). Plant functional types are generally well adapted to the hydrological conditions where they

root. In the presence of sustained surface or subsurface flows, mesic riparian environments are common, which sustain a range of plant and animal species that cannot thrive in the xeric dryland environment, thus creating complex landscapes with unique ecohydrological dynamics (Makings 2005; Stromberg et al. 2005; Stromberg et al. 2013). Dryland vegetation is generally well-adapted to the marginal conditions of their environment. However, many dryland regions are affected by rapid changes in vegetation cover and desertification (Wang et al. 2012).

With water being the main growth-limiting factor to dryland vegetation, vegetation dynamics and water stress are directly correlated to declining soil moisture availability, which subsequently affects other biophysical interactions with the atmosphere, such as carbon sequestration, through vegetation shifts or reduction in photosynthetic activity and vegetation functioning (Huang et al. 2017; Zhou et al. 2019). Vegetation cover and density can be broadly explained in terms of spatial and temporal availability of water, from streamflow, to shallow soil moisture, to groundwater access, which lead to distinct vegetation zones and patterns across the landscape (Caylor et al. 2006; D'Odorico et al. 2007; Sabathier et al. 2021). The fraction of water used by vegetation varies greatly by vegetation cover type, season and overall vegetative health, with differential responses between ecohydrological process at patch, hillslope or catchment scale (Notaro et al. 2010; Moore et al. 2015). At patch scale, vertical patterns of ecohydrological processes primarily affect local vegetation-soil moisture interactions, such as transpiration drainage and vegetation growth. At the hillslope scale, vegetation distribution plays an important role as the associated ecophysiological properties drive larger-scale hydrologic processes (Rodriguez-Iturbe 2000; Moore et al. 2015; D'Odorico et al. 2019). More importantly, lateral redistribution of water through surface and subsurface partitioning links vegetation dynamics to hydrologic processes, invariably driving the spatial redistribution of water and vegetation across the landscape. At the catchment scale, vegetation can exert considerable influence on the regional the water balance, with dense vegetation driving runoff and recharge processes and the redistribution of water across the landscape. Still, the effects of vegetation on the catchment water balance can be difficult to quantify due to the inherent spatial heterogeneity of

vegetation across the landscape and their influence on surface and subsurface water fluxes (Porporato et al. 2002; Moore et al. 2015).

The fluxes of water through the dryland soil-plant-atmosphere continuum are expected to change under future climate, as evapotranspiration, soil moisture and runoff are tied to magnitude and direction, and spatial patterns of precipitation (Garfin and Jardine 2013). Nevertheless, the quality, timing and amounts of water remain critical in dryland ecosystems, not only to runoff, recharge processes, plant water availability and sedimentation processes, but also to a variety of threatened and endangered species that seek refuge from extreme temperatures and dryness (Garfin and Jardine 2013; Huang et al. 2017).

1.4 Climate change and drought: The example of the Southwestern USA

One particular area of the world's dryland regions, the semi-arid Southwestern USA, is the focus of study in this thesis and has experienced recurring periods of drought since medieval times (Cook et al. 2015a). However, an extremely dry 22-year period during the early 21st century and continuing to the present, aggravated by anthropogenic climate change, has resulted in an emerging megadrought, a period of aridity of such severity than any of the worst multi-year droughts recorded during the 20th century (Ault et al. 2016). These droughts are characterized by persistent severe soil moisture deficits and acute water shortages exceeding any historical records of past drought events (Cayan et al. 2010; Cook et al. 2015c; Williams et al. 2022a). Global warming has contributed towards the amplified drought severity and frequency of recent decades, with warming global temperatures and evaporative demand amplifying drought severity (Cole et al. 2002; Cook et al. 2014; Cook et al. 2015c). Anthropogenic climate change will arguably play a defining role in future drought occurrences throughout the Southwest, propagating drought even beyond historically known drought prone regions (Cook et al. 2014; IPCC 2014).

The semi-arid climate of the Southwestern USA is characterized by a strong natural climate variability with climatologically low precipitation, soil moisture and

humidity (Notaro et al. 2010; Garfin and Jardine 2013; Gonzalez et al. 2018). The climate varies across spatial and temporal scales due to orographic effects, ocean-land interactions and the presence of atmospheric rivers, resulting in distinct climate gradients between coastal and inland regions (Dettinger 2013; Garfin and Jardine 2013). More specifically, the Mediterranean climate of California with its hot, dry summers and cold, intermittently wet winters with episodic rainstorms, stands in stark contrast to the monsoon-dominated interior states, such as Arizona, with its extremely hot summers and heavy monsoon rainfall between July and September and highly variable winter – early spring precipitation between November and March (Dettinger et al. 2011; Steenburgh et al. 2013). Coastal climates are generally moderated through the proximity to the Pacific Ocean, leading to much lower average maximum temperatures and increased humidity, while with increasing distance from the coast, a strong temperature gradient extends into the interior, with regions such as Southwestern Arizona being considerably more arid. Average maximum temperatures frequently exceed 40°C during the summer and the strong interannual variability in precipitation affects hydrology, soils, vegetation, and carbon storage in these arid regions (Steenburgh et al. 2013; Gonzalez et al. 2018).

Throughout the Southwest, ecosystem structure and functioning are broadly defined by seasonal water availability, either through shallow soil moisture or access to groundwater. As the hydrology of the Southwest is strongly tied to the seasonal and interannual climate variability, it is inherently sensitive to changes in the water cycle that alter the seasonal water availability (Cayan et al. 2010). The effects of the recent warming and drying has propagated throughout lowland grasslands in Southern California, to desert grasslands and riparian forests in Southeast Arizona. Ecosystems in these areas have experienced the direct and effects of climate change, resulting in widespread mortality, vegetation cover changes and loss of species diversity because of the anomalously dry periods of recent decades (Cook et al. 2015a; McKinnon et al. 2021).

1.5 Regional examples of climate change from the Southwest

1.5.1 The lowland grasslands of Southern California

Throughout California, grassland ecosystems constitute a major component of the state's wildlands comprising >10% of its area, which can be broadly divided into coastal prairie and valley grasslands (Bedsworth et al. 2018). Throughout the 19th and 20th centuries, the continued transition from native to non-native species, which may have started with the arrival of Spanish explorers, has resulted in an increasing dominance of annual non-native grasses and forbs and significant fragmentation and habitat loss (Reynier et al. 2016). As a result, the percentage of introduced non-native species now almost exceeds the number of native species, especially due to the diversity of habitats that appeal to non-native species of predominantly Mediterranean origin (Stromberg et al., 2007).

The coastal plains of California contain a mixture of native and non-native grasslands, intergraded with oak woodlands and minor drought deciduous shrublands, which benefit from the influence of the Mediterranean climate. There, winter rainfall and summer fog contribute to increased soil moisture availability and provide a moisture buffer during the summer dry periods. Species distribution can vary significantly between years, due to rainfall variability, with significant amounts of both native and exotic perennial species. Farther inland, species compositions transition to semi-arid grasslands and valley oak woodlands (Figure 1.1 a), with higher species variability in some areas where no disturbance from grazing or farming is present. Overall, non-native annual grasses have expanded considerably across arid and semiarid lands, including various brome grasses (*Bromus hordeaceaus L., Bromus diandrus*) (Roberts et al., 2010; Stromberg et al., 2007). The significant increase in invasive annual species such as cheatgrass (*Bromus tectorum*), red brome (*Bromus rubens*) and buffelgrass (*Pennisetum ciliare*), has been directly linked to increased fire activity and land degradation during recent decades (Abatzoglou & Kolden, 2011; Wallace et al., 2016).

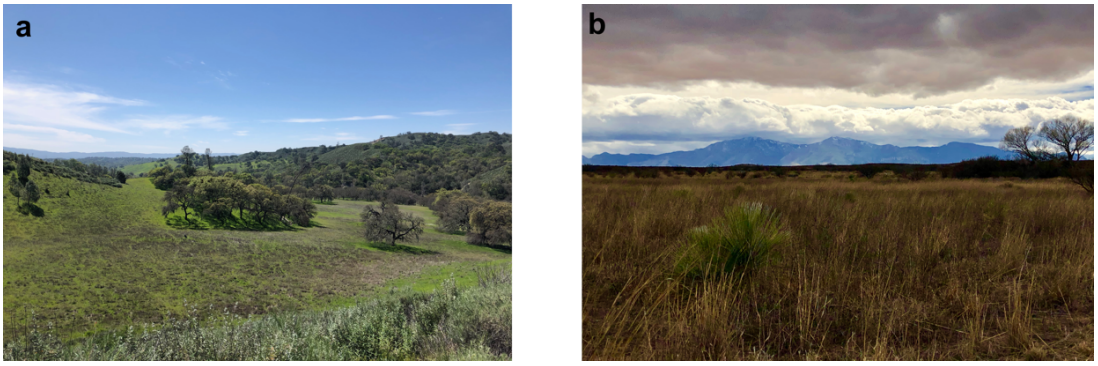

Figure 1.1: a) Native grassland and valley oaks at Sedgwick Ranch, Santa Barbara country.b) Desert shrubland in a dryland ecosystem along the San Pedro River National Conservation Area in Southeastern Arizona.

The persistent multi-year drought between 2012-2019 in California severely affected natural ecosystems throughout the state (Liu et al. 2012; Bachelet et al. 2016; Reynier et al. 2016; Thorne et al. 2016). While native perennial grasses tend to be more resilient to short-term drought periods than shallow-rooted non-native annual grasses, due to their deeper rooting systems, the prolonged drought periods and persistent soil moisture deficits have led to a significant decline in native perennial grass cover, exposing grasslands to further invasion of exotic species (Wallace et al. 2016). The expansion of invasive annual grasses not only results in irreversible changes in grassland physical structure but also increases fuel availability, raising the risk of wildfire frequency and extent to unprecedent levels (Westerling and Bryant 2007; Abatzoglou and Kolden 2011). Even though California's landscapes are historically dominated by brown vegetation during the dry summer, significant shifts in grass phenology and earlier browning may propagate due to soil moisture deficits, which limit recovery and green-up in subsequent growing seasons (Harrison et al., 2018; Mann & Gleick, 2015).

1.5.2 Dryland riparian forests of Southeastern Arizona

Riparian zones are considered important landscape features,as they provide a wide array of ecosystem functions and regulate a number of ecological processes at the intersection between terrestrial and aquatic systems (Stromberg et al. 2006; Pettit and Froend 2018). Riparian areas are known to sustain regionally rare biotic

communities and provide habitat for a large variety of plants and animals, as well as food and shading (Richardson et al. 2007). The riparian microclimate also contributes to the moderation of stream water temperatures, thus keeping riparian zones cool via plant evapotranspiration and shading and contributing to the removal of pollutants and enhancement of bank storage and stabilization along the channel (Richardson et al., 2007; Stromberg et al., 2006). The relative importance of riparian zones has led them to be characterized as "critical transition zones", as they occupy only small parts of the landscape while simultaneously standing at the interface of intense human activity and the natural environment (Richardson et al. 2007). Riparian vegetation exerts a strong influence on hydrological processes, and vice-versa, through its moderation of interception, infiltration, runoff and uptake, storage and return of water to the atmosphere through evapotranspiration (Williams and Scott 2009). These ecohydrological interactions are particularly strong in the arid and semi-arid regions of the Southwest, such as SE Arizona, where the inherent strong spatial and temporal variations of water availability broadly determine the structure and functioning of vegetation-atmosphere interactions (Tabacchi et al. 2000; Williams and Scott 2009; Stromberg et al. 2013).

Figure 1.2: A characteristic narrow band of cottonwood trees surrounds the San Pedro River channel at the SPRNCA in Southeastern Arizona. Upland areas are dominated by mesquite and other xeric grasses and shrubs. Source: Romy Sabathier, August 2019.

Among the most prominent riparian areas in the arid Southwest is the San Pedro Riparian National Conservation Area (SPRNCA) in Southeastern Arizona, which is considered one of the most diverse ecosystems of the country and has been studied extensively in recent decade due to its declining status (Stromberg et al. 1992; Stromberg and Tiller 1996; Scott et al. 2000; Snyder and Williams 2000; Lite and Stromberg 2005a; Williams and Scott 2009; Mayes et al. 2020; Sabathier et al. 2021). Owing to its relative resource abundance and surface water access, it serves as an important migratory corridor and functions as a thermal and moisture refugium for many threatened and endangered species (Makings 2005; Stromberg et al. 2006). The San Pedro River itself is a low gradient, alluvial desert river originating in Sonora, Mexico and a tributary to the Gila River, which then flows into the Colorado River.

Generally, riparian zones consist of a narrow band of channel adjacent vegetation (Figure 1.2), which in the presence of reliable access to shallow alluvial groundwater tends to be favored by obligate phreatophytes that develop roots primarily into the capillary fringe and saturated zone (Pettit and Froend 2018). The responsiveness of riparian vegetation to nonstationary conditions of water stress leaves them particularly sensitive to extreme groundwater and stream flow fluctuations and thus highly vulnerable to the negative effects of warmer and drier climate conditions and changes to the water cycle (Bréda et al., 2006; Stromberg & Tiller, 1996). Among the most common obligate riparian tree species found in the SPRNCA are willows (*Salix spp.),* cottonwoods (*Populus spp*.) and tamarisk (*Tamarix spp.*) with varying degrees of dominance and density across the landscape (Stromberg et al. 2017). The upland zones above the river channel (riparian terraces) are inhabited by a variety of facultative phreatophytes, such as mesquite (Prosopis spp.), with dense mesquite forests known as “bosques“. Even though mesquite has a large ecological range, the densest mesquite forests are found above the riparian floodplains where plants have adapted to accessing water from a variety of sources, including shallow soil moisture, stream water and shallow groundwater (Snyder & Williams, 2000; Stromberg et al., 2006; Williams & Scott, 2009).

Further upland, various xerophytic desert shrubs, such as creosote bush (Larrea tridentata), whitethorn acacia (Acacia constricta) or tarbush (Flourensia

cernua) inhabit the drier regions with increasing distance from the channel (Makings 2005). Generally, plant distributions throughout the riparian and upland zones vary with the level of available moisture, soil properties and elevation, resulting in distinct vegetation patterns with varying drought sensitivities and tolerance (Makings 2005; Stromberg et al. 2006; Stromberg et al. 2017; Sabathier et al. 2021). In contrast to grasslands in Southern California, desert grasslands dynamics are strongly tied to monsoon precipitation, resulting in peak vegetation activity throughout the summer (Scott et al. 2000).

1.6 Uncertainties about the impact of climate change on dryland vegetation

Despite the increasing complexity of global climate models, the true extent of projected temperature and precipitation changes on climate-vegetation interactions in dryland environments remains largely uncertain (Huang et al. 2017). The sensitivity of dryland hydrology and vegetation to changes in the seasonal delivery of precipitation presents a significant challenge in terms of quantification and predictability of water resources. Even though the evolution of key hydrological processes and associated vegetation-climate interactions are closely linked to precipitation they remain poorly understood across different vegetation communities (Tietjen et al. 2010; Scott et al. 2014). The current lack of understanding consequently impedes any efforts to anticipate the changes of key components of the dryland water balance in response to changes in the timing and intensity of precipitation and their overarching effects on plant water availability (Tietjen et al. 2010; Wang et al. 2012; Huang et al. 2017; Quichimbo et al. 2021). Indeed, the main challenge in managing ecohydrological systems is the inherent difficulty of quantifying impacts of certain climate changes (i.e. evaporative demand, precipitation) on ecohydrological processes. However, identifying the specific contributions of climate drivers on ecohydrological dynamics is essential to predict and assess the effects of global water cycle changes on ecosystem dynamics. Especially in dryland ecosystems, where changes to precipitation variability exert disproportionate pressure on vegetation and surface and groundwater resources, models are a key tool that must consider the

feedbacks between hydrologic flows and climate, and how they control ecohydrological processes across multiple scales.

While a substantial decrease in average annual rainfall and increases in the frequency and intensity of droughts will undoubtably incur large-scale changes in vegetation structure and functioning, the level of impact on individual species likely varies significantly. As such, the diverging sensitivities between soil moisture and groundwater dependent dryland plant functional groups inhabiting distinct locations in the landscape to climate forcing, require a disaggregation of the individual key hydroclimate drivers (Gremer et al. 2015; Munson and Long 2017). Considering the effects of changes in the timing and amount of seasonal precipitation on soil moisture dependent species in conjunction with temperature changes; the effects of water deficits and plant water stress on phenology and species interactions need to be further explored to create sustainable management practices that account for the non-stationarity of future climate conditions. Prolonged droughts constitute a considerable threat to grassland ecosystem functioning and species distribution, calling into question the plasticity of vegetation responses to more frequent and severe water stress and long-term soil moisture deficits, and future wildfire regimes (Gremer et al. 2015; Reynier et al. 2016; Zhu et al. 2016; Munson and Long 2017).

The complex interactions between climate and weather play a key role of wildfire activity, especially in Southern California, where strong seasonal wind patterns (i.e. Santa Ana winds) regularly propagate extreme fire-weather conditions (Westerling et al. 2004; Garfin and Jardine 2013). The persistent dry conditions undoubtedly contributed to recent wildfire occurrences, however anthropogenic influences severely exacerbated the extent and severity of wildfires. Still, the uncertainties regarding future climate trajectories and the lack of understanding and predictive modeling frameworks of future vegetation shifts present a challenge in terms of understanding and evaluating future fire regimes in similar arid and semiarid environments such as Southern California (Westerling and Bryant 2007; Liu et al. 2010; Keeley and Syphard 2016).

For groundwater dependent vegetation, the major uncertainties over future vegetation dynamics are frequently linked to declines in surface flow and depth to

groundwater, as well as interannual precipitation fluctuations. The changes to precipitation can drive soil moisture levels persistently below plant wilting points, thus significantly reducing recharge fluxes and compromising ecologically sustainable water table depths (Baird et al. 2005; Stromberg et al. 2013; Condon et al. 2020; Anurag et al. 2021; Sabathier et al. 2021). The observed trends in declining riparian vegetation functioning presage the effects of chronic physiological stress induced by declining water table accessibility. However, there are remaining uncertainties regarding the deleterious impacts on groundwater-dependent vegetation to long-term changes in the mean state and variability of climate. Furthermore, there is a lack of understanding regarding hydrologic partitioning between surface and subsurface fluxes between riparian zones and upland areas, and how riparian forest water stress is expressed under various climate change scenarios (e.g., warmer and drier or warmer and wetter). This topic of research has important implications not only for the quantification of the overall dryland water balance but on the spatial distribution of vegetation and broader ecosystem responses to future water limitations (Rodriguez-Iturbe 2000; Loik et al. 2004; Tamea et al. 2009). The current lack of understanding of riparian forests to water stress and the expression of climate on surface and subsurface water availability impedes any efforts to develop adaptive management practices that consider the potential climatic and ecohydrological thresholds of sensitive riparian species.

1.7 Advances in monitoring and modeling vegetation dynamics

Remote sensing techniques have been instrumental in tracking contemporary global and regional changes in the terrestrial surface over seasonal and interannual scales and a wide range of species and biomes (de Beurs and Henebry 2010; Choler et al. 2010; Walker et al. 2014; Lu et al. 2015; Moon et al. 2021). Remotely sensed vegetation information such as the Normalized Difference Vegetation Index (NDVI), Enhanced Vegetation Index (EVI) or Soil Adjusted Vegetation Index (SAVI) are widely used as indicators of terrestrial vegetation productivity and health, and to track global and regional land cover changes and phenology (Wang et al. 2000; Helman et al. 2015; Gillespie et al. 2018; Sabathier et al. 2021). Especially in the context of drought, the integration of climate data with remote sensing information, strengthens

monitoring and quantification of vegetation responses across different spatial and temporal scales (Kibler et al. 2021; Rohde et al. 2021b; Sabathier et al. 2021)

The state-of-the-art remote sensing products have been essential in the analysis of global drying trends and shifts in vegetation phenology, with the purpose of determining drought timescales and elucidating the role of ecosystem processes within the broader Earth system (Gouveia et al. 2017; Smith et al. 2019). Yet, drylands present a unique challenge even to remote sensing, due to irregular and unpredictable growing seasons, rapid vegetation responses to seasonal rainfall and high soil background reflectance. Nevertheless, vegetation indices such as SAVI, which account for the higher soil background reflectance provide valuable information about seasonal vegetation dynamics over large spatial scales. Especially, for model simulations of dryland ecohydrological processes, an accurate representation of surface and subsurface fluxes is equally important to an accurate and moreover dynamic representation of phenology (Richardson et al. 2012).

Vegetation dynamics are often neglected or purposefully kept simple, with static prescriptions of greenness and vegetation cover (Montaldo et al. 2005a; Richardson et al. 2012). However, phenology is a key regulator of ecosystem processes and vegetation-atmosphere feedbacks with hydrology. Especially in dryland ecosystems, an accurate assessment of vegetation dynamics is vital for assessing ecosystem responses to environmental changes (Walker et al. 2014; Wallace et al. 2016; Pastick et al. 2018). The complex interactions between environmental and biological mechanisms arguably complicates modeling of ecohydrological processes in water-limited dryland environments. However recent modeling advances brought on more inclusive and efficient models that can capture key hydrologic processes over a range of spatial and temporal time scales, despite lacking a comprehensive parameterization of surface vegetation dynamics (Quichimbo et al. 2021).

In this context, the combination of remote sensing information with climate data has considerable potential to enhance the evaluation and parameterization of models, and therefore improve quantification and understanding of vegetation responses in vulnerable dryland ecosystems. This is particularly the case since the

true extent of climate induced phenological shifts and overall changes to species composition within both groundwater and soil moisture dependent dryland vegetation communities remains unclear (Walker et al. 2012; Gremer et al. 2015; Munson and Long 2017; Schlaepfer et al. 2017).

1.8 Aims and objectives of the thesis

The recent warming and drying trends have had widespread effects on dryland ecosystems and water resources, including soil moisture, streamflow and groundwater. However, despite the mounting scientific evidence, it is still unclear how vegetation will respond to future climate variability and how future trends in drought, precipitation and aridity will propagate across ecosystems with differential water and moisture dependencies. From lowland grassland biomes to dryland riparian woodlands, the effects of future changes to precipitation and temperatures on vegetation functioning and ecohydrological processes are not yet fully understood. More specifically, the negative effects on composition, structure and functioning of riparian habitats in response to prolonged water deficits are relatively unexplored. Ultimately, a more accurate understanding of the abiotic and biotic thresholds to water limitations and disaggregation of key hydroclimate drivers of vegetation responses is important to delineate the diverging sensitivities of existing vegetation communities and develop predictive models that are able to quantify the changes to the hydrological cycle and ecosystem dynamics under changing environmental conditions. To that end, the research in this thesis is guided by the following specific research questions:

i. How is a multi-year drought expressed in dryland hydrology and vegetation changes at a patch scale?
ii. What are the key hydroclimate drivers of vegetation dynamics and vegetation water stress for different plant functional groups in a water-limited environment?
iii. How will vegetation-hydrology interactions and overall dryland ecosystem functioning be affected by climate change on a catchment scale?

1.8.1 Objectives

To address these research questions, I set several objectives with the aim to improve the scientific understanding of vegetation responses to water stress under historic and future climate by exploring climate-vegetation interactions across different spatial and temporal scales, and different biomes and geographical regions throughout drought prone regions of the Southwestern USA (Figure 1.3). Generally, I aim to use historic observations and climate data as well as remotely sensed vegetation information to determine the effects of drought on ecohydrological processes and quantify the impact on the relationships between hydroclimate and vegetation, and on the propagation of vegetation water stress. Furthermore, I aim to address questions regarding the prediction of future vegetation responses and key challenges of dynamic parameterizations in ecohydrological model frameworks.

The research presented in this thesis is defined by the following objectives:

Objective 1: Determine how drought affected soil moisture availability to lowland grassland vegetation in the recent California drought and how grasslands might respond to future warming and drying trends in this region.

Objective 2: Disaggregate phenology-hydroclimate interactions of different dryland plant functional groups in SE Arizona and determine the key hydroclimate drivers of phenology.

Objective 3: Explore dryland phenology-climate interactions under future climate scenarios though modeling.

Objective 4: Improve the parameterization of climate-vegetation interactions in ecohydrological models.

Objective 5: Determine the effects of altered climate conditions on climate-vegetation-soil interactions in a dryland environment.

Specifically, I address **Objective 1** by exploring how the recent multi-year drought in California propagated throughout local soil moisture and affected vegetation responses. By disaggregating the locally observed effects of the drought on precipitation, soil moisture and vegetation responses I aim to generate a broader understanding of how sensitive ecohydrological processes are to soil moisture and

climate across a topographical gradient. I aim to further explore this sensitivity through simple modeling experiments to quantify the differential impacts of changing climate, specifically prolonged drought periods and reduced precipitation intensity, on soil moisture dynamics and how this would broadly affect existing regional challenges regarding species invasion, wildfire and overall ecosystem degradation.

To address **Objective 2**, I aim to disaggregate the influence of hydroclimate drivers on vegetation phenology of different dryland plant functional groups occupying distinct spaces in the landscape. This is an essential part to improve the parameterization of vegetation in ecohydrological models and the quantification of water stress, which is the ultimate goal of this study. To do this, I first use multiscale remote sensing and climate data to generate a broad understanding of seasonal vegetation dynamics. Subsequently, to address **Objective 3**, I aim to develop simple predictive models that are driven by individual hydroclimate-phenology relationships for different plant functional groups. This approach will allow me to explore potential changes to phenology under future climate scenarios over extended temporal scales.

To address **Objective 4**, I will use the broader understanding of climate-vegetation feedbacks and the established phenology model to improve the parameterization of soil-vegetation interactions within an existing dryland water partitioning model, DRYP, to improve the predictive capabilities of ecohydrological processes dryland ecosystem dynamics to climate and environmental changes. Finally, I address **Objective 5** by evaluating the functionality of the new parameterization through synthetic experiments and then testing the model using different scenarios of altered climate forcing. This will help to further quantify the effects of climate on the dryland hydrological cycle. It will also allow for an improved quantification of vegetation water stress to seasonal changes in water availability. Ultimately, the goal of this entire body of work is to generate a broader understanding of future climate-vegetation interactions in drought prone regions and modeling tools that are most useful and transferrable to land and resource managers.

Figure 1.3: Study sites across the Southwestern USA. Chapter 2 focuses on two grassland sites in Southern California and Chapter 3 explores desert grassland and riparian forests in Southeast Arizona

CHAPTER 2

2 Onset and propagation of drought into soil moisture and vegetation responses during the 2012-2019 drought in Southern California

2.1 Introduction

Current understanding of the California drought's impacts is frequently based on research within particular regions and biomes. However, little is known about the propagation of drought from the atmosphere into soil moisture, and its associated effects on lowland vegetation, especially within water-limited regions where grasses and shrubs dominate the landscape. These lowland, water-limited, grassland ecosystems exhibit complex relationships between vegetation and water availability that affect the spatial pattern and extent of different vegetation types, as well as the relative responses of different species to drought stress (Caylor et al. 2006; D'Odorico et al. 2007; Caylor et al. 2009; Okin et al. 2018).

The progression of climate change and its potential impacts on the water balance demand a better understanding of how mean climate (temperature, precipitation) and soil water availability drive vegetation dynamics in lowland grasslands. Soil moisture is one of the key drivers of plant growth and -health and accordingly, there are strong seasonal responses of vegetation to temperature and precipitation changes (Roberts et al. 2010; Coates et al. 2015).

Therefore, in this chapter, first the evolution of soil moisture and associated vegetation responses during the recent California drought is explored at two different grassland sites, one coastal and one further inland. Multi-year climate, in-situ soil moisture and remote sensing data was used to understand the broader patterns of soil moisture and associated vegetation responses during drought periods of different intensity. Second, a simple parsimonious soil moisture bucket model based on the FAO approach by Allen et al. (1998) is used to explore soil moisture responses to plausible future climate scenarios. Finally, conclusions are drawn from the analysis and the implications of climate shifts on grassland habitat survival are discussed.

2.2 Data & Methods

2.2.1 Study sites

The natural geography of the Santa Barbara region is characterized by coastal plains, oak woodlands divided by the Santa Ynez mountain range (Roberts et al. 2010). The two study sites were chosen from a network of several sites as they had the continuous climate and soil moisture data spanning over 10 years, while also representing the diverse geography of the region: a coastal grassland plain and an inland grassland site, north of the Santa Ynez Mountains (Figure 2.1). Both sites are characterized by a Mediterranean climate, with strongly seasonal precipitation during the winter and prolonged dry periods in the summer. The majority of precipitation falls between November and March, with an average of 352 mm (coastal) and 314 mm (inland) per water year (October-September), with growing season water availability strongly controlling annual growth cycles and senescence of vegetation throughout the region (Roberts et al. 2010; Liu et al. 2012).

The coastal site is located at the Coal Oil Point Reserve at an elevation of 6 mASL on a coastal floodplain, while the inland site is situated at Sedgwick Reserve Airstrip in the Santa Ynez Valley on the University of California's Sedgwick Natural Reserve at an elevation of 381 mASL. The second site is an open grassland, and neither site is grazed. The inland site is situated in a relatively dry valley in the rain shadow of the Santa Ynez mountain range, resulting in a higher evaporative demand during the summer due to higher temperatures (May-Aug average 28.5°C), compared to the coastal site (May-Aug average 20.6°C). Temperatures are generally more moderate at the coastal site, due to the presence of cooler, moister ocean air and coastal stratus clouds and thus lower insolation, enhanced by a coastal current, all of which reduce the overall evaporative demand (Roberts et al. 2010).

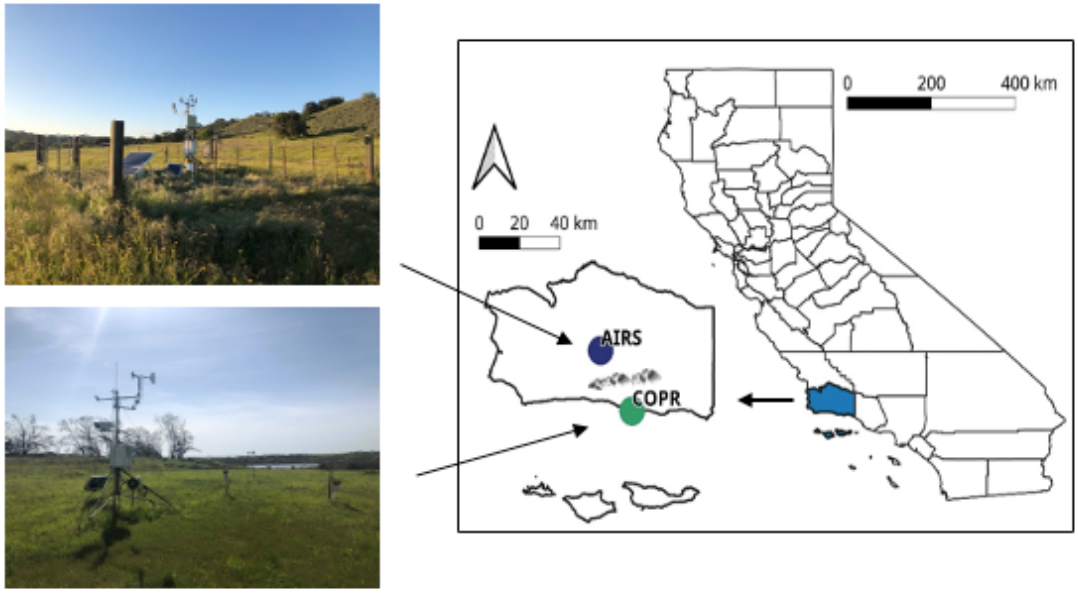

Figure 2.1: Location of stations in the Santa Barbara County showing the coastal grassland site (COPR, green) with a marine microclimate and the semi-arid inland grassland site (AIRS, blue), north of the Santa Ynez mountain range.

The coastal and inland sites vary in soil textural properties and water holding capacity, with soil types varying from clay loam at the coastal site to loam at the inland site, where there are distinctly higher sand contents (Table 2.1). Soil samples from several depths were taken at the time of sensor installation in 2007 by University of California Santa Barbara (UCSB) and texture, porosity, field capacity and wilting point were determined from volumetric moisture content measurements.

Table 2.1: Soil hydraulic properties at the coastal () and inland site in Santa Barbara, California.

Site	*Depth [cm]*	*Texture*	*Sand [%]*	*Clay [%]*	*Silt [%]*	*Porosity*	*θfc*	*θwp*
Coastal	10	Clay Loam	28	30	42	0.71	0.4	0.13
	20		24	37	39	0.66	0.48	0.15
	50		24	36	40		0.47	0.22
Inland	15	Loam	39	17	44	0.34	0.28	0.07
	23		38	16	45	0.39	0.3	0.07
	46		39	17	45		0.28	0.07

2.2.2 Historical climate

The United States Drought Monitor (USDM, https://droughtmonitor.unl.edu/) defines drought as a moisture deficit of such severity that it causes social, environmental, or economic effects. The USDM identifies and labels areas of drought within the United States based on a semi-quantitative intensity scale, derived from a combination of key indicators and information on soil moisture, precipitation, streamflow and drought severity, along with local condition and impact reports and ranges from D0 (Abnormally Dry) to D4 (Exceptional Drought) (NDMC 2020). The recent multiyear drought affected the majority of the state of California between 2012-2016 (Dong et al. 2019) at varying levels according to the USDM (Figure 2.2a), whereas Santa Barbara County was under continuous drought conditions much longer (until 2019) (Figure 2.2b).

The county was under 'extreme' (D3) to 'exceptional' (D4) drought from mid-2013 until early 2017, with the entire area remaining in the most severe category for several year. By spring 2017 the county was still under 'moderate' drought (D1), following a single wet winter season. However, the accumulated moisture deficit was so high after several years of exceptional drought conditions, that the state reverted to a state of 'severe' drought (D2) in 2018 after another abnormally dry year. The region finally came out of the drought completely in early 2019 after the wettest rainy season since 2005. Based on the drought designations from the USDM, we defined the following three drought categories: i) No drought (January 2010 - March 2012, February 2019 - October 2019 end of data), ii) Moderate Drought including periods of D0 and D1 and iii) Extreme Drought including Drought including periods of D2, D3 and D4. The three different categories to characterize the meteorology of the drought and assess the changes in mean climate and vegetation responses.

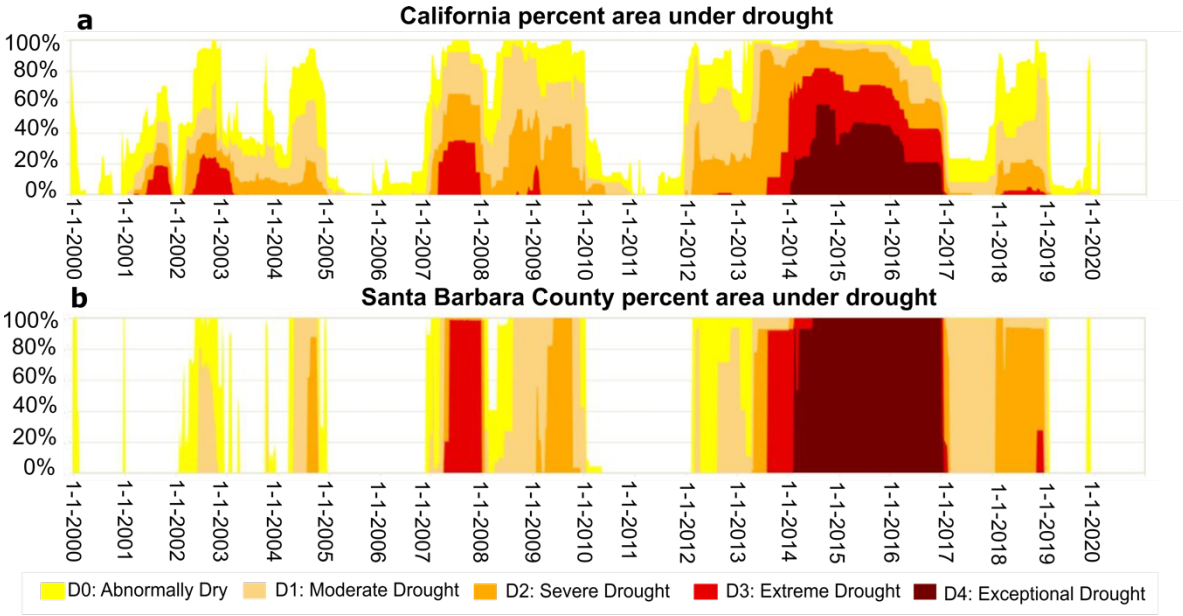

Figure 2.2: Timeseries of a) percentage area of California under drought and b) percentage area of Santa Barbara County under drought. [The U.S. Drought Monitor is jointly produced by the National Drought Mitigation Center at the University of Nebraska-Lincoln, the United States Department of Agriculture, and the National Oceanic and Atmospheric Administration. Map courtesy of NDMC.]

2.2.3 Meteorological and soil moisture data

Meteorological and soil moisture data was obtained from a network of several sites where data have been continuously recorded at 15-min resolution since 2007 by the University of California, Santa Barbara (UCSB) for educational purposes (Roberts et al., 2010). The data are generated as part of a long-term environmental sensing network, which was established in 2007. The network consists of three stations across southern California and are publicly available and continuously updated (https://ideas.geog.ucsb.edu/). Data include air temperature (T), relative humidity (RH), net radiation, wind speed and direction, and precipitation (P) among others. For each site, temperature and humidity were summarized to daily maximum daytime values and precipitation into daily totals to define the meteorology during our study period. Other variables from the dataset, such as soil temperature, wind speed and net radiation were used to estimate the necessary parameters to calculate the reference evapotranspiration (ET_0) via the Penman-Monteith approach (Allen et

al. 1998). The date of onset (day of the year of last recorded precipitation for more than three months) and length of the dry season for each year was analyzed and compared the timing between moderate drought, extreme drought, and non-drought periods. Two-sample Kolmogorov-Smirnov (KS) tests and/or Pearson's correlation were used to determine statistical differences between these periods, and to quantify correlations between variables, such as T, RH, P, ET0, available P (aP= P – PET), soil moisture saturation, and NDVI. I defined available P as the remaining amount of water in the soil after incoming precipitation is reduced by atmospheric demands, thus defining the potentially available amount of water in the soil and to vegetation.

Volumetric soil water content and soil temperature were measured using in-situ probes (Stevens Hydro Probe II, Stevens Water Monitoring Systems Inc., Portland) at three different depths (10, 20 and 50 cm at the coastal and 15, 23 and 46 cm at the inland site) (Roberts et al. 2010). For the purposes of this study, only the shallowest soil moisture was used at each site to capture the precipitation and evapotranspiration dynamics of the shallow soil horizon, which comprises the majority of the shallow moisture availability to grasses. Historical soil moisture is presented as relative saturation levels, ranging from dry (0%) to fully saturated (100%), defined as the ratio of volumetric moisture content to the volume of pore space (porosity). This allows for a direct comparison of soil moisture between the two sites, considering the differing soil textural properties While the data recovery for both meteorological stations was continuous for the period of interest, the soil moisture probes at the inland site experienced significant data loss between 2016 – 2018, due to battery and sensor failure; these gaps in the data are indicated in the results.

2.2.4 Normalized Difference Vegetation Index

Vegetation indices from remote sensing have been widely used to monitor the effects of drought on vegetation, as well as the links between precipitation, soil moisture, and plant sensitivity (Gu et al. 2008; Small et al. 2018; Dong et al. 2019). Multispectral indices, such as NDVI, provide good spatial and temporal representation of drought conditions, which can be combined with in situ measurement of soil moisture for a more detailed understanding of drought

propagation and drought stress on vegetation (Gu et al. 2008; Okin et al. 2018). To analyze the seasonality and relationship between soil moisture and vegetation for the study period, I used NDVI, as it is the most commonly used vegetation index, where vegetation cover is generally high. Other indices such as the Soil Adjusted Vegetation Index (SAVI) is more commonly used in less densely vegetation areas, where the influence of bare soil surface reflectance must be accounted for(Huete 1988). NDVI is computed from visible (VIS) and near infrared (NIR) surface reflectance data. It is distributed by the USGS for Landsat-5 (Thematic Mapper), Landsat-7 (Enhanced Thematic Mapper) and Landsat-8 (Operational Land Imager) - each with a 16-day acquisition interval and 30-m resolution. NDVI is estimated as:

$$\mathrm{NDVI} = \frac{\mathrm{NIR-VIS}}{\mathrm{NIR+VIS}} \qquad \text{Eq. 2.1}$$

where NDVI ranges from +1 to -1, reaching its maximum (saturated) value of 1 primarily in conditions of high plant vigor and photosynthetic activity, most common in forested areas and cultivated fields. As such, low or negative values are mostly representative of bare ground, senescent vegetation or water surfaces (Gillespie et al. 2018). Because multiple Landsat instruments were used to generate a continuous timeseries of NDVI, Landsat-5, and 7 were homogenized to Landsat-7 using the approach of (Goulden and Bales, 2019). Furthermore, if a pixel was cloudy the whole image was removed to create a consistent timeseries of pixels over the sampling area. Through regressions determined by comparing consecutive observations between the different instruments, NDVI was normalized as:

$$\mathrm{LS_8NDVI} = (\mathrm{LS_7NDVI} + 0.0232)/0.9553 \qquad \text{Eq. 2.2}$$

$$\mathrm{LS_8NDVI} = (\mathrm{LS_5NDVI} * 1.0630 + 0.0136)/\ 0.9553 \qquad \text{Eq. 2.3}$$

Polygons were defined around the measuring stations at each site to capture a broader area of homogenous grassland vegetation and soil textural properties at the coastal (19,800 m2) and inland site (35,100 m2). The polygons are based on field surveys made during site installation and on NDVI image analysis, delineating regions of relatively homogenous NDVI including only grassland vegetation (no trees). NDVI was spatially averaged over each polygon to obtain a monthly time series for the period January 2008 to October 2019. Through a pixel-wise visual

analysis of NDVI and comparison of different cover types (grassland, bare ground, forest, water) over the grassland sites, green grassland vegetation was generally represented by values >0.3, while NDVI values <0.3 are more indicative of brown or senescent (non-photosynthesizing) vegetation.

2.2.5 Soil Moisture Balance Model

2.2.5.1 Model description

A simple, parsimonious model was developed to better understand the linkages between climate, plant water availability and plant health and include experimental manipulations of climate variables to explore plausible future climate scenarios. Rather than attempting to model detailed soil moisture processes, a simplified soil moisture balance model (SMBM) established by the FAO was used, which is based on a 'bucket' approach (Allen et al. 1998), and a variant of a code previously developed for estimating groundwater recharge (Cuthbert et al. 2013; Cuthbert et al. 2019).

Simple modeling frameworks capable of linking vegetation to water availability can be useful tools to assess past and future ecohydrological dynamics in a range of water-limited environments (D'Odorico et al. 2007; Caylor et al. 2009; Evans et al. 2018; Quichimbo et al. 2020). Therefore, model inputs are equally kept as simple as possible and include information on soil properties, vegetation cover and climate (precipitation and the meteorological variables required to estimate reference evapotranspiration (ET0). Due to the flat topography of the study sites, runoff is assumed to be zero, thus precipitation at the study site is assumed to be either infiltrating into the soil and contributing towards recharge or returned to the atmosphere through evapotranspiration. Figure 2.3 shows a simplified conceptual design of a homogenous soil column and the relevant incoming (P) and outgoing (AET, runoff and drainage) fluxes, as established by Allen et al. (1998).

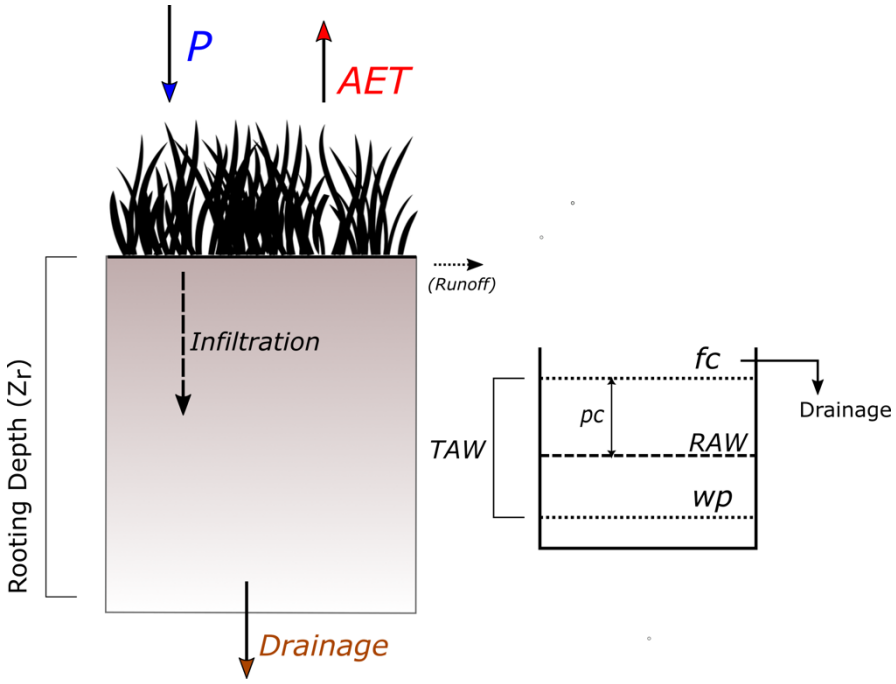

Figure 2.3: Conceptual model of a homogenous soil column and relevant incoming and outgoing fluxes and soil parameters defining the amount of available water.

The model uses the concepts of total available water (TAW) and readily available water (RAW), which are dependent on soil textural properties, to estimate the amount of water available for plants and by extension the soil moisture deficit. For this study, information on soil properties is available (Table 2.1). However, if field measurements are unavailable typical ranges for field capacity, wilting point, and rooting depths can also be found in the FAO56 Manual (Tables 19 and 22 in Allen et al., 1998). TAW is defined as the total water available in the root zone (mm), while RAW is the proportion of TAW that can be used by vegetation without the reduction of transpiration. The depletion fraction (pc) that decreases TAW to RAW is generally dependent on vegetation/crop type and was set to a vary between a commonly used range of 0.2-0.6 (Allen et al. 1998). The SMBM was driven by precipitation from meteorological data and reference evapotranspiration estimated through Penman-Monteith, using meteorological data from the weather stations. Due to the richness of the IDEAS dataset, variables such as soil temperature, wind speed and net radiation were available, which allowed us to estimate the necessary parameters such as ground heat flux and conductance, to apply the Penman-Monteith

model. A conceptual summary of all model parameters and processes is presented in Figure 2.4.

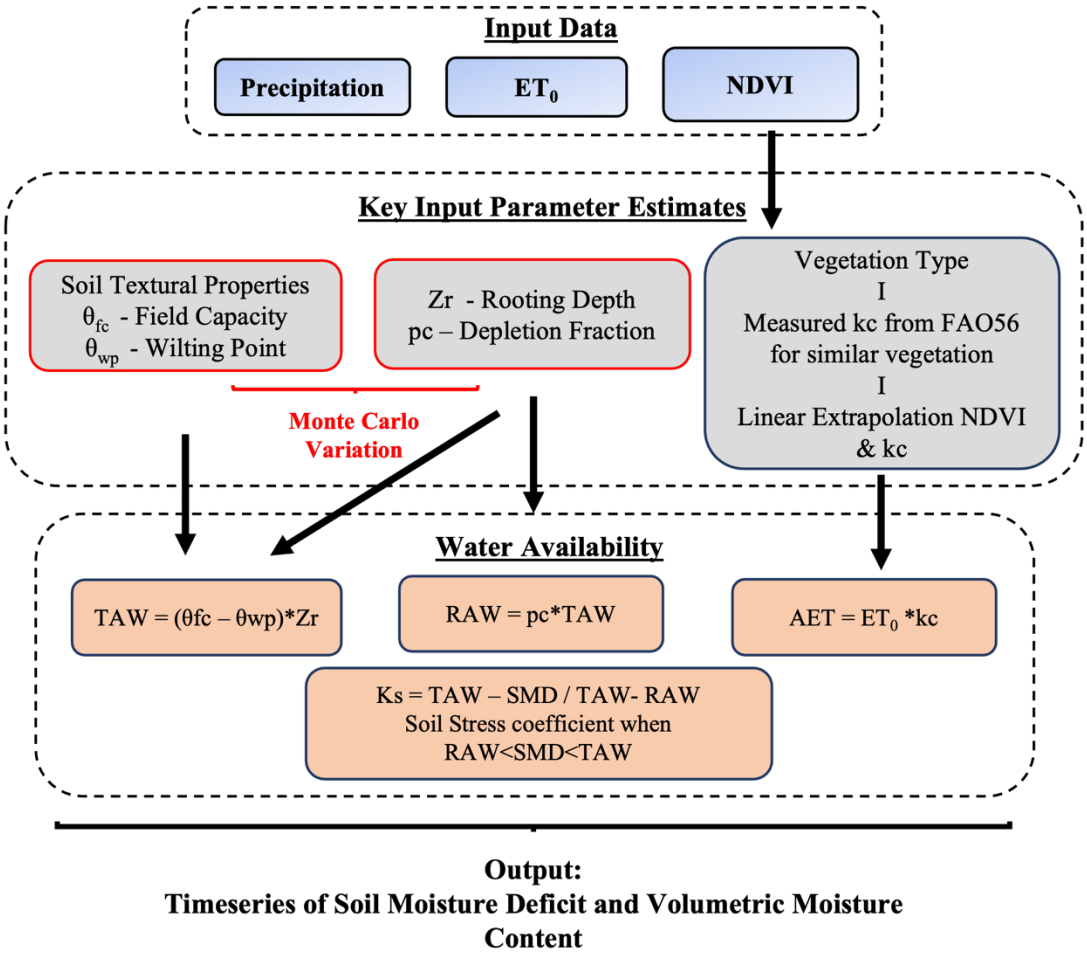

Figure 2.4: Schematic representation of the SMBM showing the key input parameters of soil textural properties and vegetation information, and the main model concepts of the parameterization of water availability.

2.2.6 Dynamic vegetation responses

Within the SMBM actual evapotranspiration is estimated using a crop coefficient (kc) as the empirical ratio relating plant ET to a calculated reference ET (ET0) and to account for changes in evaporative demand over a growing season. Previous studies have explored the relationship between multispectral vegetation indices, such as NDVI, and crop coefficients, and have applied it successfully to estimate kc at the field scale for different locations and climate conditions (Hunsaker et al. 2005; Glenn et al. 2011). Since kc traditionally does not account for variations

in plant growth due to climate variations or uneven water distribution, the alternative use of vegetation indices allows for a more accurate and dynamic estimation of ET (Nagler et al. 2005). NDVI was found to be closely correlated to ET, where maximum ET and maximum NDVI coincide at approximately the same time during a growing season, thus making NDVI a suitable proxy to estimate crop coefficients (Glenn et al. 2011). We use the same linear relationship between NDVI and kc to model a temporally varying crop coefficient derived from vegetation indices to quantify plant ET as follows:

$$\mathrm{kc_{VI}} = (VI^*)^{\eta} \qquad \text{Eq. 2.4}$$

where $\mathrm{kc_{VI}}$ represents a plant transpiration coefficient, η is an exponent determined by the relationship of ET0 with a vegetation index (i.e. NDVI) as measured by Pearson's correlation, and the vegetation index used in Eq. 2. VI* is the vegetation index of choice (i.e. NDVI, SAVI) normalized between 0 and 1 to represent bare soil/dead vegetation and fully transpiring and unstressed vegetation respectively, and calculated as:

$$\mathrm{VI} *= 1 - \frac{\mathrm{NDVI_{max}} - \mathrm{NDVI}}{\mathrm{NDVI_{max}} - \mathrm{NDVI_{min}}} \qquad \text{Eq. 2.5}$$

where NDVImax is the value when ET is maximal and NDVImin the ET of bare soil. Actual evapotranspiration under unstressed conditions can then be estimated as:

$$\mathrm{AET} = \mathrm{ET_0} * \mathrm{kc_{VI}} \qquad \text{Eq. 2.6}$$

2.2.7 Model implementation

The soil moisture and climate data were separated into calibration and validation sets and model performance in each period was evaluated for acceptance or rejection of models. Calibration, was done using data from January 01, 2008, to December 31, 2014. This time frame was chosen to include the natural variation of soil moisture dynamics, including non-drought and drought period. The model was then validated against data from January 01, 2015, to September 30, 2019. This period also includes natural variations in soil moisture, including the drought, individual very wet and dry years to account for the possibility of different combinations of parameter values (soil hydraulic properties, depletion fraction) that may all be equally

successful at reproducing the observed soil moisture data. Quantitative measures of acceptance/rejection criteria were defined through Kolmogorov-Smirnov (goodness of fit) testing to identify parameter combinations that achieve statistically similar ($p > 0.01$) distributions in observed versus simulated soil moisture. The temporal dynamics of soil moisture were evaluated via Nash Sutcliffe Efficiency (NSE) to identify parameter combinations that adequately simulated the observed soil moisture series ($NSE > 0.5$).

The models accepted during calibration and validation periods were then evaluated via goodness-of-fit and the best model and its parameters was used for simulating soil moisture under simple climate change scenarios. We developed an envelope of uncertainty based on Monte Carlo sampling (1000 simulations from a uniform distribution), using a range between the measured values soil textural properties and more general estimates of soil water storage properties found in the literature. For rooting depth and depletion fraction I used estimates from Allen et al., (1998, Table 22). Final model simulations included ±1 standard deviation of all accepted models in the results to show the range of working models.

2.2.8 Representing future drought scenarios

The projected shifts in precipitation frequency and variability during the dry season and anticipated increases in evaporative demand and extreme temperatures (see chapter 1.4) is likely to have detrimental effects on arid and semi-arid grassland ecosystems of Southern California. Through the SMBM model the possible effects of variations in P and ET0 on soil moisture and grassland vegetation were explored in a simple parsimonious way, based on projections of shifting precipitation variability and evaporative demand (Berg and Hall, 2015b; Pierce et al., 2018). These explorations of specific types of climate change used monthly input data and did not include any alterations to other key parameters, such as soil properties and vegetation cover type. The approach of only altering the climate forcing allowed a separate analysis of the influence of precipitation changes and the effects of increased evaporative demand on seasonal moisture and plant water availability. The historic period of 2012-01-01 to 2018-12-31 was used as a reference climate. The experimental climate scenarios are represented as a deviation from it as follows:

i) Scenario A): Simulation of the effects of a truncated rainy season (November – February) that reflects a loss of spring rains. This scenario represents an extreme decline in annual precipitation totals (average ~30% loss of annual P), the loss of precipitation in the shoulder seasons and prolonged dry periods.
ii) Scenario B): Simulation of a redistribution of lost spring rains from Scenario A into the truncated rainy season from November – February, thus increasing the precipitation intensity and frequency during the compressed rainy season, combined with an increase in dry season length. Projections of CMIP5 indicated a potential increase in the number of dry days in combination with more extreme events, overall increasing interannual precipitation variability over California (Berg and Hall, 2015b).
iii) Scenario C): Simulation of the effects of more extreme drought. A truncated rainy season from Scenario A is combined with an increase in evaporative demand and an additional 25% reduction of winter rainfall totals. Annual evaporative demand was increased to represent an average 4°C increase in annual temperature, characterized by more warming in the dry season, which is based loosely on projected changes in temperature for Southern California and much of the Southwest under RCP 8.5 (Cook et al. 2015b).

To maintain dynamic vegetation responses, simple linear regression models between observed NDVI and concurrent as well as antecedent available precipitation (aP) were established, and their correlation strength assessed through Pearson's correlation. The relationships were used to create a leading indicator to estimate NDVI using internally created aP under different climate change scenarios.

2.3 Results

2.3.1 Climatology of the drought

The 2012-2019 drought in Southern California was marked by several years of high evaporative demand, and low precipitation. The seasonal temperature differences during the March – October dry season between drought periods was +0.7°C between non drought and moderate drought, +1.9 between non drought and extreme drought and +1.3 between moderate and extreme drought at the coastal site, and +1.1, +1.9 and +0.8 for the inland site, respectively. Daily maximum temperatures during March – October were on average 6.2°C warmer at the inland site. Temperature differences were significantly different between all drought periods at both sites (Figure 2.5 a). Due to the moderating effects of cooler/moister oceanic air and coastal fog, relative humidity at the coastal site averaged at 81%, (Figure 2.5b). Inland, the relative humidity was lower, averaging 54% under non-drought conditions, and decreasing significantly during the extreme drought to an average of 48%. The more moderate temperatures and high relative humidity at the coastal site were also reflected in a lower evaporative demand, resulting in ~50% lower annual ET_0 compared to the inland site. Monthly ET_0 averages at the coastal site were 265 mm/y and 515mm/y at the inland site during non-drought periods, with significant increases during the extreme drought period, especially at the inland site (Figure 2.5 c).Historical annual precipitation over the 11-year period was on average 20% less at the inland site than at the coast, as the site lies in the rain shadow of the Santa Ynez mountain range. Precipitation averaged 147mm/y at the coastal site and 119 mm/y at the inland site during the non-drought period, with precipitation at the coastal site showing a significant shift towards lower monthly totals during drought periods (Figure 2.5 d). A correlation matrix of all parameters is presented in Table 2.2.

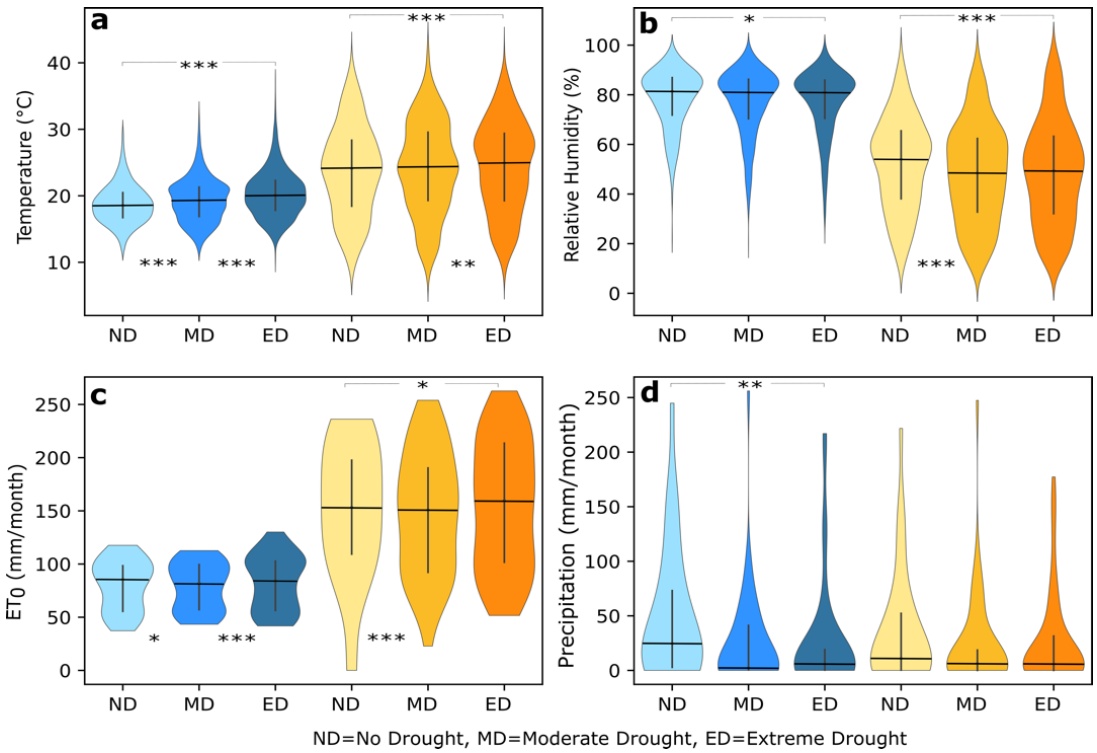

Figure 2.5: a) Monthly mean daytime temperatures, b) monthly mean relative humidity, c) monthly cumulative reference evapotranspiration and d) cumulative monthly precipitation during the non-drought, moderate and extreme drought periods at the coastal (blue) and inland site (orange). The vertical black line indicates the interquartile range and the black horizontal line the median. Statistically significant differences between drought periods are indicated at the 0.05 (*), 0.01 (**) and 0.001 (***) level.

The lowest October-September totals at both sites were recorded at the height of the drought in 2014, with 170 mm/y at the coastal and 162 mm/y at the inland site. A period of intense precipitation occurred from late 2016 to spring 2017, but the area remained in a state of severe drought until early 2019. A single dry year in 2018 temporarily increased the drought stress on the region again, before a very wet rainy season in 2019 finally relieved the pressure on ecosystems and water resources in Santa Barbara County locations and much of the entire state (Figure 2.2).

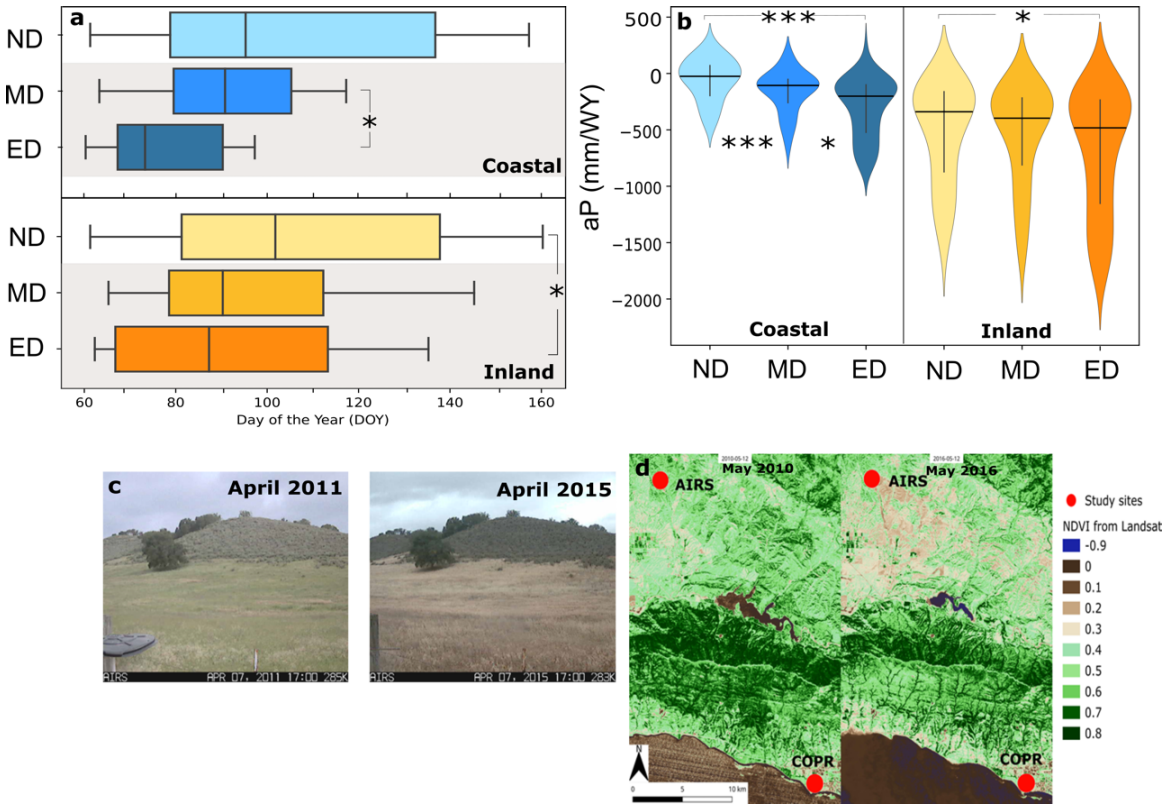

Figure 2.6: a) Onset of the dry season for the coastal (blue) and inland (orange) site. Vertical black lines indicate the median DOY, whiskers indicate the maximum and minimum DOY recorded. b) Available precipitation (aP) over the water year for the individual drought periods. Black horizontal lines indicate the median aP and vertical lines the interquartile range. Statistical significances are indicated at the 0.001 (***) and 0.05 (*) level. c) Webcam images of the inland site during non-drought (April 2011) and extreme drought (April 2015). d) Declines in greenness are visible during the drought period throughout the Santa Barbara County.

Most notable was the emergence of a shift in the onset of the dry season, after which no more precipitation was recorded for three consecutive months or more, until the start of the rainy season again in the fall (Figure 2.6 a). At the coastal site, the shift of the onset of the dry season was most significant between non-drought and extreme drought, with a shift from DOY 95 to 73, which translates to a temporal shift roughly from early April to mid-March, whereas at the inland site, the shift was most pronounced, with a shift from DOY 103 (non-drought) to 90 (moderate drought) to 87 (extreme drought). This shift in early dry season onset from mid-April to late

March triggered visible vegetation browning during the extreme drought by late March/early April at the inland site, as opposed to a more gradual browning between May and June in the years preceding the drought (Figure 2.6 c, d). The increased evaporative demand and reduced precipitation during the drought also resulted in significant changes to available P during drought periods, implying limited water availability for infiltration and replenishment of soil moisture, especially inland (Figure 2.6 b).

Table 2.2: Summary of correlation coefficients between drought periods, as measured by Pearson's correlation. Significance levels are noted at the 0.05, 0.01 and 0.001 level and significant relationships highlighted in bold.

Site	*Variable*	*ND-MD*		*ND-ED*		*MD-ED*	
		Stat.	Signif.	Stat.	Signif.	Stat.	Signif.
Coastal							
	AT	0.14	0.001	0.21	0.001	0.12	0.001
	RH	0.05	0.21	0.05	0.05	0.03	0.38
	ET0	0.06	0.05	0.03	0.39	0.07	0.001
	P	0.3	0.06	0.36	0.01	0.12	0.77
	NDVI	0.3	0.001	0.32	0.001	0.22	0.001
	Saturation	0.25	0.17	0.45	0.001	0.34	0.01
	aP	0.47	0.001	0.55	0.001	0.26	0.05
Inland							
	AT	0.05	0.06	0.08	0.001	0.06	0.01
	RH	0.11	0.001	0.1	0.001	0.03	0.46
	ET0	0.08	0.001	0.04	0.05	0.05	0.065
	P	0.18	0.45	0.16	0.51	0.09	0.96
	NDVI	0.19	0.001	0.18	0.001	0.11	0.001
	Saturation	0.25	0.16	0.36	0.01	0.25	0.05
	aP	0.25	0.15	0.29	0.05	0.20	0.20

2.3.2 Soil moisture and plant responses to drought

The drought was expressed differently in the soil moisture at each site. Soil moisture observations showed increased drying of soils during drought periods at

both sites, compared to the non-drought period, reaching extremely low moisture levels in 2013 and 2014 (daily relative saturation (S_e) fell below 5% inland). Similar low soil moisture occurred at both sites in 2008, a particularly dry year for the region. At both sites, relative saturation was significantly different between the non-drought and drought periods at both sites, with significantly lower levels during the drought at both sites (Figure 2.7 a). Relative saturation was similar at both sites during the non-drought period (40%) but decreased to an average of 30% at the coastal site and 23% at the inland site during the extreme drought.

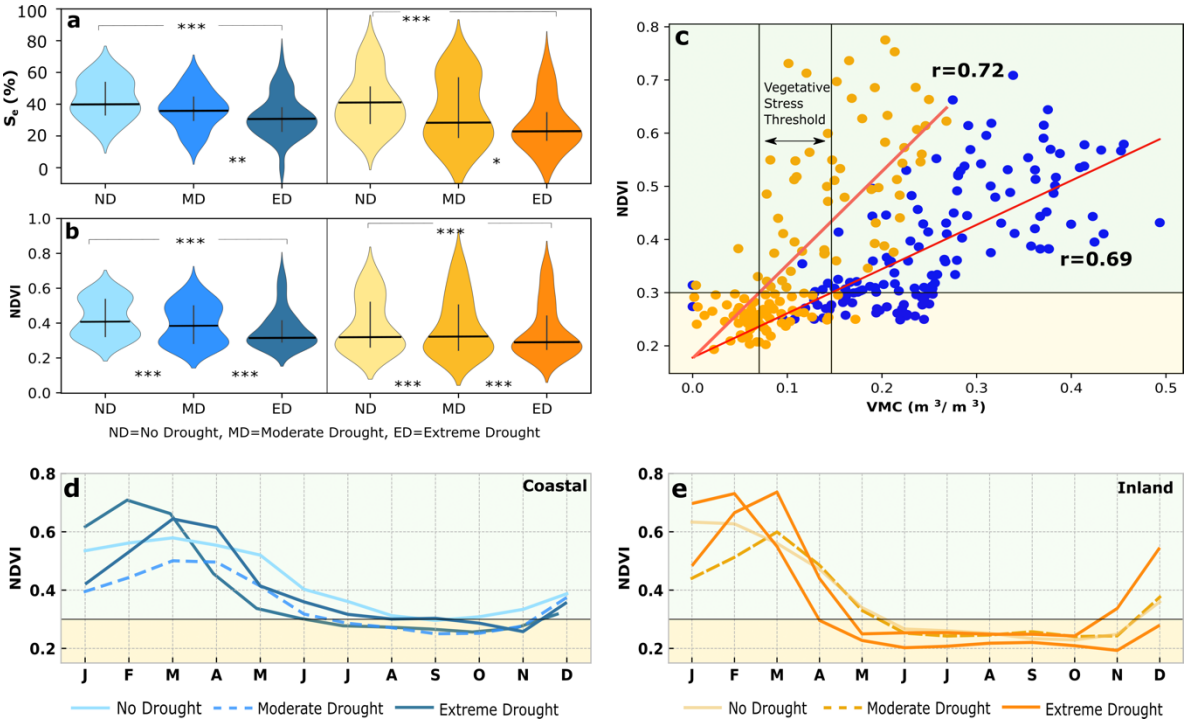

Figure 2.7: a) Monthly average relative saturation (S_e) of soil moisture and b) daily mid-month NDVI during non-drought, moderate and extreme drought periods at coastal (blue) and inland (orange) sites. Medians are indicated as black horizontal lines. Significance is indicated at the 0.001 (***), 0.01 (**) and 0.05 (*) level. C) Relationship between monthly average soil moisture and NDVI, which was used to establish a heuristic vegetative stress threshold (horizontal line), below which vegetation is most likely senescent. d) and e) Seasonal dynamics of NDVI during years of non-drought, moderate and extreme drought.

At both sites average monthly NDVI during the non-drought period was significantly higher than during the drought periods (Figure 2.7 b). Monthly NDVI values over selected non-drought and drought years illustrate the strong seasonality of annual grass cover in the region, with a marked green-up period after the winter rains, followed by a decline into brown conditions over the dry season (Figure 2.7 d,e). In particular, there was a rapid increase of greenness during the extreme drought, following the winter rains in 2015 and 2016, and the subsequent unusually rapid and early decline of greenness in spring. Surprisingly, NDVI reached maximum values at the height of the drought in 2015 that were nearly double the non-drought averages (0.70 and 0.77 coastal and inland, respectively). It is most notable that the NDVI peak values during drought were higher than those for the non-drought period at both sites, but very short-lived as NDVI declines rapidly back to low values, in contrast to the shoulder of greenness and slower decline of NDVI that occurred in most non-drought years. During the extreme drought, NDVI dropped rapidly below 0.3 in April at the inland site, which was also visible in webcam images and spatial NDVI imagery over the region (Figure 2.6c,Figure 2.7e). These differences in the seasonal variation of NDVI suggest a strategy of rapid grass green up after winter rains, accelerated by mild winter temperatures during the drought and especially during the exceptionally warm winter in 2014-2015. The growth of additional vegetation under these conditions likely led to the observed rapid decline in moisture during spring, as vegetation quickly depleted any excess moisture, and subsequently experienced increased browning and senescence due to the early onset of the dry season (Figure 2.6a).

Correlation between NDVI and soil moisture of the concurrent month over the study period was strongly positive and statistically significant for both sites ($r = 0.68$ coastal and inland, $p < 0.001$), a relationship that was used to establish a heuristic vegetation stress threshold at VMC = 0.15 m3/m3 for the coastal and VMC = 0.07 m3/m3 for the inland site. We associated these thresholds with very low rates of photosynthetic activity, based on an NDVI threshold of 0.3 (Figure 2.7 c). Correlation analysis between NDVI and aP over antecedent months revealed a three-month lag in aP and NDVI at the coastal site ($r=0.82$), and a two-month lag at the inland site

(r=0.74). To develop a predictor (leading indicator) of vegetation response to aP, we fitted linear regression models as follows:

$$NDVI_i = \alpha * aP_m + \beta \quad \text{Eq. 2.7}$$

where $NDVI_i$ denotes an estimated monthly NDVI, aPm is the amount of aP accumulated over a number of months m, and α and β are regression coefficients. A threshold of maximum NDVI was applied to both sites (0.75 coastal and 0.7 inland) during the regression analysis to account for the fact that NDVI saturates beyond a maximum amount of available water.

2.3.3 Model performance evaluation

Given the simple structure of the SMBM, results were reasonably effective at capturing and predicting the timing and magnitude of interactions between P, ET0, and soil moisture (Figure 2.8 a, b). Kernel density estimates (KDE) for observed and simulated soil moisture distributions were statistically similar (Figure 2.8c; ks=0.12 and p=0.24 coastal and ks=0.12 and p=0.49 inland) and simulated and modelled soil moisture showed good correlation (r=0.84 coastal and r=0.84 inland). However, it should be noted that the best-fit simulated soil moisture at both sites at times over- or under-estimates observed VMC.

Notably, the best model from the Monte Carlo simulations at the inland site was not able to capture the extreme dryness in 2013 and 2014. The SMBM assumes plant wilting point as the lowest level of soil moisture. However, in reality soil moisture declined below wilting point during the extremely dry periods. Under such conditions, soil evaporation may still occur even though plants are senescent or even dead. potentially further compounding the effects of soil drying by bare soil evaporation (Briggs and Shantz 1912). As the model does not distinguish between evaporation and plant transpiration, no independent estimates can be obtained for the two fractions. Nash Sutcliffe Efficiency (NSE) coefficients showed good predictive abilities of the model with high values of 0.63 and 0.7 for the coastal and inland site respectively.

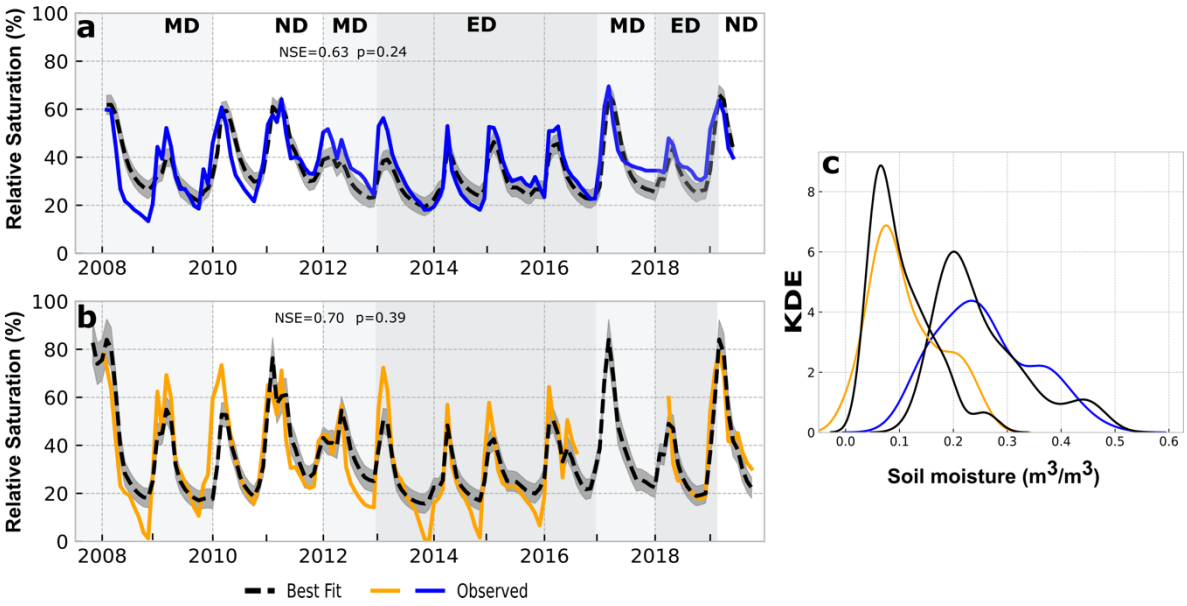

Figure 2.8: SMBM results for the a) coastal and b) inland site. Observed soil moisture is indicated as a solid line (blue-coastal, orange-inland), while simulations are shown as a dashed black line. Grey shading indicates ±1 Standard Deviation based on the output of 1000 Monte Carlo simulations. Grey vertical shading indicates historical non-drought (ND), moderate (MD) and extreme drought (ED) periods. c) KDE curves of observed(black) and simulated (colored) soil moisture confirm model performance.

2.3.4 Soil moisture responses to plausible future drought scenarios

Under historic drought conditions, simulations for both coastal and inland sites reveal a clear seasonal pattern of time below the vegetative stress threshold in the fall, prior to winter rainfall, which by extension represents the senescent periods typical for grasslands in Southern California (Figure 2.9 a, b). The differences in the extent of time below the threshold as well as the minimum saturation levels are visible between sites and can be attributed to differences in soil water holding capacity and aridity. Inland, soil saturation is below the appointed threshold more than half (64%) the simulation time, compared to about 47% at the coastal site. Scenarios A and C noticeably shift soil moisture towards a drier baseline, leading to more extended periods of low saturation and the accumulation of an extreme soil moisture deficit extending over several years (Figure 2.9 c, d, g, h). Under Scenario C, for example, the time below the threshold would increase from the historical simulation by almost

50% at the coastal site and only 25% at the already dry inland site. This suggests that the previously buffered coastal locations would suffer disproportionally more from extended dry periods under more extreme drought, as moisture reaches increasingly low levels previously unseen at this site.

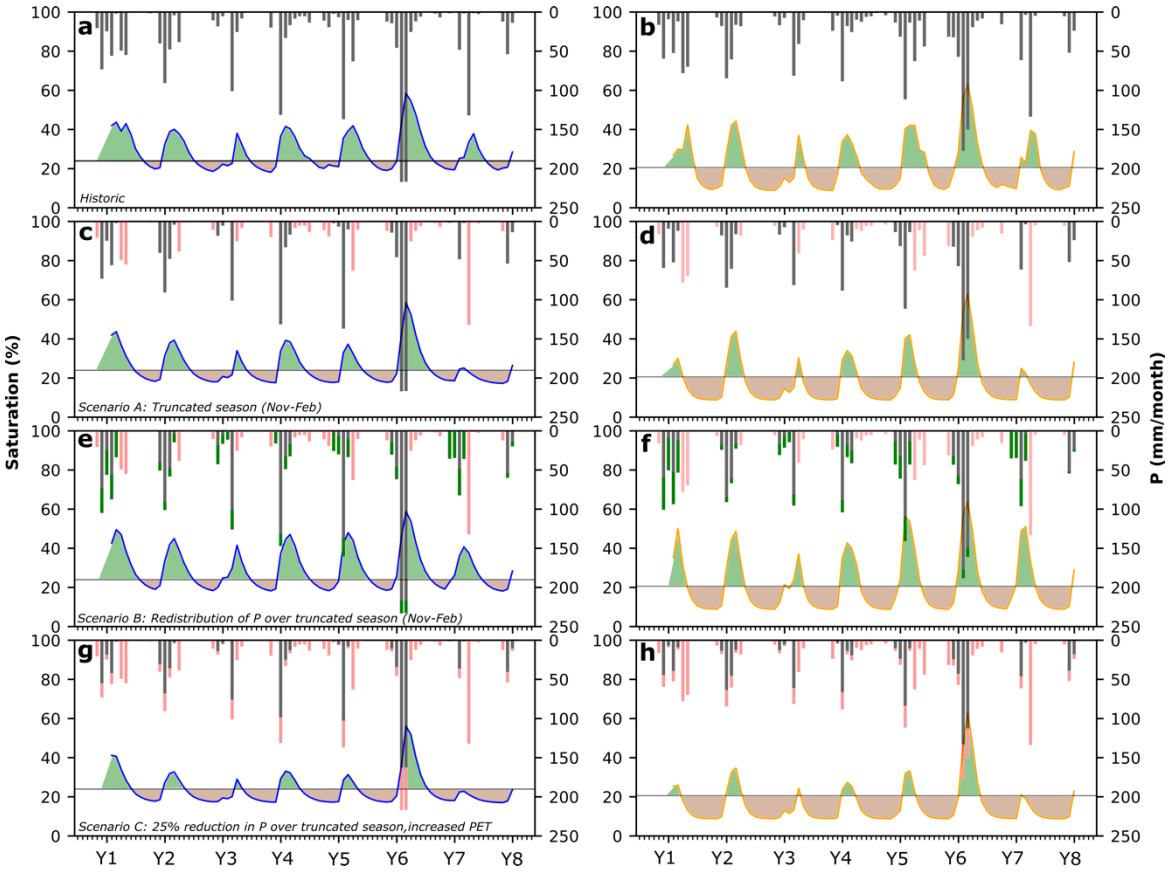

Figure 2.9: Simulations for the coastal and inland site. a) and b) show historic simulations. c) and d) Scenario A showing a truncated rainy season, with ed bars indicating a precipitation loss. e) and f) Scenario B showing a redistribution of annual P over the truncated season, with green bars indicating additional P, while red bars indicate P loss. g) and h) Scenario C showing a truncated season with additional 25% loss of P and an increased evaporative demand equal to a +4°C increase in mean annual temperature. The horizontal line indicates a vegetation stress threshold below which water becomes limiting to plants. Green shading indicates periods of greenness while brown shading highlights periods of senescence.

In contrast, the higher intensity P over a shortened rainy season in Scenario B would actually reduce the amount of time below the stress threshold at the inland site (by 2% or 76 days over the 8-yr simulation), and only increase minimally by 2% at the coastal site (Figure 2.9 e, f). In other words, redistributing the same annual P total into a briefer rainy season seems to mitigate the effects of no spring rains, and also suggests a longer residence time of water in the soil (especially at the coastal site) that persists into the summer. This would allow plants to access legacy soil moisture even after precipitation has stopped and likely support normal plant growth over the season, without any extensive or premature drying. As such, the risk of extensive wildfires would likely be less acute, as plants are not likely to suffer the level of intense and early senescence and drying, as seen in the other scenarios.

In Scenario A, the loss of spring rains, with precipitation limited between November – February would artificially extend the dry period to a total of 8 months of the year (Figure 2.9 c, d), resulting in a loss of ~30% of the annual precipitation. The climate simulations indicate that the loss of spring precipitation pulses in Scenario A seems to have a larger effect on the inland than on the coastal site. While the overall water input is reduced at both sites with a shortening of the rainy season, the amount of water removed through AET would be only minimally reduced (<5%) at the coastal site. However, at the inland site the loss of these cool season events would result in the reduction of AET by 10%, suggesting that the spring precipitation is a more important component of the water balance at semi-arid sites (Figure 2.10 b, e). The lowered moisture holding capacity due to a higher sandy content at the inland site and the more arid climate makes the inland site seemingly less resilient to reduced spring precipitation at the time when plant development is about to start and soil moisture is needed to support seed germination and biomass accumulation.

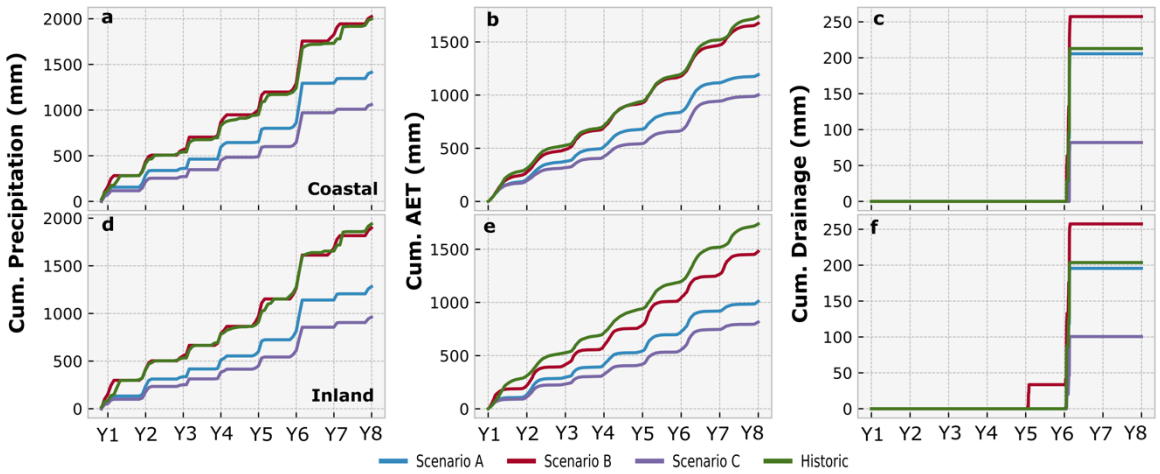

Figure 2.10: Cumulative water balance for the coastal (top panels) and inland (bottom panels) site under the different climate change scenarios. a) and d) cumulative precipitation, b) and e) cumulative evapotranspiration, c) and f) cumulative drainage, which only occurs after reaching a certain threshold of monthly precipitation, where the higher intensity of Scenario B benefits the inland site as additional drainage occurs in Y5.

Further analysis of the water balance suggests that the loss of spring rains seems to have only a minor effect on drainage (i.e. local potential groundwater recharge) at both sites, as drainage totals are only minimally reduced under Scenario A compared to historic values (Figure 2.10 c, f). This suggests that precipitation events large enough to overcome antecedent soil moisture deficits and produce drainage historically only occur during the main winter months (Nov, Dec, Jan, Feb). Hence any precipitation lost by the shortening of the season would not have contributed towards groundwater recharge either way.

At the coastal site, the redistribution of precipitation (Scenario B) seems to have little effect on the percentage of P removed by AET, suggesting a tight coupling of AET to precipitation. At the inland site, however, the fraction of precipitation removed as AET declines by ~10% compared to historical simulations (Figure 2.10 b, e). It appears that higher intensity rain events at the inland site may be large enough to promote deep infiltration and local drainage below the evaporation zone (e.g., in Y5), due to the low water holding capacity of the soils. Rainfall event size and antecedent conditions together are the main control of drainage in the SMBM, with

results suggesting certain rainfall thresholds that need to be overcome on daily and monthly timescales for drainage to occur. Historically a monthly total of >140 mm of precipitation at the inland site is the threshold above which drainage occurs. The historic events in Y6 both exceeded this threshold and thus produced considerable drainage for all simulations, with more than 50% of the incoming precipitation in those months becoming drainage. In contrast, the coastal site requires more precipitation to produce drainage with a monthly threshold >230 mm, suggesting that much more of the annual rainfall is recycled to the atmosphere. On a daily timescale, drainage occurrence at the inland site corresponds to events of >20 mm/d, which produced an additional drainage peak in Y5, while the coastal site requires several days of rainfall between 20 – 55 mm/d to produce drainage. Overall, it is evident that the higher precipitation intensity would contribute towards increasing the overall amount of drainage at both sites (Figure 2.10 c, f), with the added intensity increasing the potential for additional drainage and groundwater recharge at the inland site, despite the extended dry periods.

Under the extreme drought conditions of Scenario C, the effects of increased precipitation loss and heightened ET0 would affect several aspects of the water balance. The reduction of precipitation in conjunction with a shortened season would have a major impact on soil moisture, leading to low levels of saturation at both sites. As less water would be available at both sites, cumulative drainage is reduced by more than 50% compared to the historical simulation (Figure 2.10 c, f) while AET would be reduced at the inland site by up to 5%, due to less water being available to be used by plants. Interestingly, at the coastal site AET exceeds input precipitation by ~6% over the simulation period, reflecting an overall increased drying of these coastal soils under extreme drought.

2.4 Discussion

In light of the progression of climate change in semiarid environments such as Southern California, a better understanding of drought propagation and the climatic drivers of shifts in soil moisture and water availability to grassland vegetation (and correspondingly, to the health and functioning of grassland ecosystems), would enable anticipation of how soil moisture and grassland dynamics might respond to intensified moisture limitations under future scenarios of climate change across the region. Through simple climate scenarios, the combination of increased evaporative demand and decreased precipitation intensity and frequency was explored. The results highlighted the potential for multi-year soil moisture droughts to occur at previously less affected coastal sites as reduced precipitation variability and increase soil drying affect the seasonal distribution of moisture. Such conditions would put a new strain on these ecologically sensitive areas and in future render them potentially unsuitable as climate refugia and habitats for critical threatened and endangered species.

The analysis revealed that winter/spring precipitation deficits, coupled with higher evaporative demand in Southern California, led to temporal shifts in the onset of the dry season, which subsequently incurred increased soil drying in spring and summer. The loss of essential precipitation pulses in spring months generated large soil moisture deficits and induced a faster die-off (browning) of grasses, especially at the inland site. A shift in dry season onset was further explored by simulating soil moisture responses under an even shorter rainy season. The model results suggest that arid sites such as the inland site with low water holding capacities, widespread over the region and more broadly over the Southwest and other Mediterranean climate systems, would become increasingly vulnerable to climate change that favors milder winter and hotter summer temperatures, and decreased precipitation in key months during spring.

Sites with low moisture holding capacities due to sandy soils and more arid climate, appear less resilient to the loss of rain at the time when plant development is about to start, and moisture is needed for seed germination and plant growth. Interestingly, the potential for apparent local groundwater recharge seems to remain

unaffected by the loss of spring rains, suggesting that drainage only occurs during the winter months and surprisingly under prolonged periods of drought there appears potential for local groundwater recharge. A noted caveat of the model results is that parameters such as hydraulic conductivity and infiltration rates are not explicitly considered in the SMBM. Hence, the simulations of soil moisture may underrepresent the exact magnitude of infiltration fluxes and potential recharge contribution. Still, the model was purposefully kept simple to broadly illustrate the sensitivity of soil moisture to climate variability and possible future climate change scenarios.

The explored changes to the seasonal delivery of precipitation would arguably increase the soil moisture drought frequency and magnitude, leading to much earlier senescence of vegetation and widespread desertification of the landscape, while selectively priming the landscape for large and destructive wildfires. Such extreme conditions would suggest that already arid ecosystems might be brought to their physiological limit. Furthermore, climate simulations revealed that the occurrence of extreme events after prolonged periods of drought, as simulated in Scenarios A and B, would provide erstwhile relief to soil moisture, and most likely support considerable green up and production of biomass during that season. However, if climate conditions revert to extreme dryness and minimal precipitation input during subsequent years, soil moisture deficits would increase again to levels unlikely to support the extensive growth from the previous season. Under these conditions the senescent vegetation would turn into large amounts of easily ignitable fuel that, coupled with the dried-out soils, would prime the landscape for extensive wildfires, potentially creating severe chain reactions of extreme events as previously seen during the Montecito fires and mudslides.

Overall, the results from this study can be viewed alongside prior work in the Southwest that suggested chapparal landscapes (Okin et al. 2018) and perennial (C4) grasslands (Gremer et al. 2015) are and will become increasingly prone to the negative impacts from drought. Given how widespread the recent drought was in terms of spatial footprint and temporal length, more frequent occurrences of extreme drought conditions as expected under future climate change and increased emission scenarios could be devastating to perennial grasses and chapparal communities with

larger consequences for entire grassland/shrubland ecosystems over a broad spatial extent (Gremer et al. 2015; Petrie et al. 2015; Okin et al. 2018). As such, the need for action and the implementation of sustainable and adaptive management and mitigation strategies is now greater than ever as the effects of increased precipitation variability and higher temperatures ravage natural grassland habitats.

CHAPTER 3

3 Modelling seasonal vegetation phenology from hydroclimatic drivers for contrasting plant functional groups within drylands of the Southwestern USA

3.1 Introduction

The grassland responses in Southern California to shifts in seasonal precipitation and moisture availability I described in the previous chapter provided an initial illustration of the strong coupling of greenness and phenology to hydroclimate. The shifts in spring and summer precipitation incurred significant shifts in the onset of greenness and annual maximum greenness, which exacerbated the risk of extensive wildfires and degradation of the landscape. While the soil moisture balance model used in this study was able to predict soil moisture dynamics under potential future climate change, it opened up the question of how vegetation responses can be more efficiently predicted in response to varying future climate. From the previous study open questions remain how hydroclimate drives seasonal vegetation phenology patterns in monsoon dominated soil moisture and groundwater dependent dryland plant functional groups and how seasonal phenology changes can be parameterized within an ecohydrological modeling context. This is particularly relevant when exploring questions about how seasonal phenology will respond to climate change.

Since terrestrial vegetation responds to local and regional climate and its expression of the water cycle through distinct phenological events, they are influenced by the seasonal variations in temperature and precipitation (Cleland et al. 2007; Richardson et al. 2013). Plants experience the direct and indirect effects of temperature and precipitation through the timing of leaf-on and leaf-off, as well as the seasonal availability of water in the unsaturated and saturated zone respectively, which drives vegetation productivity and composition (Richardson et al. 2013; Schlaepfer et al. 2017). Phases of green-up, maturity, senescence and dormancy, as well as annual peaks and troughs of greenness define the seasonal phenology as an expression of plant growth and vegetative health in response to hydroclimate forcing. Species-level observations have identified temperature as the main driver of spring

onset in temperate and boreal forests (Hunter and Lechowicz 1992; Hänninen and Kramer 2007; Berra and Gaulton 2021), however the level of climatic controls have been shown to vary between temperate and dry ecosystems (Jolly & Running, 2004; Xin et al., 2015). Particularly in semi-arid ecosystems, seasonal moisture availability is recognized as the primary controlling resource of vegetation growth and functioning (Rodriguez-Iturbe et al. 1999; Rodriguez-Iturbe 2000). The critical link between phenology and climate variability, particularly temperature and precipitation, is considered a powerful indicator of past climate change with observed phenological changes also serving as guidance to predict the causes and consequences of potential future phenological shifts (Diez et al., 2012; Matthews & Mazer, 2016; Menzel et al., 2006; Munson & Long, 2017; Rafferty et al., 2020; White et al., 2009).

Despite the sensitivity of phenology to climate change and observations of vegetation responses to changing climatic conditions, the magnitude and extent of the effects on vegetation phenology for specific plant functional types remain poorly understood (Cleland et al. 2007; Körner and Basler 2010; Richardson et al. 2013). Nevertheless, there is a growing urgency to expand and generalize our understanding of temporal vegetation responses to hydroclimate forcing in different plant biomes, to support a more complete historical understanding of vegetation response to hydroclimate extremes. The true extent of phenological shifts and overall changes to species composition within both groundwater and soil moisture dependent dryland vegetation communities is not yet fully understood, requiring further analysis over a range of spatiotemporal scales (Walker et al. 2012; Gremer et al. 2015; Munson and Long 2017; Schlaepfer et al. 2017). This would also improve the representation of phenology within ecohydrological and phenological modeling, allowing for a better characterization of future climate-phenology interactions and generally creating a more accurate representation of phenology within climate models and global change studies (Peñuelas et al. 2009; Diez et al. 2012; Richardson et al. 2012; Haynes et al. 2019).

Therefore, in this chapter through remotely sensed vegetation information and contemporary hydroclimate data, I aim to explore the linkages between climate variability and phenology of different plant functional types occupying distinct

rooting locations within a dryland ecosystem in SE Arizona on a seasonal scale. In particular, I aim to identify the seasonal phenology patterns by exploring historical climate-phenology relationships and determine key phenological events along a seasonal phenology curve. Finally, I present an empirical modeling approach to estimate synthetic seasonal phenology curves that capture vegetation greenness in response to variable hydroclimate forcing.

3.2 Data & Methods

3.2.1 Study region

Vegetation greenness was sampled through remote sensing at two distinct and complementary areas in SE Arizona, the Walnut Gulch Experimental Watershed and San Pedro Riparian National Conservation Area. The San Pedro and Walnut Gulch are both well studied dryland vegetation environments due to their characteristic hydrology and vegetation dynamics (Renard et al. 2008; Skirvin et al. 2008; Singer and Michaelides 2017; Stromberg et al. 2017; Mayes et al. 2020; Sabathier et al. 2021). The presence of the North American monsoon strongly drives the hydrology of SE Arizona, with annual precipitation ranging between 300 – 400 mm/y, and two-thirds of the annual precipitation and 90% of its runoff delivered during the summer months between July and September (Nichols et al. 2002; Stromberg et al. 2006; Moran et al. 2008).

Based on hydrology and geomorphological characteristics, the San Pedro has been divided into reach types that summarize flow conditions and associated vegetation communities along the river (Stromberg et al. 2006). The major vegetation communities include riparian woodlands on low floodplains, xero-riparian trees and shrubs on river terraces, and grasses and desert shrubs on piedmont surfaces further upland (Makings 2005; Sabathier et al. 2021). The narrow gallery forest along the river channel is primarily populated by obligate phreatophytes such as Fremont cottonwood (*Populus fremontii*) and Goodding's willow (*Salix gooddingii*), which prefer constant access to groundwater and are therefore strongly influenced by variations in connectivity between surface and subsurface water flows (Makings 2005; Stromberg et al. 2017). Bordering the riparian corridor are terraces dominated

by mesquite woodlands (*Prosopis velutina*), which have been observed to be less dependent on groundwater and more flexible in their use of seasonally available water sources, including soil moisture (Snyder and Williams 2000; Stromberg et al. 2017).

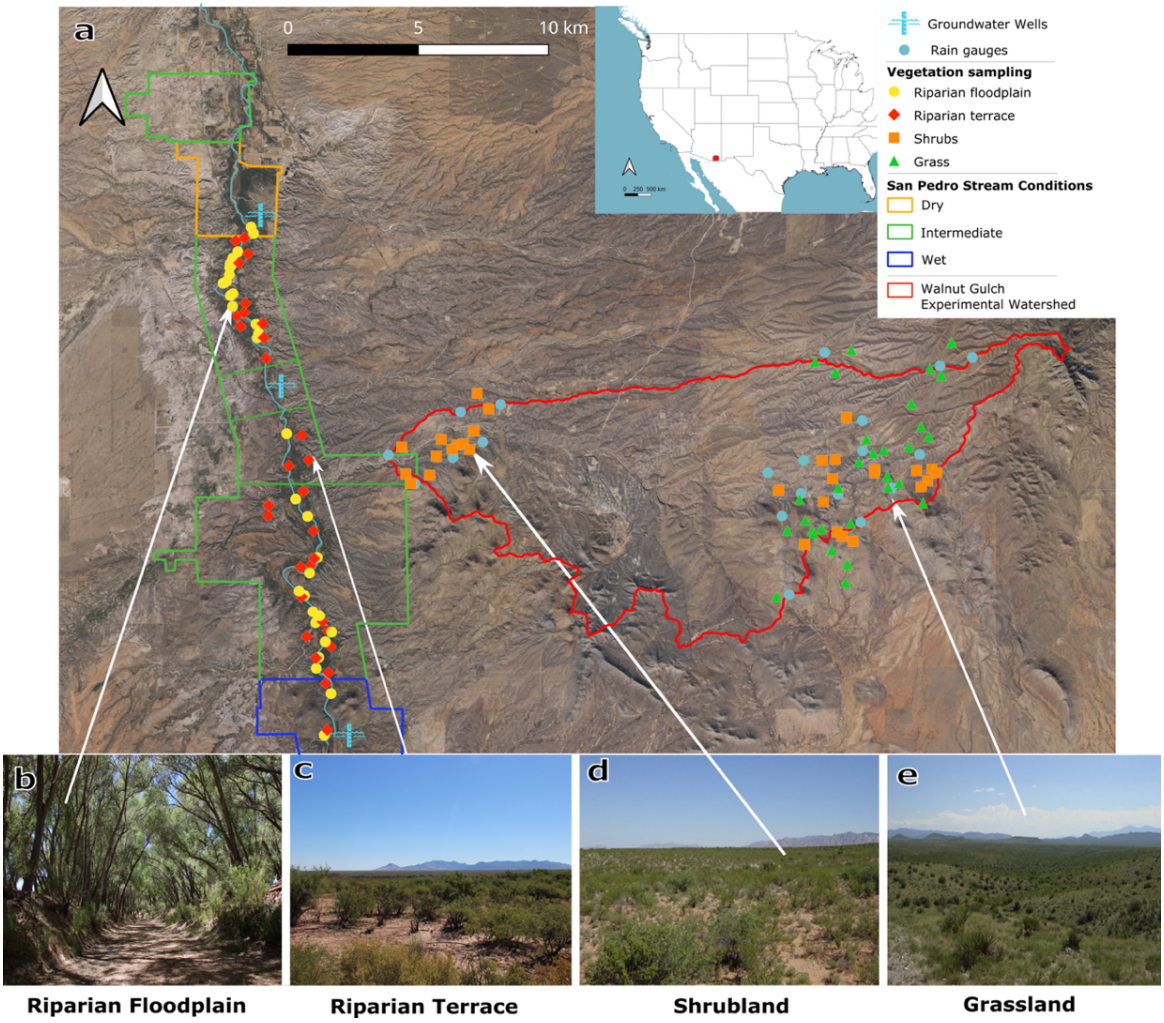

Figure 3.1: Map and outline of the San Pedro Riparian National Conservation Area and Walnut Gulch Experimental Watershed. Vegetation sampling points are colored by biome, with stream flow conditions outlined along the sampling stretch in the SPRNCA. b) Dense cottonwood corridor along the riparian floodplain and c) riparian terrace trees further upland from the channel. d) Shrubs and e) grasses at the WGEW show varying levels of density (Source: https://www.tucson.ars.ag.gov/).

Vegetation from phreatophyte-dominated riparian floodplain and mesquite woodland terraces was sampled longitudinally along a 28-km stretch of the river, which includes wet, intermediate and dry riparian flow reaches, spanning a gradient

from perennial to intermittent flow (Sabathier et al., 2021; Stromberg et al., 2006, 2017). (Figure 3.1 a). The delineation of reaches is based on a riparian assessment model, whereby the riparian zone was divided into 14 homogenous reaches with similar stream flow hydrology and geomorphological traits (Stromberg et al., 2006). Based on vegetation bioindicators, for example species composition and biomass structure, the reaches are classified into three condition classes (dry, intermittent and perennial), which incorporate plant functional groups and structural traits of riparian vegetation, rather than individual species (Stromberg et al., 2006, Lite et al. 2005). This delineation is widely used to differentiate vegetation and hydrological conditions throughout the San Pedro Riparian Area in the context of ecohydrological studies.

At Walnut Gulch, vegetation distribution is dominated by a variety of native and exotic grass (i.e. black grama (*Bauteloua eriopoda (Torr.)*), sideoats grama (*Bouteloua curtipendula*), Lehman lovegrass (*Eragrostis lehmanniana*) and shrub species (i.e. creosote bush (*Larrea tridentata*) tarbush (*Eremophila glabra*), and snakeweed (*Gutierrezia sarothrae*), which comprise the two main structural vegetation types (Figure 3.1 d, e) (Skirvin et al. 2008). Total vegetation cover at Walnut Gulch is generally sparse and highly variable in space, with species distribution and density linked to soil type, aspect, and spatial precipitation variability (Skirvin et al. 2008). Based on these predominant vegetation types four characteristic plant functional groups can be considered (with local analogues) in similar dryland environments: i) semi-arid grasses, ii) semi-arid shrubs, iii) riparian phreatophyte floodplain trees and iv) xeric riparian terrace trees (Figure 3.1 a-d).

3.2.2 Data

3.2.2.1 Hydroclimate

Several datasets of climate variables were downloaded to support the analysis of hydroclimate controls on phenology. Daily precipitation and minimum/maximum air temperature data for the SPRNCA were extracted from the National Oceanic and Atmospheric Administrations (NOAA) Climate Prediction Center's (CPC) Unified Gauge-Based Analysis of Daily Precipitation

(https://psl.noaa.gov/data/gridded/data.cpc.globalprecip.html) and Global Daily Temperature (https://psl.noaa.gov/data/gridded/data.cpc.globaltemp.html). Datasets were generated for the period 1996–2019 with a spatial resolution of 0.5° x 0.5° for grid cells covering the study area along the San Pedro River. At Walnut Gulch, precipitation data were extracted from the Southwest Research Center Data Access Project (https://www.tucson.ars.ag.gov/dap/) for the period between 1994-2019, using only a selection of the available rain gauges (Gauge Nr: 1, 3, 4, 5, 7, 8, 45, 46, 48, 50, 53, 56, 57, 58, 59, 62, 63, 64, 67, 72), which are closest to the vegetation sampling pixels of grass and shrub, and creating a spatial average of daily precipitation (Figure 3.1 a).

Daily potential evapotranspiration was extracted from the hPET dataset (https://data.bris.ac.uk/data/dataset/qb8ujazzda0s2aykkv0oq0ctp). To characterize water availability to phreatophytes, mean daily depth to groundwater (DTG) from the US Geological Survey's National Water Information System (https://waterdata.usgs.gov/az/nwis/) was used, focusing on monitoring wells with the most continuous measurements and longest monitoring periods within the sampling area. Records of several groundwater wells were used (USGS ID: 313738110102901 (GS_SP17), 314511110120601 (GS_SP23) and 314904110125001 (GS_SP27)), located in the wet, intermediate, and dry reaches respectively (Figure 3.1 a). DTG records for GS_SP17 and GS_SP23 contain daily data between 2001-2018, with 80% and 52% of the respective records complete. GS_SP27, being a periodic monitoring well, only has limited observations available between 2007-2010. DTG generally varies among reaches due to local differences in the underlying geology and geomorphology, as well as proximity to tributaries and groundwater pumping sites (Lite and Stromberg 2005b). The time frame of the water year was determined from November 1st until October 31st to best represent the bimodal precipitation regime of this monsoon dominated ecosystem and the associated vegetation dynamics of the region.

3.2.2.2 Soil Adjusted Vegetation Index

To measure how vegetation greenness evolves seasonally and responds to inter-annual variations in climate, SAVI was used as it is considered a suitable metric

in regions with relatively low vegetation cover (Huete 1988). Cloud-free images were extracted from the Landsat 5 Thematic Mapper (TM), and Landsat 8 Operational Land Imager (OLI) / Thermal Infrared Sensor (TIRS), which are available at 30-meter spatial resolution every 16 days. SAVI is generally closely related to NDVI but considered less sensitive to soil brightness. The effects of soil background reflectance in areas where vegetation cover is less dense are accounted for by including a soil brightness correction factor (L) (Huete 1988). SAVI is defined as:

$$SAVI = \frac{(NIR-RED)}{(NIR+RED+L)} * (1 + L) \quad \text{Eq. 3.1}$$

where L is the soil brightness correction factor, commonly set to 0.5, which is considered applicable to suit most land cover types (Huete 1988).

To avoid mixed SAVI signatures of multiple vegetation types at Walnut Gulch, homogenous areas of grasses and shrubs as the dominant vegetation cover type were identified using a map of vegetation classes previously established by Skirvin et al. (2008), as well as aerial imagery from the National Agricultural Imagery Program (NAIP) with a 1 m spatial resolution (https://www.fsa.usda.gov/programs-and-services/aerial-photography/imagery-programs/naip-imagery/index). Adopting a single pixel approach, 30 sampling points were selected in a cloud polygon and SAVI values between 1996-2019 were extracted. Similarly, at the SPRNCA high-resolution NAIP imagery was used to delineate the riparian floodplain and mesquite terraces and sample individual pixels for each plant functional type longitudinally along the 28-km river stretch (Figure 3.1 a).

To obtain the most homogenous signature of vegetation greenness for the riparian floodplain, only pixels in areas where the width of the cottonwood corridor exceeded 30 m were selected. Furthermore, the obtained SAVI data was filtered to include only years with images in June, July and August, as these usually corresponds to the period when riparian vegetation is leafed out and plants exhibit maximum greenness values. First, the sampled pixels were summarized into a spatial median for each reach and plant functional group over the study period. Second, SAVI was resampled to mean monthly values to generate 12 monthly values per year, which were then averaged across years into a seasonal monthly composite. This not only smoothed SAVI

signals, but also removed any issues regarding aligning sampling dates from remote sensing data with climate data of a different temporal resolution. Finally, the seasonal composite was used to characterize the phenology and determine the key phenological events and controls on timing and amplitude of greenness.

3.2.3 Phenological model development

The framework and stepwise approach for the proposed methodology of creating synthetic phenology curves is illustrated in Figure 3.2. To model the key controls of seasonal greenness of different plant functional groups, first the statistical relationships between hydroclimate and remote sensing data were analyzed. Then seasonal composites of all plant functional groups were used to characterize the key phenological events along the seasonal phenology curve, such as maximum greenness and start of green-up. Next, empirical relationships between greenness and a relevant hydroclimate variable were established and used to develop regression models to predict the timing of key phenological events and the amplitude of greenness during each event under variable hydroclimate forcing. Finally continuous seasonal phenology predictions are created using interpolation, which is explained in detail in subsequent sections.

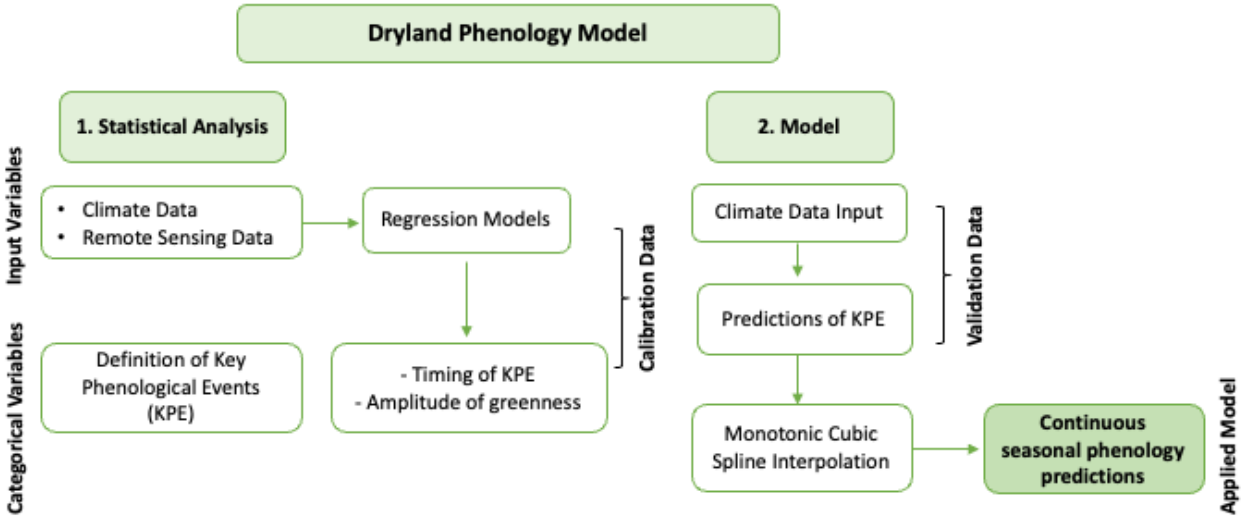

Figure 3.2: Overview of the stepwise approach to create synthetic phenology based on hydroclimate forcing.

3.2.3.1 Key phenological events

For defining the key phenological events for all plant functional groups we considered the shape of the mean seasonal SAVI composites. The seasonal cycle of vegetation in SE Arizona can show a characteristic unimodal or bimodal cycle in response to the local hydroclimate and water availability, and depending on the plant functional type (Jenerette et al., 2010; Notaro et al., 2010). Grasses and shrubs generally displays a bimodal seasonal cycle which can be attributed to seasonal interactions with temperature and precipitation. The plants' sensitivity to soil moisture drives the dual greenness peaks, with a first small seasonal peak in spring in response to a break from cold season dormancy mediated by temperature and the accumulation of cool season precipitation (Notaro et al., 2010). The increased transpiration and declining moisture resources incur a period of low photosynthetic activity before the arrival of the monsoon. This leads to a second larger seasonal peak, after which greenness starts to subsequently decline on a steady downwards trend (Figure 3a). In contrast, the unimodal cycle of riparian trees exhibits a monotonic green-up in spring and a single seasonal peak at the height of the growing season between July and August (Figure 3b) (Notaro et al., 2010; Walker et al., 2014).

We defined several key phenological events based on the two characteristic phenology distributions (unimodal and bimodal), which we use as hinge points to reconstruct the seasonal phenology curves . The start of green-up (SGU) for all plant functional groups is defined as the day of the water year (DOWY) on which the median SAVI shows consistent increase and upwards trend, representing a break in dormancy and the onset of photosynthetic activity. For bimodal plant functional types (Figure 3a) we define a spring greenness peak (POS_1). The next hinge point is the start of the monsoon (SOM) from where a steady increase in greenness leads to the second larger greenness peak at the height of the growing season (POS_2). After this point, plants can be considered to start senescing as greenness starts to steadily decline until the end of the season (EOS), which is estimated as the last day of the water year (DOWY 365). In unimodal vegetation, after green up they only exhibit a single seasonal peak (POS_2), after which senescence sets in and greenness declines towards the end of season. For certain trees, the peak of season shows a broader peak,

indicating a more extended period of maximum greenness and maturity. In this case, an additional hinge point is defined to characterize the start of the peak greenness period (ps).

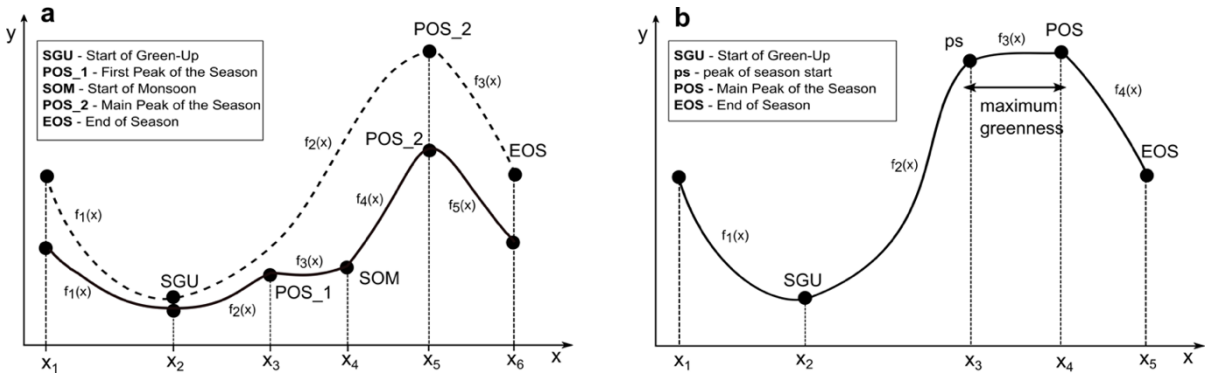

Figure 3.3: Graphic representation of seasonal phenology composites of a) bimodal and b) unimodal phenology cycles with key phenological events indicated along the phenology curve.

Table 3.1: Summary and description of key phenological events for bimodal and unimodal phenology cycles.

Key Phenological Event	*Description*
Bimodal seasonal cycle	
SGU_t	The time when greenness starts to increase
SGU_g	The value of minimum seasonal greenness
POS_1_t	The time of the first seasonal greenness peak
POS_1_g	The value of greenness of the first seasonal greenness peak
SOM_t	The time of the start of the monsoon rains
SOM_g	The value of greenness at the start of the monsoon
POS_t	The timing of peak of season and start of senescence
POS_g	The value of greenness at the second seasonal peak
EOS_g	The value of greenness at the end of the season (DOWY=365)
Unimodal Seasonal Cycle	
SGU_t	The time when greenness starts to increase
SGU_g	The value of minimum seasonal greenness
POS_t	The time of seasonal maximum value of greenness
POS_g	The value of seasonal maximum greenness
ps	The timing of the start of the seasonal peak in floodplain trees

3.2.3.2 Timing of key phenological events

The first step in creating a synthetic phenology is to establish the timing of key phenological events based on greenness responses to hydroclimatic drivers. Once these are determined and greenness values are calculated for them, a synthetic curve can be fit via splines (Figure 3.3). Previous studies observed a close link between the intra-seasonal timing of phenological events and temperature, as well as precipitation. However, temperature is typically considered the main driver of the timing of green-up and senescence (Jolly et al., 2005; Renwick et al., 2019; Richardson et al., 2013), so I adopted that concept here to define the start of the phenological green up (SGU_t) and to indicate the timing of the highest peak of season greenness (POS_2_t). To extract the phenological timing for these two events, I used daily SAVI and temperature data. Given that SAVI is only measured every ~16 days, but temperature is measured daily, I accounted for the time lags between temperature and SAVI by applying the delayed moving average method (Wu et al., 2021) to the timeseries of daily maximum temperature, using 16-day averages to match the temporal resolution of SAVI. Thus, I developed synchronized curves of both SAVI and temperature from which to analyze the timing of phenological metrics (Figure 3.4).

Next, to identify the timing of SGU and POS for all plant functional groups as a function of temperature, I computed derivatives of these time-matched curves by the curve derivative method (Zhang et al., 2004). Then, I quantitatively compared seasonal SAVI derivatives to derivatives of the seasonal cycle of temperature to identify when the slopes of both curves cross zero (change of sign, for example, where a change from negative to positive values indicates an increase in greenness associated with the start of green-up, SGU). The timing of the peak of season (POS_2t) is determined as the date when the SAVI derivative crosses zero again (from positive to negative), indicating the start of a monotonic decline in greenness, defined as the start of senescence (Figure 3.4), which continues until the End of Season (EOS_t) and which is defined as the end of the water year. Note the

relationships between these metrics in derivative space and how they compare to the actual SAVI curves (c.f Figure 3.3 & 3.4)

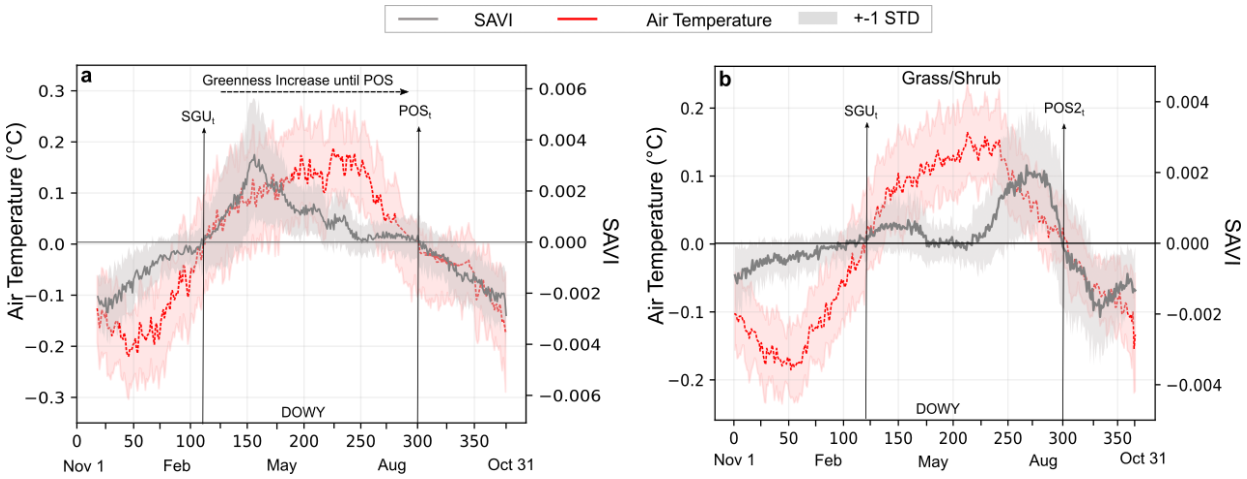

Figure 3.4: Derivatives of mean maximum daily air temperature (red) and mean seasonal composite SAVI (grey) for a) unimodal, b) bimodal phenology curves. The zero crossing points of SAVI and temperature indicate the slope changes from negative to positive (and vice-versa) and determine changes in greenness and seasonal temperature respectively. The dates of the zero crossing points determine the timing of SGU_t and POS_t and POS_2_t for unimodal and bimodal vegetation respectively.. ± 1STD is shown as red and grey shading around the composites of air temperature and SAVI respectively.

These steps can be carried out to determine the timing of phenological events to compute a unimodal synthetic phenology curve, for example that of riparian terrace trees such as mesquite. However, some plant species exhibit more complex phenologies that require additional information. For example, riparian floodplain trees such as cottonwoods in the Southwest USA may have a prolonged, broader peak greenness that needs to be delineated by an additional hinge point, which denotes the start of the period of maximum greenness. The timing of this event is also forced by temperature, as the date when the temperature derivative exhibits maximum change (see Figure 3.4).

For bimodal plant species with two seasonal peaks in greenness, such as for grasses and shrubs, I separately computed the timing for each peak (POS_1 and POS_2, Figure 3.3a). However, for these plant functional groups, I found that the

temperature derivative curve does not help in defining the timing of the first spring peak, which is associated more with antecedent precipitation, and which defines the store of root-zone water availability in these water-limited environments (Jolly et al., 2005; Tang et al., 2015). Because the bimodal phenology is more closely linked to the dual precipitation distribution of the region, I determined the timing of the first peak, POS_1, and the start of the monsoon, SOM, through the derivatives of seasonal precipitation instead of temperature. SOM_t is determined by the onset of the monsoon, as the inflection point with the steepest increase along the cumulative seasonal precipitation composite mean (Figure 3.5 a). POS_1t is determined using the derivative of precipitation at the point where the derivative equals zero, which indicates the end of the spring rains and thus the peak of the first period of green-up (Figure 3.5b).. It should be noted that the role of soil hydraulic properties and soil moisture is not directly within the model. This is due to the availability of direct soil moisture data at the sampling locations.

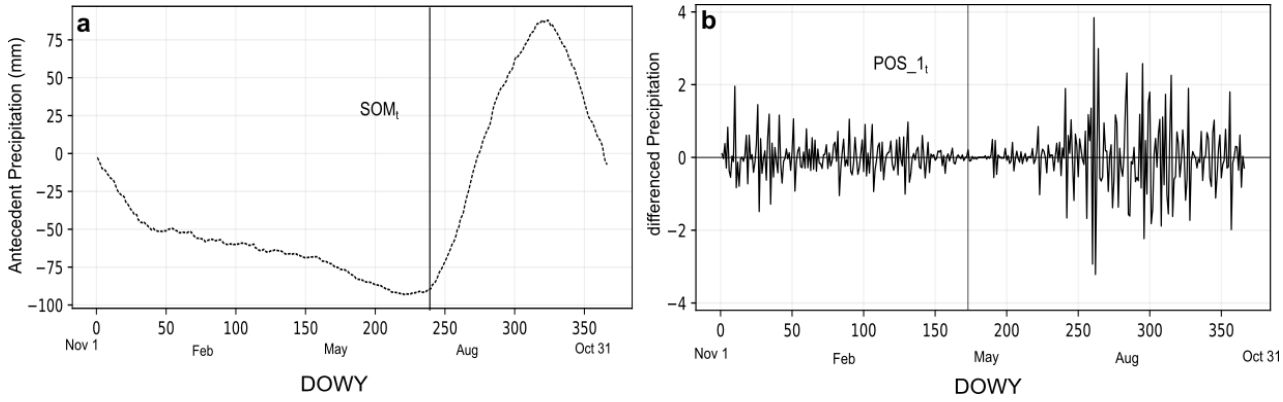

Figure 3.5: a) Differenced cumulative precipitation composite to determine the onset of the monsoon and SOM_T. b) Differenced precipitation to determine the timing of POS_1 at the end of the spring rainy season.

3.2.3.3 Greenness amplitude of key phenological events

To estimate the sensitivity of different hydroclimate variables on greenness amplitude, correlation analyses between hydroclimate and observed SAVI values of key phenological events was performed. Annual values for each phenological event were extracted from the historic SAVI timeseries and correlation strengths were tested between observed SAVI and concurrent and antecedent/lagged hydroclimate

variables. Given the direct sensitivity of shallow rooted soil moisture dependent species, such as grasses and shrubs, to accumulated antecedent precipitation in the soil (Laio et al. 2001; Porporato et al. 2002; D'Odorico et al. 2007), I applied the moving average method to the timeseries of daily precipitation by using multiple 16-day composite periods and testing lags of up to 96 days to account for antecedent rainfall contributions to water availability (Ukkola et al. 2021).

Vegetation dynamics of deeper rooted phreatophyte species such as riparian floodplain trees, are known to respond primarily to variations in water table depth and depend on root zone access to the water table (Laio et al., 2009; Porporato et al., 2002; Stromberg et al., 2017); however, it has also been shown that riparian trees may access water from the upper soil layers to supplement water demands (Snyder and Williams 2000; Singer et al. 2014). The role of soil water availability was reasonably generalized as antecedent available precipitation (aaP = P - PET) and considered a proxy for deeper root zone water availability, for which no measured data was available at the sampling lcoations. Therefore, both depth to groundwater and aaP were analyzed as potential controls on seasonal greenness of riparian floodplain and terrace trees by testing the relationships between SAVI and DTG and between SAVI and aaP. Due to the unimodal phenology cycle in riparian trees, POS was determined as the most responsive phenological event to hydroclimate variations, while SGU and EOS only showed minimal interannual variations. Therefore, normal distributions were created for these events based on observed greenness values to be used for determining synthetic phenology curves.

To account for the differences in DTG of different wells, observed data were normalized to the same range and scale (0-1), irrespective of absolute values. DTG values are expressed as DTG_{norm} and normalized as:

$$DTG_{norm,i}(t) = (dtg_{t,i} - dtg_{i,min})/(dtg_{i,max} - dtg_{i,min}) \quad \text{Eq. 3.2}$$

Based on the functional form of regressions between observed SAVI and the relevant hydroclimate variable for each phenological event, regression models were fitted and calibrated. I used antecedent precipitation for grasses and shrubs and DTG as well as antecedent available precipitation for riparian floodplain and terrace trees. Specifically, they were calibrated to a subset of data using either odd or even years

between 1994-2021 (n = 13 years) and the goodness of fit was assessed using either Pearson's R or Spearman's Rho correlation depending on (non)linearity. For the purposes of creating the most dynamic synthetic phenology curves, the inherent uncertainty in these relationships was considered by introducing a prediction interval (*PI*) around all regression models. The 95% *PI* denotes 95% confidence that this area will contain a new observation of greenness in response to a climate forcing and was defined as:

$$PI\left(y_{pred}\right) = T_{n-m}^{0.0975}\sigma\sqrt{1+\frac{1}{n}+\frac{(x^{*}-\bar{x})^{2}}{\sum_{i=1}^{n}(x_{i}-\bar{x})^{2}}} \qquad \text{Eq. 3.3}$$

where y_{pred} is the predicted value of greenness in response to climate forcing x*, T denotes the 97.5th percentile of the student's t-distribution with n-m degrees of freedom, and σ is the standard deviation of the residuals at the confidence level (Bevington and Robinson 2003). The prediction interval was used as a range for Monte Carlo sampling to create multiple simulations (N=100) of stochastic greenness values that would represent the spatial and temporal variability of observed greenness values in response to hydroclimate forcing at the temporal location of each phenological event.

3.2.3.4 Modeling of synthetic phenology curves

Continuous synthetic phenology curves were created by using the coefficients from the regression models of each phenological event to estimate annual synthetic SAVI values at the timing of a key phenological event in response to hydroclimate forcing. All stochastic simulations of greenness (N=100) for each event were summarized into a sample median. The performance of the regression models and the models' ability to capture greenness responses to variable hydroclimate forcing were evaluated by using the other half of the hydroclimate data, comprising the remaining years between 1994-2021 not used for calibration (n=13 years).

Through monotonic cubic spline interpolation between phenological events of an individual year, piecewise cubic polynomials were fitted between events to create smooth continuous functions which pass through all data points without inducing unwanted oscillations in the fitted curve and ensure monotonicity, thus representing seasonal phenology curves (Wolberg and Alfy 2002). The cubic spline

was fitted at an interval between phenological events, with the number of data points and intervals varying between bimodal (n = 5) and unimodal (n = 3) phenology cycles (see Figure 3.3). In python, the *PchipInterpolator* function was used to automate the process of fitting splines between events for every year. (https://docs.scipy.org/doc/scipy/reference/generated/scipy.interpolate.PchipInterpolator.htm). This function requires 1-D arrays of *x* and *y*, representing time and synthetic SAVI respectively, as well as optional parameters *extrapolate*, which was set to *True.*

The synthetic SAVI timeseries over the validation period were summarized into a seasonal mean composite, which was compared to the observed SAVI composite of each plant functional group. Correlation strength was assessed using Spearman's Rho correlation, while seasonal distributions were compared using the 2-sample Kolmogorov-Smirnov statistic at a significance level of $\alpha = 0.05$. Additionally, to determine whether a phenological model was able to capture the variability of observed SAVI, synthetic greenness values of each key phenological event were assesses through Kruskal-Wallis testing at a significance level of $\alpha = 0.05$. I also evaluated timeseries of mean synthetic and observed values through Nash-Sutcliffe Efficiency (NSE), as well as the coefficient of determination (R^2) to estimate the measure of the variance explained by my phenology model. Overall model performance was deemed adequate if no significant statistical differences between modeled and observed values were detected.

To further test and demonstrate the functionality of the model and explore the potential impacts of climate change on phenology, simple plausible climate change scenarios were created that included simple changes to key hydroclimate variables. Based on climate projections of Southwest precipitation (Anderson et al. 2010; Berg and Hall 2015; Aghakouchak et al. 2018), a simplified scenario of reduced precipitation intensity by 20% during winter/spring (JFMA) as well as during the monsoon (JJAS) was applied, without changing the frequency of events. Furthermore, a reduction of PET by 20% was included to represent the projected rise in evaporative demand due to the overall warming and drying trend. Similarly, groundwater levels in dryland areas are vulnerable to increased warming and drying

((Stromberg and Tiller 1996; Meixner et al. 2016; Kibler et al. 2021; Williams et al. 2022b)). Therefore, a plausible scenario of a lowered water table depth by 0.5m was implemented to explore differential vegetation responses to a deeper water table independently of climate, as a representative of the potential effects of lowered precipitation and increased PET. Furthermore, the effects of temperature shifts and earlier warming were explored, a trend which has been observed to affect vegetation phenology and advance the onset of green-up as well as senescence (Xin et al. 2015; Munson and Long 2017; Warter et al. 2020). The impacts of such changes on vegetation responses were examined for all plant functional groups, comparing mean growing season greenness distributions (March-September) between historic observations and model results through 2-sample Kolmogorov-Smirnov testing.

3.3 Results

3.3.1 Timing of phenological events

A comparison of derivatives of composite SAVI and composite maximum air temperature predicted the timing the start of green-up in riparian floodplain trees in early February (~DOWY 110), while in terrace trees it occurred in early March (~DOWY 125). The timing of the peak of season was similar for trees, occurring around the same time in late August (~DOWY 300), linking the timing of the start of green-up and the peak of season to air temperature. Grasses and shrubs showed similar links between air temperature and SAVI regarding timing of green-up and the peak of season. Green-up in spring occurred in early March (~DOWY 124), while the main summer peak occurred at the end of August (~DOWY 300), correlating well to the seasonal changes in maximum air temperature. The timing of the onset of monsoon generally occurred between mid-June to early July (~DOWY 245) while the first peak of season in shrubs and grasses usually occurred post spring rains and prior to the onset of the early dry season around mid-April (~DOWY 170).

3.3.2 Greenness responses to hydroclimate

Significant correlations were found between maximum greenness of riparian floodplain and terrace trees and DTG as well as antecedent available precipitation (**Error! Reference source not found.**). The groundwater well in the perennial reach is near the river (<20m), with a shallow annual mean DTG of 1.8m and small inter-annual fluctuations (±0.2 m). A significant negative linear relationship could be observed between maximum SAVI and DTG (r= -0.71 for floodplain and r= -0.72 for terrace trees) (**Error! Reference source not found.** e, f). At the same time, there was also a statistically significant positive linear trend between aaP and maximum SAVI present (r=0.91 for floodplain and r=0.82 for terrace trees) (**Error! Reference source not found.** g, h). Overall, the mean annual peak of season greenness values were similar in both riparian floodplain and terrace trees, however a slight upwards trend was visible over the observation period, despite short term dry periods between 2018-2021 (**Error! Reference source not found.** a, b). This trend can likely be attributed to the relatively stable groundwater level and minimal seasonal fluctuations, providing trees with relatively constant access to groundwater to satisfy their transpiration demands despite seasonally limited precipitation and soil moisture. Due to the lack of groundwater observations during these dry years for this well location, this interpretation cannot be fully verified, however previous studies have shown that flow in the perennial reach of the San Pedro river is consistently maintained by the presence of shallow bedrock and a strong connection between the riparian aquifer and the river, thus buffering the effects of short-term dry periods and allowing vegetation to maintain a high level of photosynthetic activity (Stromberg et al. 2006; Baillie et al. 2007; Sabathier et al. 2021).

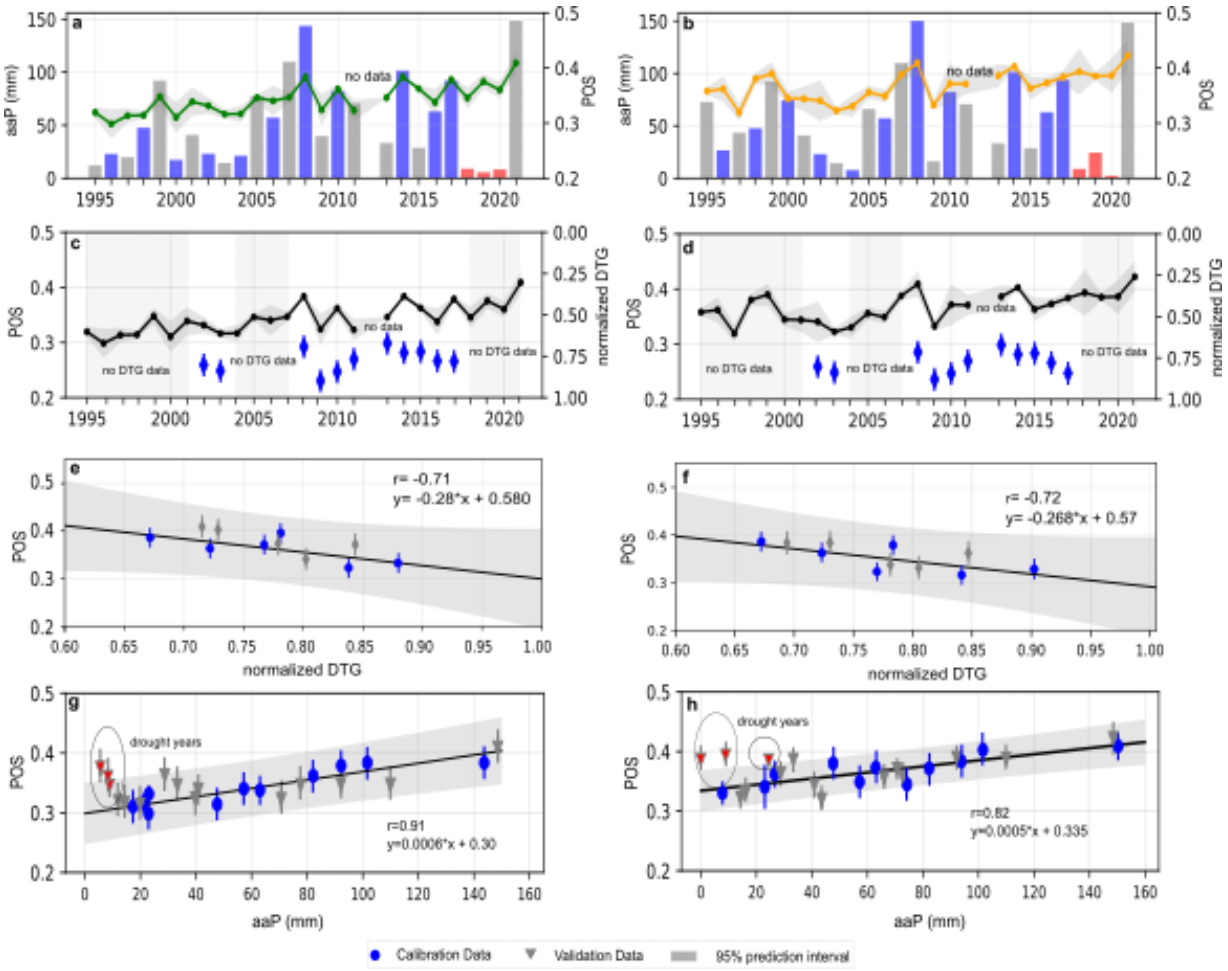

Figure 3.6: Observed median of annual peak of season greenness and antecedent available precipitation (aaP) of a) riparian floodplain and b) riparian terrace trees in a perennial reach of the San Pedro. A data gap exists between 2012-2013. Grey shading around the median greenness indicates the interquartile range over the sampled area. c) and d) Annual peak of season greenness and concurrent normalized DTG with ± 1STD indicated around DTG measurements. e) and f) Regression models between peak of season greenness and normalized DTG. Periods of no DTG records are highlighted in grey. g) and h) Regression relationship between annual peak of season and aaP, with drought years indicated in red (2018-2021). Grey shading around all regression models denotes the 95% prediction interval, while different symbols indicate calibration and validation data.

Overall, the presence of significant relationships to two different water sources would makes sense, as riparian forest sites have been observed to also use shallow soil water during the rainy season (Snyder and Williams 2000). At the intermediate reach, I found the same significant relationships between the peak of season and depth to groundwater (r= -0.75 and r=-0.81) as well as antecedent available precipitation (r= 0.72 for floodplain and r=0.73 for terrace trees) (Figure 3.7 Figure 3.7a-b). The water table in this reach was moderately shallow with a mean annual depth of 2.8 m and larger interannual fluctuations than in the perennial reach (± 0.9m). Ultimately, I only used the strong linear relationship between DTG and the peak of season in the perennial reach to establish the synthetic phenology curves, as DTG is the more direct measure of vegetation greenness in dense, mature groundwater-dependent riparian ecosystems. However, where groundwater data are unavailable, I used antecedent available precipitation as a proxy to force greenness responses.

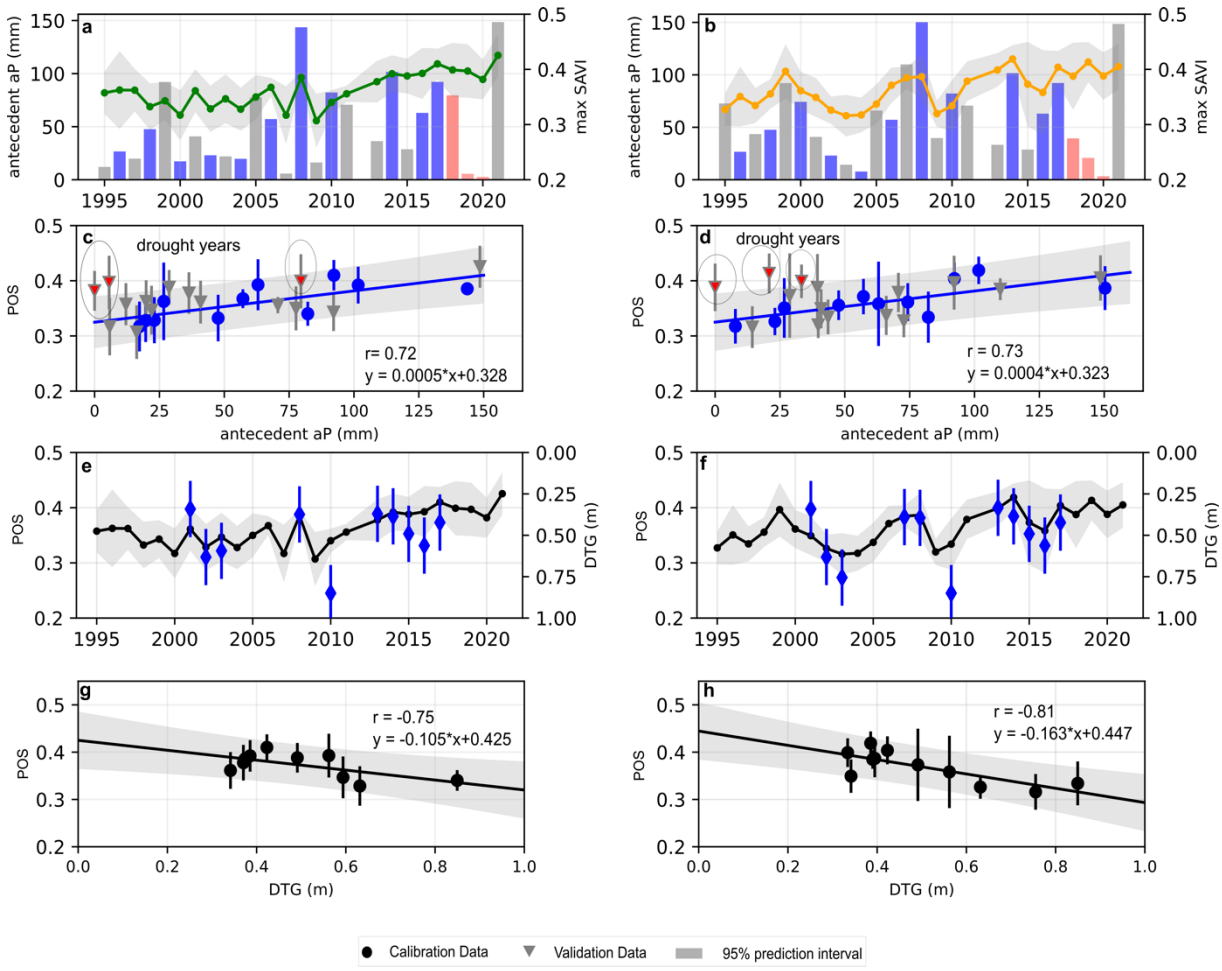

Figure 3.7: Regression relationships for the intermediate reach of the San Pedro. a) and b) Median maximum SAVI and aaP, c) and d) Regression model for max SAVI and aaP c) and d) Mean maximum SAVI and DTG, g) and h) Regression relationship between max SAVI and DTG. Symbols denote calibration and validation data. The 95% prediction interval is indicated as grey shading around the mean model fit.

In grasses and shrubs, the second larger peak of season showed visibly larger interannual variations than in riparian trees, due the strong link to recent precipitation and the dual precipitation cycle of the region (Figure 3.8). Mean values of greenness were similar in grasses and shrubs (0.22 and 0.20, ±0.05 respectively) and showed a strong variability in response to interannual precipitation differences (Figure 3.8 a, b). More specifically, lower greenness values can be seen in years of lower antecedent moisture and weaker monsoon (< 50mm), such as in 2003 and 2004, during which >50% of Arizona was under extreme drought, as well as during summer 2020, which

was an exceptional drought year throughout the Southwestern US (U.S. Drought Monitor, https://droughtmonitor.unl.edu/DmData/TimeSeries.aspx). The highest greenness value during the second larger peak of season was observed in response to larger monsoon totals such as in 1999 and 2000 (> 140mm) as well as in 2017, which had a particularly strong monsoon (>200mm). Overall, greenness at the peak of the season in summer was significantly related to antecedent monsoon precipitation of the previous month (r= 0.86 grasses; r= 0.88 shrubs, Figure 3.8 e, f).

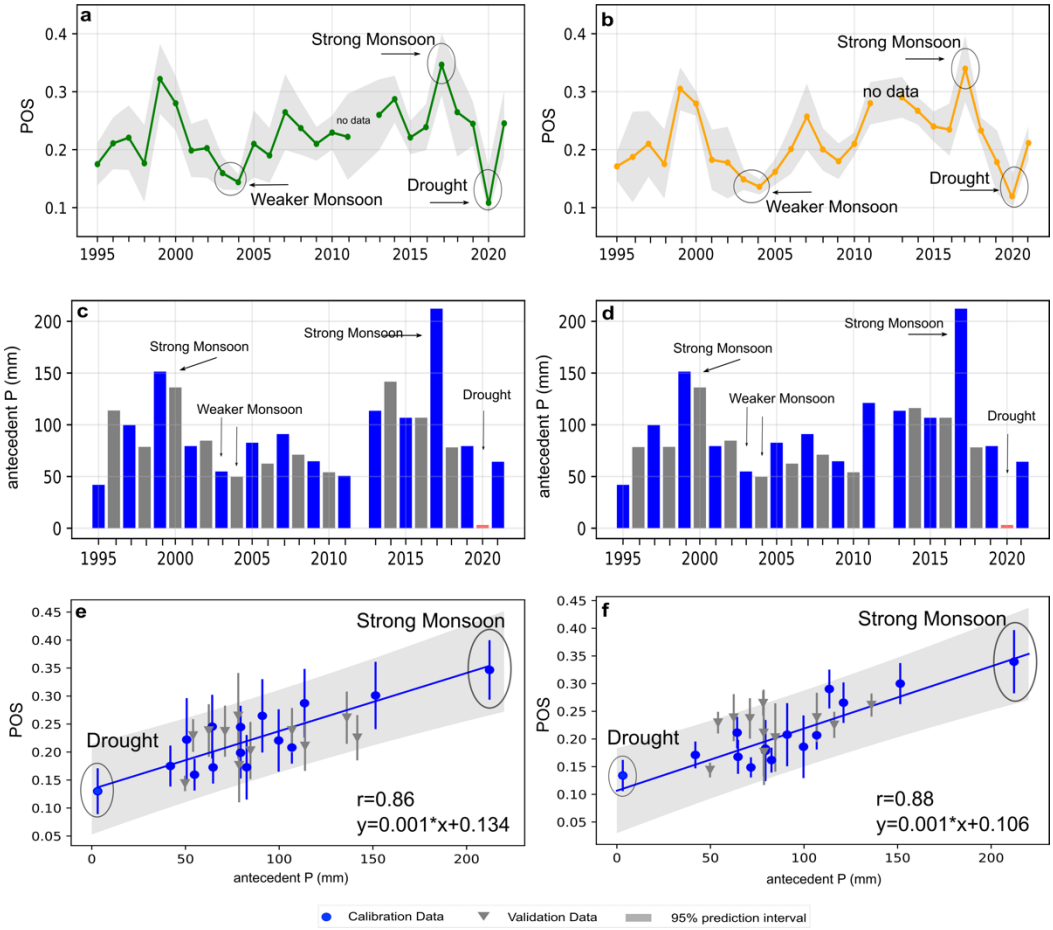

Figure 3.8: Mean SAVI of greenness at the peak of season in summer for a) grasses and b) shrubs. c) and d) mean antecedent precipitation. Grey shading in a) and b) indicates the interquartile range across all available sampling pixels of observed SAVI. A data gap exists between 2012 and part of 2013, where no SAVI data was available. e) and f) Regression models between greenness during the peak of season and antecedent precipitation. Calibration and validation data are indicated with different symbols and the 95% prediction interval is indicated as grey shading around the mean fit.

Antecedent precipitation was the most significant variable also for other key phenological events. The spring peak of season for grass and shrubs was significantly related to accumulated moisture from weak synoptic rain events during the cool season (Figure 3.9 a, b), while greenness prior to the start of the monsoon correlated to the limited precipitation during the early summer dry period, during which time only limited increases in greenness occurred (Figure 3.9 c, d). Finally, greenness at the end of the season was most significantly related to antecedent precipitation from late monsoon and early autumn precipitation (Figure 3.9 e, f).

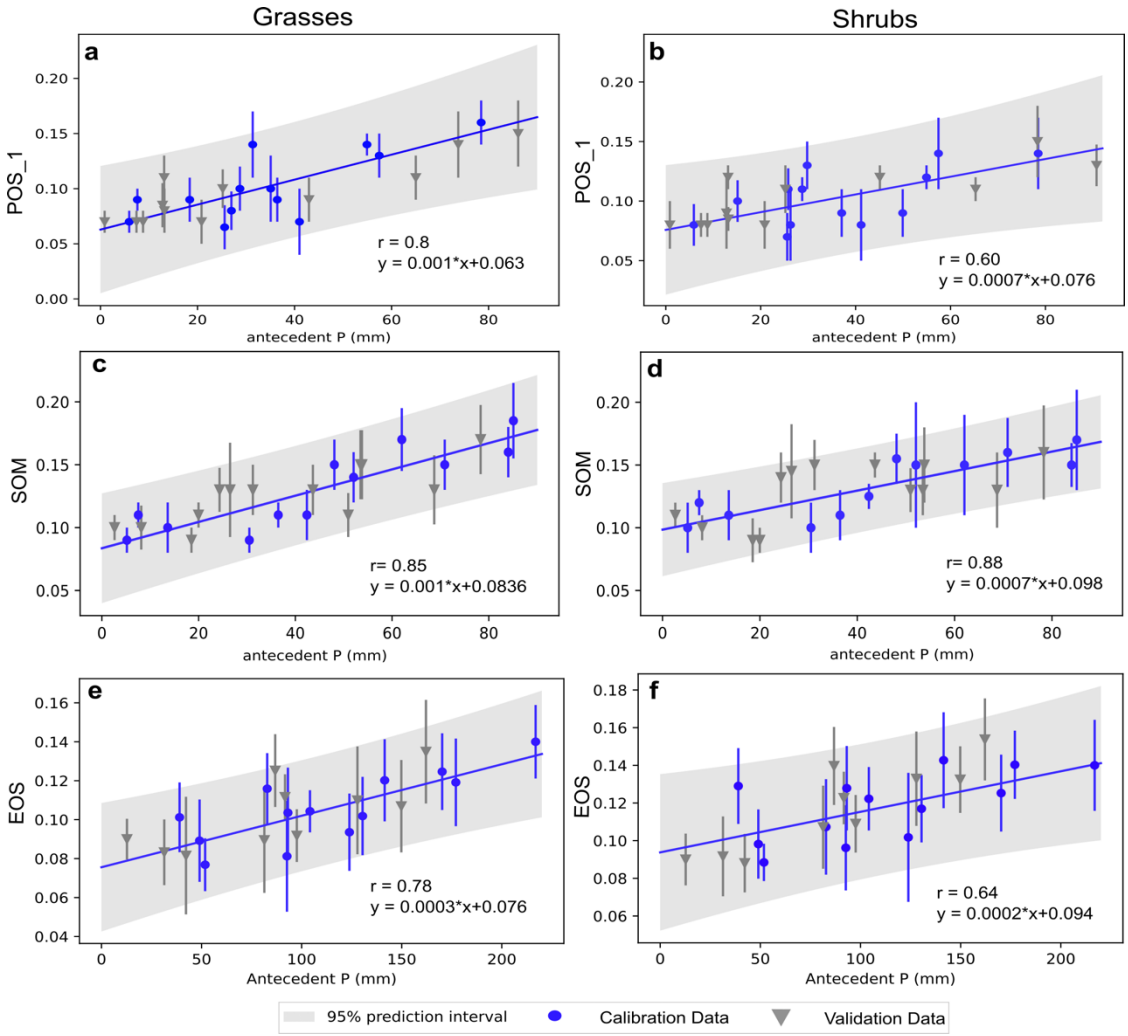

Figure 3.9: Regression relationships for greenness during a) and b) the first peak in spring, c) and d) prior to the star of monsoon, and e) and f) at the end of the season for grasses and shrubs respectively. Symbols denote calibration and validation datasets with grey shading around the mean model fit indicating the 95% prediction interval.

3.3.3 Synthetic phenology

Modelled greenness values for riparian floodplain and terrace trees at the peak of season were forced by DTG and showed no statistically significant difference to observed values (p=0.81, ks =0.3; p=0.62, ks =0.25). Similarly, values at the start of green-up were also not significantly different (p=0.07, ks =0.24; p=0.83, ks =0.06) (Figure 3.10 a, b). The model showed strong predictive abilities, with a Nash-Sutcliffe efficiency of 0.94 for riparian floodplain and terrace trees between modelled and observed timeseries (Figure 3.10 c, d). Median composite values showed strong correlation with observed values, with the model capturing well the interannual variations in greenness in response to variable DTG (r = 0.92 riparian corridor, r = 0.96 terrace trees), and no significant differences between the distributions of mean seasonal modelled and observed composites (p=0.72, ks =0.2; p=0.83, ks =0.2) (Figure 3.10 inset).

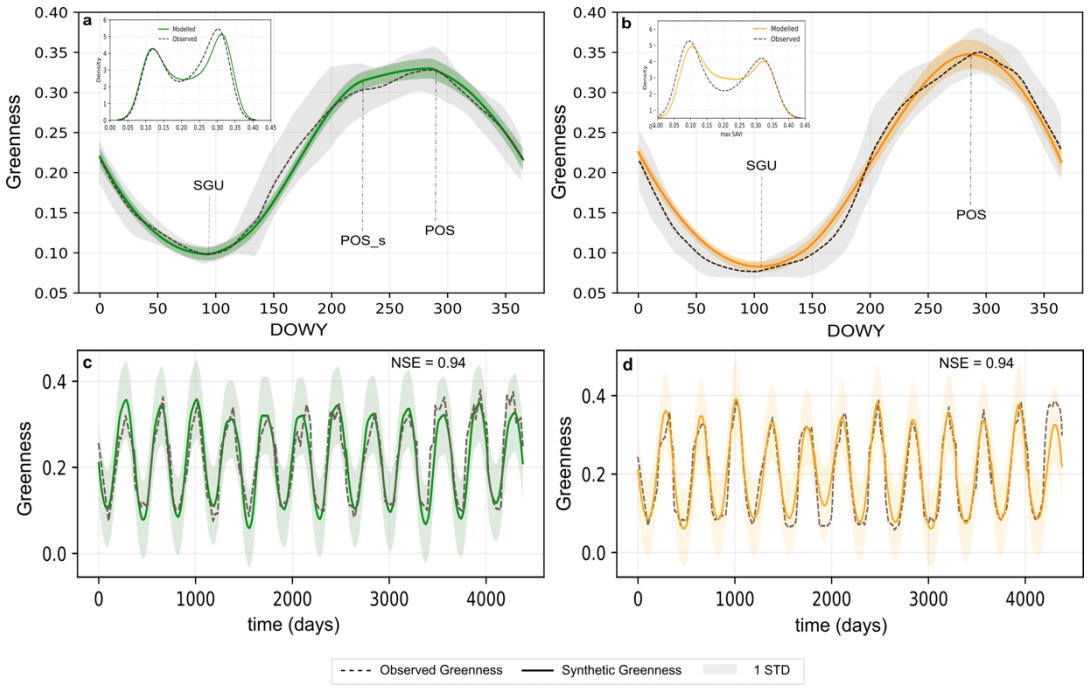

Figure 3.10: Seasonal composite of modelled (colored) and observed (grey) greenness for a) riparian floodplain (green) and b) riparian terrace trees (orange) against observed composites. Distributions of observed and modelled greenness are shown in the inset. c) and d) Timeseries of observed and modelled greenness over the validation period. ±1 STD is shown as colored or grey shading around the modelled and observed composite respectively.

In grasses and shrubs, modelled values of greenness during the spring peak, forced by antecedent precipitation, showed no statistically significant difference to observed greenness (p = 0.6, ks = 0.28; p = 0.89, ks = 0.02). The timing of the start of the monsoon was accurately captured and greenness values showed no significant differences to observations (p = 0.93, ks =0.006; p=0.81, ks = 0.06), Modelled greenness also showed similar interannual variability in response to variable precipitation totals during the early summer dry period (Figure 3.11 a,b). Modelled greenness values during the larger peak of season in summer showed interannual variations in response to variable monsoon totals within the historic range. Annual modelled greenness values during the larger peak of season in summer showed no significant differences to observed values (p = 0.62, ks= 0.25; p = 0.9, ks = 0.01).

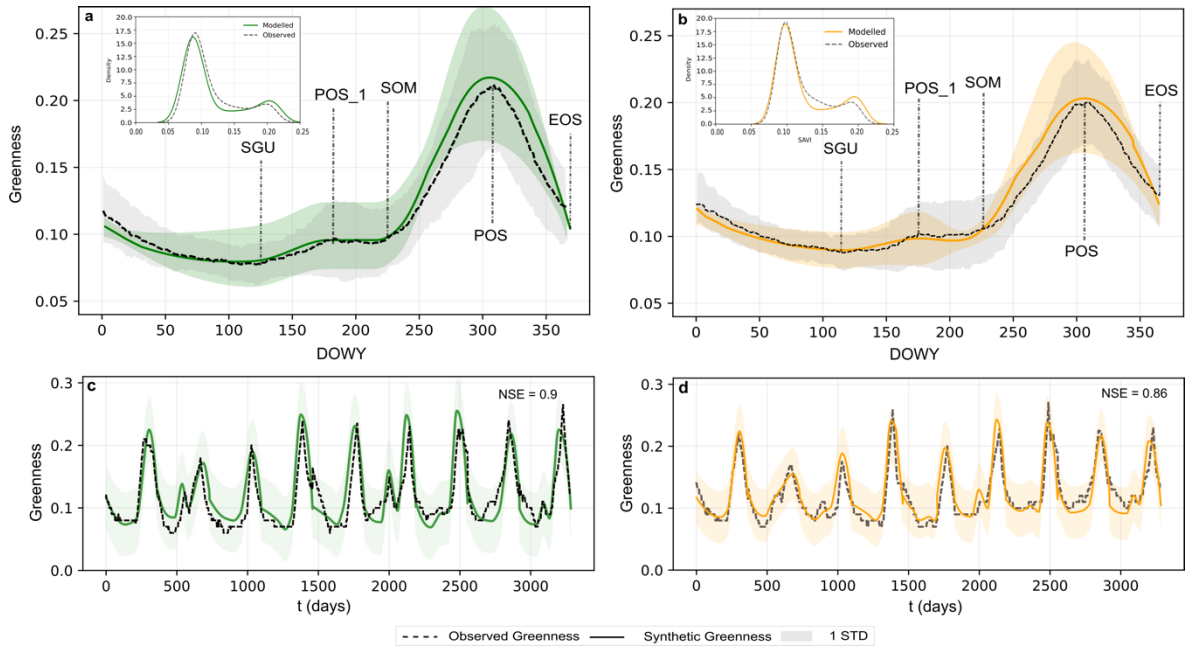

Figure 3.11: Seasonal composites of modelled (colored) and observed (grey) greenness for a) grasses (green) and b) shrubs (orange) against the historic composite (grey). Distribution of modelled and observed greenness shown in the inset. c) and d) Timeseries of synthetic (colored) and observed (grey) greenness. ±1 STD is indicated as shading around the composites and the modelled timeseries.

Model performance was confirmed with modelled and observed composite medians showing no statistically significant differences for grasses and shrubs, as well as a strong overall correlation between observed and synthetic composites

(r= 0.81 grasses; r = 0.77 shrubs). Accepatable predictive power was confirmed through high Nash-Sutcliffe efficiency coefficients (NSE = 0.9 grass;NSE = 0.86 shrubs) (Figure 3.11 c, d). Table 3.2 contains a summary of goodness-of-fit statistics for all key phenological events and plant functional groups, which were compared through Kolmogorov-Smirnov testing.

Table 3.2: Summary of goodness of fit statistics between synthetic and observed greenness for all plant functional group.

	Rip. Floodplain		*Rip. Terrace*		*Grass*		*Shrubs*	
	p	ks	p	ks	p	ks	p	ks
SGU_G	0.07	0.24	0.83	0.06	0.51	0.41	0.29	0.19
POS_1_G			0.6	0.28	0.89	0.02		
SOM_G			0.93	0.006	0.81	0.06		
POS_G	0.85	0.3	0.62	0.25	0.9	0.01	0.58	0.3
EOS_G			0.2	0.8	0.16	1.9		
Composite	0.71	0.2	0.12	0.22	0.21	0.2	0.83	0.2

3.3.4 Phenological responses to plausible future climate change scenarios

In riparian trees a drop in DTG of 0.5m led to a significant reduction in annual greenness values during the peak of season of approximately 17% in riparian floodplain and 13% in riparian terrace trees (p=0.02, ks =0.57; p= 0.02, ks =0.6, respectively) (Figure 3.12 c,d). Composite means of greenness further highlight the effects of shifted temperature, whereby an early onset of the start of green-up and the peak of season is visible. The shift towards an earlier peak of season can be considered as a two-way effect on seasonal greenness, as groundwater may still be at its seasonal low level, prior to the onset of the monsoon and increase in baseflow, thus resulting in a lower greenness value. Growing season distributions show significant differences for riparian floodplain and terrace trees (p=<0.05, ks =0.37; p = <0.05, ks =0.32, respectively), highlighting the shift towards lower greenness values at the peak of season (Figure 3.12 c, d, inset).

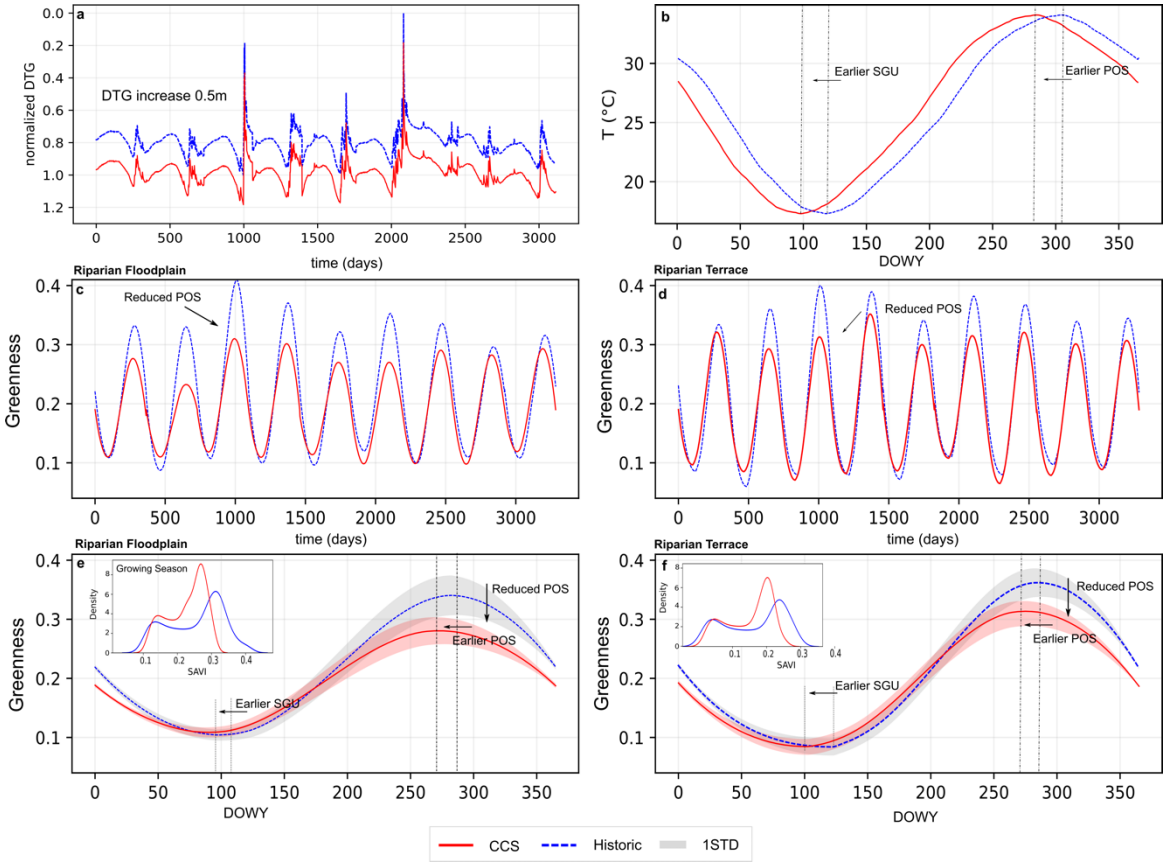

Figure 3.12: Observed (blue) and modelled (red) greenness for riparian floodplain and terrace trees underclimate change scenarios of a) a deeper water table and b) shifted seasonal temperature. c) Modelled timeseries of greenness of riparian floodplain and d) riparian terrace trees show a reduction in annual peak greenness values in response to lower DTG. e) and f) Composite greenness means further highlight the temporal shift towards earlier green-up and peak greenness, while the shift towards lower peak greenness can be seen throughout the growing season distributions (inset). Grey shading around the composite means indicates ±1 STD.

In grasses and shrubs, a 20% reduction in monsoon precipitation was sufficiently large to result in a significant decrease in greenness during the peak of season by 15% in grass and 13% in shrubs (p= 0.03, ks =0.67; p=0.03, ks= 0.66, respectively). Similarly, the reduced spring precipitation resulted in more muted green-up in spring (Figure 3.13 c, d). The seasonal composite mean highlights the effects on seasonal phenology patterns, showing the loss of a clear spring green-up peak and shift towards a more prolonged period of senescence during spring, while the shift in temperature resulted in an earlier timing of the start of green-up and the

peak of season (Figure 3.13 e, f). Growing season greenness between March and September showed strong correlation to reduced antecedent precipitation (r=0.77 for grass and r=0.81 for shrubs) and a significant difference between historic and observed (p = <0.05, ks =0.18 for grass; p= <0.05, ks = 0.17 for shrubs), with a clear trend towards lower greenness at the peak of season and an increased frequency of lower greenness values in spring and summer (Figure 3.13 e, f inset).

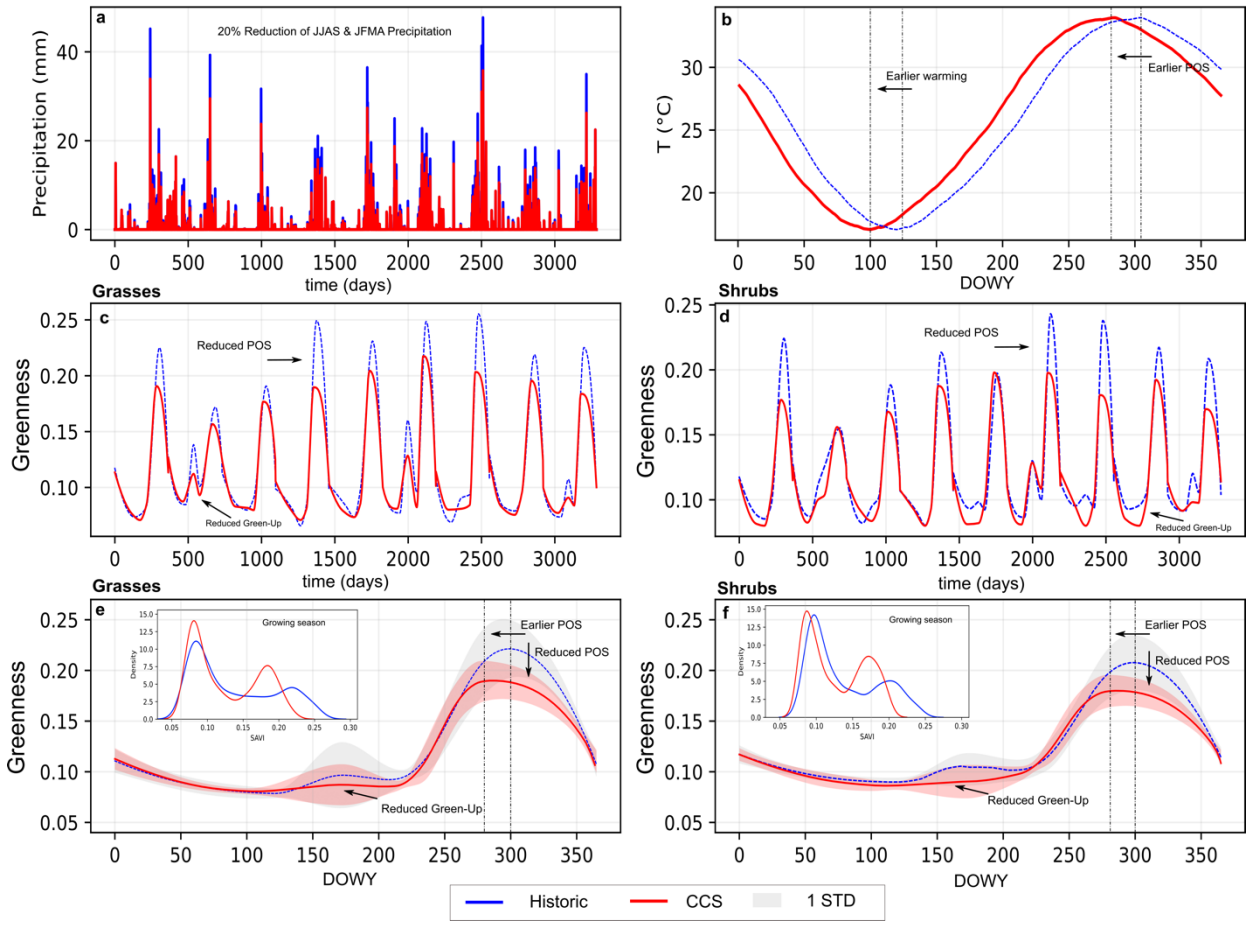

Figure 3.13: Modelled (red) and observed (blue) greenness for grasses and shrubs under plausible scenarios of a) reduced monsoon (JJAS) and spring (JFMA) precipitation by 20% and b) shifted seasonal temperature dynamics. c) and d) Timeseries of historical and modelled greenness show a reduction of greenness during the peak of season as well as lowered green-up in spring. e) and f) Seasonal composite means show the effects of reduced precipitation on phenology and and timing of phenological events. Inset: Growing season distributions (March-Sept) show a shift towards lowered peak of season in the summer and increasing frequency of low greenness.

3.4 Discussion

In the context of shifting phenology due warming temperatures, there is a need to prioritize high-resolution temporal and spatial analyses of climate drivers on plant phenology, to improve our understanding of what might be expected in the future (Ganguly et al., 2010; Moon et al., 2021; Zhang et al., 2003). The mechanisms of bimodal seasonal phenology cycles have previously been explored in regions where the North American monsoon dominates, however there is remaining uncertainty associated with the complex ecohydrological relationships in arid and semiarid environments throughout the Southwest USA. The results have illustrated the complex relationships between observed vegetation greenness and different hydroclimate drivers and their potential to be explored within an empirical modeling framework. Such modeling capabilities open up avenues for exploring climate-phenology feedbacks under future climate change scenarios and support the proactive development of appropriate adaptation strategies to mitigate the effects of warming temperatures, increased precipitation variability, and declining groundwater (Joyce et al. 2013; Polley et al. 2013).

While individual drought years (e.g., 2020) had a relatively strong effect on grasses and shrubs (Figure 3.8 a, b), riparian trees remained apparently unaffected. This can be most likely attributed to the relatively stable influent regional groundwater, buffering such short-term drought periods. Considering, however, the effects of a climatic shift that would lead to a recession of the water table and associated temporal shifts in the timing of green-up, on greenness responses in riparian floodplain and terrace trees; significant changes to annual greenness and the timing of phenological events can be expected. Subsequently, any associated changes to groundwater-flow patterns due to increased precipitation variability, may propagate into overall reduced stream flow within perennial reaches and incur shifts within perennial systems towards more intermittent flow conditions. Such changes to the seasonal availability and overall access of water, would have far reaching implications for the health and survival of many riparian species that depend on continuous access to shallow groundwater. As such, shifts from dense riparian vegetation towards shrubbier more drought tolerant species can be expected as plants

are unable to endure extended peak physiological stress due to groundwater becoming increasingly inaccessible or unreliable.

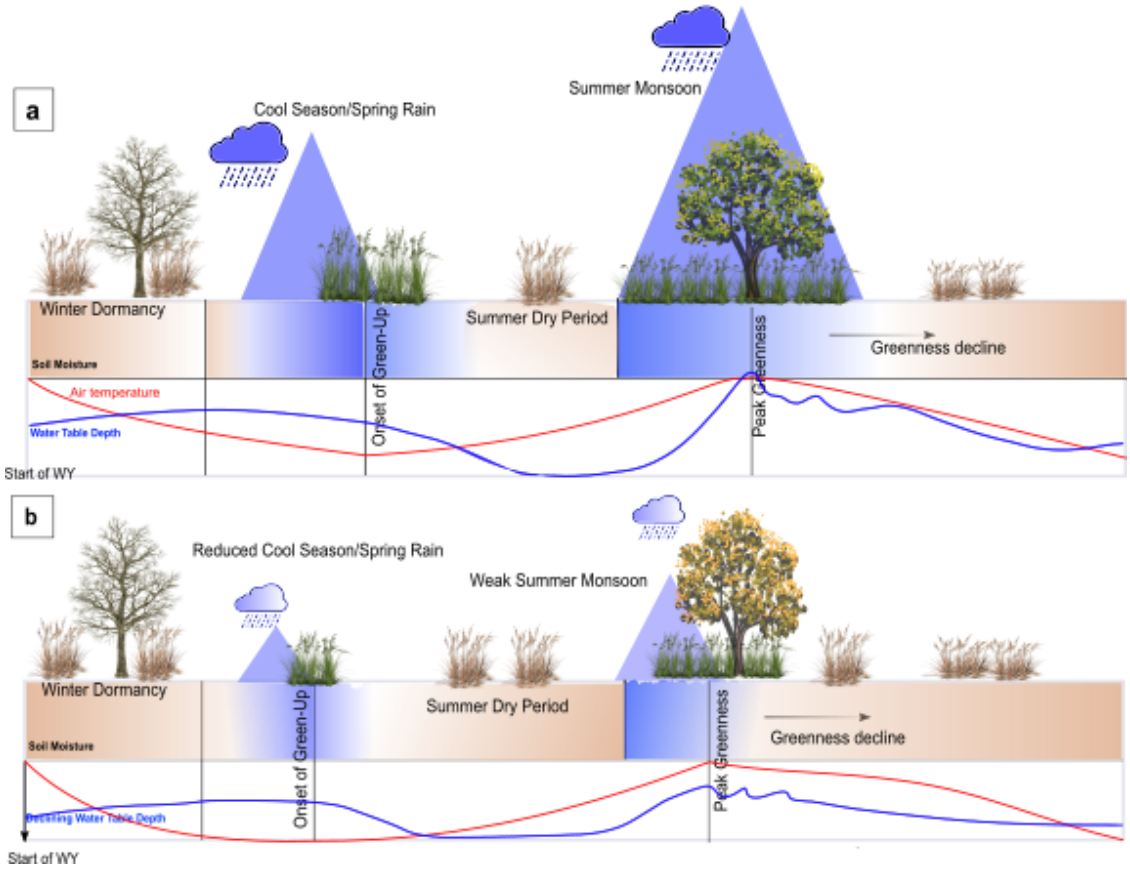

Figure 3.14: Conceptual model of the main hydroclimate controls on dryland vegetation and associated vegetation responses under a) observed conditions and b) potentially drier conditions including reduced seasonal precipitation, lower depth to groundwater and earlier warming temperatures.

Based on the simulations of greenness responses to lower DTG, the results indicate that climate-change induced groundwater decline, associated with shifts in temperature, are a primary threat to the health and survival of riparian woodlands, leading to declining greenness and a decoupling of seasonal green-up and water availability. Still, a major caveat to these simulations is that groundwater decline likely occurs over a more extended time period and changes to vegetation would be more gradual. Nevertheless, water tables have been declining more rapidly, with recession rates exceeding 0.5m/yr, leading to severe forest die-off, reduced greenness

and widespread drought responses in riparian woodlands (Kibler et al. 2021; Williams et al. 2022b),

By disaggregating phenological responses of grasses and shrubs into individual events and quantifying the seasonal and interannual variations, I gained a more detailed understanding about the precipitation-phenology relationships for grass and shrub plant functional groups and their potential vulnerability to future climate change. Simulations of simple climate change scenarios showed that a reduction of spring and monsoon totals could inherently alter phenological patterns and seasonal greenness responses (Figure 3.14). I observed similar patterns from the soil moisture perspective at two distinct grassland sites in Southern California (Chapter 2). The contrasting precipitation regimes between California and Southeastern Arizona revealed that phenology responses can be highly variable for soil moisture dependent species, which can result in distinct seasonal phenology curves and temporal trends of green-up and peak greenness. While greenness in grasses in California strongly depended on cool season precipitation to supply moisture for the spring green-up, grasses in SE Arizona were strongly tied to the bimodal precipitation regime. In both environments, I found that any changes to the delivery of precipitation (i.e. timing and amount) and associated seasonal moisture availability would dampen the seasonal phenology signal, as reduced spring precipitation or weaker monsoons drive a brown wave of grassland responses. Over multiple years, this can lead up to the loss of a clearly detectable phenological signal.

Notably, model simulations suggest that the combination of earlier green-up and limited moisture during the initial vegetation surge would most likely lead to increasingly unfavorable conditions for native vegetation communities. Particularly in semi-arid environments, this would further propagate the conversion of native shrublands into invasive annual grasslands, which are better suited to the increasingly dry conditions. The immediate implications of soil drying, and prolonged senescence and early browning further observed in grasslands of SE Arizona as well as California, extend onto increased fire activity and the availability of easily ignitable fuel. This raises the potential of recurrent wildfires of increasing extent and intensity

in grassland ecosystems across the entire arid Southwestern U.S (Westerling et al. 2006; Westerling and Bryant 2007; Abatzoglou and Kolden 2011).

The results have several implications for understanding and modeling climate-phenology interactions. My findings provide insight into differential vegetation responses of various plant functional groups to hydroclimate and outline an approach for including vegetation phenology models into other existing ecosystem models, which might currently lack a dynamic parameterization of phenology. Especially in dryland riparian environments, improved water balance estimations have recently emerged through refined modeling frameworks (Quichimbo et al., 2021), which consider all aspects of the dryland water balance. However, they mostly include simplified, static prescriptions of vegetation, which do not account for vegetation responses to climate variability. The novelty of the phenology model I developed thus lies in the explicit link between hydroclimate and phenology, which provides a more dynamic representation of greenness responses cognizant of seasonal dynamics (i.e. green and senescent periods) as well as changing atmospheric conditions.

While model simulations provided estimates of the control of seasonal water availability on vegetation greenness and seasonal dynamics, a major caveat to the configuration of the phenology model is that the phenology-hydroclimate interactions are based on empirical relationships, which leaves important feedbacks in the critical zone and between the land surface and atmosphere largely unrepresented. In the current configuration, the model hinges on long-term observational climate data to establish statistical hydroclimate-phenology relationships. To an extent, this excludes the control of other important biochemical factors such as daylength, photoperiod, nutrient availability, and stomatal activity, as well as other bioclimatic variables such as growing degree days or winter chilling. Furthermore, the use of soil moisture data and inclusion of soil hydrological processes, instead of precipitation, would be more representative in delineating climate-vegetation interactions for shallow rooted plant functional groups. Distilling the interactions and control of the water, carbon and energy cycle on phenology lies the crux of developing simple dynamic phenology models, as these parameters are frequently limited by data availability and often

require exact prescriptions of values which are often difficult to measure over large temporal and spatial scales (Richardson et al. 2012; Moon et al. 2021).

Still, predicting the sensitivity of phenology to changing climatic conditions is becoming increasingly important and essential to improve ecohydrological modeling capabilities. Improving the functionality of ecohydrological models, particularly the control of vegetation on hydrologic processes and the water balance should be a prerequisite to better forecast critical shifts in dryland ecosystem functioning to climate change and increase the representation of soil-atmosphere interactions and feedbacks, Overall, the results from my study provided an improved understanding of the impact of water availability on seasonal phenology in a water-limited dryland environment across plant functional groups. In conjunction with the modeling framework, it provides a starting point for the development and parameterization of more complex phenology models that include the relevant land-atmosphere feedbacks and phenological controls. Improving the model configuration, particularly the controls of green-up and senescence by including relevant biochemical parameters, such as growing-degree days or photoperiod, would inherently increase the predictive power of the model and its applicability to explore feedbacks on the dryland water balance as well as long-term seasonal greenness responses and potential thresholds of vegetation mortality and succession under future climate change.

In conclusion, the findings of this study can be viewed as an extension of the analysis I presented in chapter 2. The local analysis and soil moisture perspective from Southern California did not include a complete analysis of the vegetation-climate interactions and hydroclimate drivers of seasonal greenness. As such, I extended the analysis in this chapter towards an analysis of differential vegetation responses to direct hydroclimate forcing to develop a phenology model that is cognizant of climate variability. The empirical phenology model presented in this chapter is at the center of the following chapter as it is part of a newly developed dynamic vegetation module, which is incorporated within an existing dryland water partitioning model.

CHAPTER 4

4 DYNA-VEG: A dynamic vegetation module to assess and model soil-vegetation interactions in dryland environments of the Southwestern United States

4.1 Introduction

The empirically based phenology model presented in the previous chapter was explicitly developed to be incorporated into an existing ecohydrological water partitioning model, which previously lacked a dynamic parameterization of vegetation. Predicting how climate change will affect dryland ecohydrological processes remains a key challenge, which requires improved predictive models that are able to quantify soil-vegetation interactions and feedbacks that affect hydrological fluxes and vegetation health and functioning. With the design of the DNYA-VEG module, I aim to improve the modeling capabilities of the dryland water balance as well as quantify forest water stress in sensitive riparian areas.

As vegetation interacts with the hydrological cycle in complex and non-linear ways, the interactions between the water balance and plants define the fundamental differences between biomes (e.g., grassland, riparian forest) and their inherent spatial and temporal variations between hydrology and ecosystem processes (Rodriguez-Iturbe et al. 2001; D'Odorico et al. 2019; Porporato and Yin 2022). Vegetation-climate interactions have been widely explored in the context of land cover changes and changes to structural and physiological vegetation properties (Caylor et al. 2006; Villegas et al. 2010; Abatzoglou and Kolden 2011; Park et al. 2013), as well as effects on precipitation patterns and water availability (Peters et al. 2010; Anurag et al. 2021). As the drought prone vegetated landscapes of the Southwest are likely to suffer from more frequent and intense water limitations and associated vegetation water stress, there is an urgency in improving the modeling capabilities of ecohydrological interactions with a changing climate to generate more accurate water balance estimates. Such predictions would allow for an assessment of current and future vulnerabilities of lowland and upland vegetation to climatic drivers and trends and thresholds of vegetation water stress.

However, the key challenge still lies in understanding how different ecosystems will ultimately respond to shifting hydroclimate controls and how vegetation-hydrology interactions will evolve under the pressure of a changing hydroclimate (Cao et al. 2022; Castellini et al. 2022; Rinaldo and Rodriguez-Iturbe 2022). This is especially prevalent in fragile arid and semi-arid ecosystems, as they are particularly sensitive to changes in water availability and the delivery and timing of precipitation. More specifically in the context of vegetation-climate interactions, another key challenge is to anticipate how hydrologic partitioning in dryland systems will be affected by changes to precipitation and evaporative demand, and how such changes will influence ecohydrological interactions and feedbacks with drylands (Rodriguez-Iturbe et al. 2001; Porporato et al. 2002; Quichimbo et al. 2021). An improved quantitative understanding of ecohydrological process ultimately would have profound implications on future management and conservation of ecosystems and water resources in light of advancing climate change.

To date, a large number of hydrological models include only static vegetation parameterizations that do not fully account for seasonal changes or variations in response to climate (Tietjen et al. 2010; Fatichi et al. 2012; Orellana et al. 2012; Park et al. 2013). In dryland water balance estimations, this may lead to a misrepresentation of surface and subsurface fluxes, which are inherently moderated by soil-atmosphere-vegetation interactions. Changes of vegetation productivity in response to varying hydro-meteorological conditions are of particular interest in water-limited environments, where the structure and function of vegetation is predominantly driven by water availability and in turn strongly influences biosphere-atmosphere interactions (Montaldo et al., 2005).

As such, the recently published dryland water partitioning model (DRYP) by Quichimbo et al. (2021) presents a novel modeling approach designed to capture the inherent complexity of the key hydrological processes in a dryland environment over a range of spatial and temporal scales. DRYP was developed as a parsimonious alternative to existing hydrological model approaches, by considering the main hydrologic processes and timescales that control rainfall partitioning into evaporative losses, groundwater, soil moisture and runoff in dryland environments. More

specifically, the model was designed to improve the overall description of surface-groundwater interactions, including the development of ephemeral streams and focused aquifer recharge, which remain a key challenge (Quichimbo et al. 2021).. While the DRYP model is highly functional and successful in capturing important aspects of the dryland water balance, there is a need to improve the parameterization of vegetation within the model. Currently, the default representation of vegetation within DRYP is static, without temporal variation or explicit interactions and feedbacks between vegetation, root zone and surface and subsurface processes. Therefore, to account for interactions between vegetation and hydrology, and their effects on the ecohydrological water balance, I developed a novel dynamic vegetation component that characterizes and quantifies realistic dynamical behavior in response to varying hydroclimate conditions.

In the first half of this chapter, I present the framework of the novel integrative dynamic vegetation module (DYNA-VEG), which includes the previously presented empirical phenology model (Chapter 3) as well as other ecohydrological frameworks that will be used to parameterize seasonal and interannual vegetation dynamics and their interactions/feedbacks with catchment hydrology. To do so, I use a combination of insights from the previous chapter and from existing ecohydrological concepts found in the literature. The module is designed to be incorporated into the existing modular structure of DRYP, linking dynamic vegetation responses to the physical representations of the water balance. DYNA-VEG also considers new hydrological fluxes and pathways previously unaccounted for within DRYP, such as interception and canopy evaporation, and provides vegetation specific updates to existing processes such as actual evapotranspiration. Furthermore, DYNA-VEG also includes existing concepts of vegetation water stress based on vegetation specific plant water potential, to provide an explicit quantification of water stress responses.

In the second half of the chapter, I test the module and evaluate its overall model performance using a synthetic model domain. The presented model simulations use synthetic meteorological forcing and vegetation information, and present a proof of concept of the developed framework, while also contributing towards an improved understanding of the influence of climate on vegetation-soil-atmosphere interactions

within a dryland environment. More specifically, I present the setup of the synthetic model domain, the main parameters and model properties, as well as an overview of the results of the various components of the water balance. Finally, additional experiments are conducted using multiple scenarios of altered climate forcing, representing different possible futures under climate change. These will illustrate the secular effects of shifting climatological and hydrological conditions on the water balance and vegetation in a dryland environment. Finally I discuss the use and applicability of the modeling framework and meaning for future water balance assessments in dryland environments.

4.2 Methods and modeling concepts

4.2.1 The Dryland Water Partitioning hydrological model (DRYP)

The DYNA-VEG module is designed to be incorporated into the dryland water partitioning model (DRYP 1.0) developed by Quichimbo et al. (2021). As the DRYP model is published and well documented, I provide only a brief overview description of its key elements as relevant to DYNA-VEG. The DRYP model itself is a distributed, open-source, Python-based hydrological model designed to quantify the main hydrological components of the dryland water balance on a daily or sub-daily basis. It operates in a cell-based environment using spatial information of topography, soil properties, land cover and geology, and can be forced by either spatially variable or uniform time series of precipitation and potential evapotranspiration. The hydrological processes within the model are divided into three main components that control the fluxes and storage of water in a dryland environment: i) the surface, ii) the unsaturated zone and iii) the saturated zone representing groundwater flow (Figure 4.1). The original DRYP model scripts and example files are publicly available at https://github.com/AndresQuichimbo/DRYP.

The surface water component of DRYP controls the partitioning of precipitation into infiltration and overland flow, which is distributed throughout the model domain based on topography. The unsaturated zone component deals with fluxes through the soil, considering a simple linear bucket soil moisture balance model approach similar to the FAO Bucket model by Allen et al. (1998) and the SMBM I used in Chapter 2.

In the riparian unsaturated zone, additional hydrologic fluxes are considered such as stream transmission losses, focused recharge or riparian evapotranspiration through plants (Quichimbo et al. 2021). DRYP was successfully validated at the Walnut Gulch Experimental Watershed in Arizona. However, I identified a need to improve soil-vegetation interactions in the unsaturated zone to better capture the temporal variations of plant water demand under current and future climate conditions. Instead of prescribing fixed values of vegetative parameters that control AET, which do not capture seasonal changes nor interannual variations in plant transpiration, DYNA-VEG provides the necessary information to parameterize and quantify dynamic plant water demands and their effects/feedbacks on the dryland water balance*.

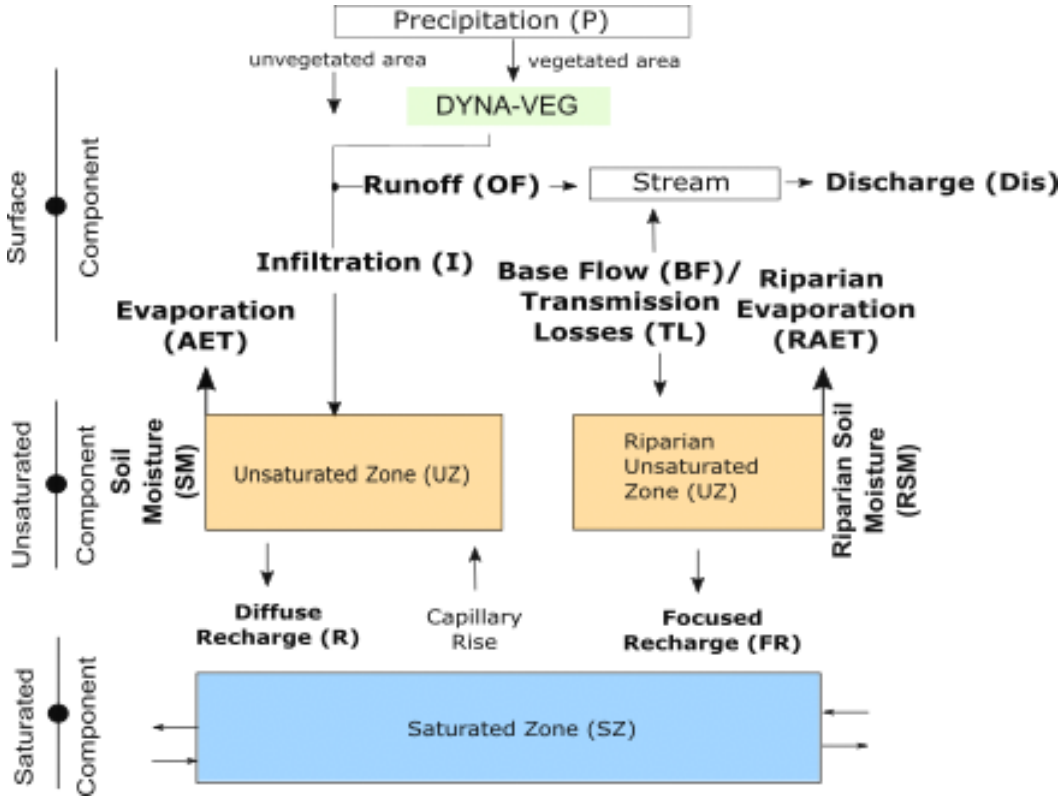

Figure 4.1 Schematic representation of the underlying model structure of DRYP and the associated hydrological processes at the surface and in the unsaturated and saturated zone within a single grid cell. The new DYNA-VEG module component is added to characterize the ecohydrological water balance. Model outputs are highlighted in bold. Figure adapted from Quichimbo et al. (2021).

* The DYNA-VEG code in DRYP can made available upon request.

4.2.2 A novel integrated DYNAmic VEGetation module (DYNA-VEG)

The integrated framework of DYNA-VEG explicitly considers the role of vegetation in affecting the water balance, by considering physiological properties, such as greenness and plant water potentials for specific plant functional types. The module provides seasonal phenological information, including timing and amplitude of phenological events (points along the curve from green up to senescence in deciduous species) that affect rainfall interception and root water uptake and represents interannual variations in potential stress responses to varying hydroclimate. The main processes considered in DYNA-VEG are: i) seasonal phenology ii) interception, iii) evapotranspiration through plant specific 'crop' coefficients and iv) an assessment of vegetation water stress through plant water potential and soil moisture (Figure 4.2).

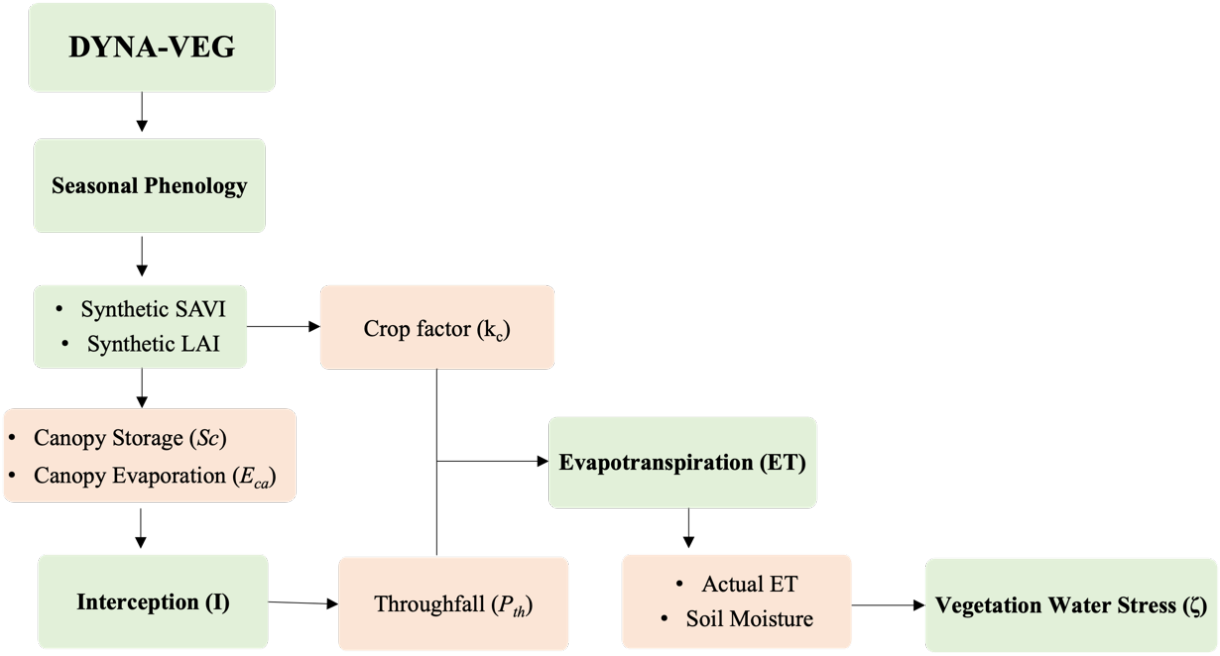

Figure 4.2: Schematic representation of the individual processes and output variables of DYNA-VEG. Red boxes indicate output variables; green boxes indicate model components..

Interception and evapotranspiration are inherently driven by changes in the vegetation dynamics through seasonal phenology and vegetation cover. The most vital link that ties climate and vegetation is soil moisture and depth to groundwater

in shallow and deeper-rooted species respectively, which determines individual vegetation responses to water stress. One of the key benefits of DYNA-VEG is its use of the same climate forcing of precipitation and potential evapotranspiration that DRYP requires. A detailed description of the main components within DYNA-VEG is given in the subsequent sections. References to the original DRYP model include equation numbers and names of model components as given in Quichimbo et al. (2021) and specified in the DRYP user guide.

4.2.3 Conceptual mdels of surface-groundwater interactions in drylands

The dynamics of groundwater dependent ecosystems, such as riparian zones, are primarily controlled through the soil moisture balance, which is affected by variations in water table depth and soil water content (Porporato et al. 2002; D'Odorico et al. 2019). With the dynamics of soil moisture tightly coupled to fluctuations in the water table, together they control several hydrological processes such as infiltration, percolation, runoff and groundwater flow, and drive climate-soil-vegetation feedbacks (Rodriguez-Iturbe 2000; Tamea et al. 2009). Vegetation-groundwater interactions primarily occur on two different levels, with vegetation first controlling the processes influencing groundwater recharge (i.e. interception, infiltration) and second, the extraction of groundwater through roots (evapotranspiration) (Huang et al., 2019; Laio et al., 2009; Orellana et al., 2012). Considering the differential water uptake strategies between groundwater-dependent species with deep roots into the saturated zone and shallow rooted soil moisture dependent species, two different formulations of water uptake and plant evapotranspiration have been made, which are presented in the following sections.

4.2.3.1 Shallow rooted plants

In general, for shallow rooted plants, such as grasses and shrubs outside the riparian zone where the water tables lies below the rooting depth (D_{root}), interactions between the unsaturated zone and water table were not considered (Figure 4.3). Instead, it was assumed that plants primarily take water from the unsaturated zone as described in section 2.4 in Quichimbo et al., 2021 (Eq. 22-24) to satisfy their water

demands. It is assumed that if there is enough water available in the unsaturated soil profile, plants do not suffer from water limitation and can transpire at the maximum rate. The total amount of water taken from the unsaturated zone by plants is assumed to vary linearly with the available moisture content, which depends on soil textural properties and the associated water holding capacities (θ_{fc}, θ_{wp}, θ_{sat}) (Figure 4.3b).

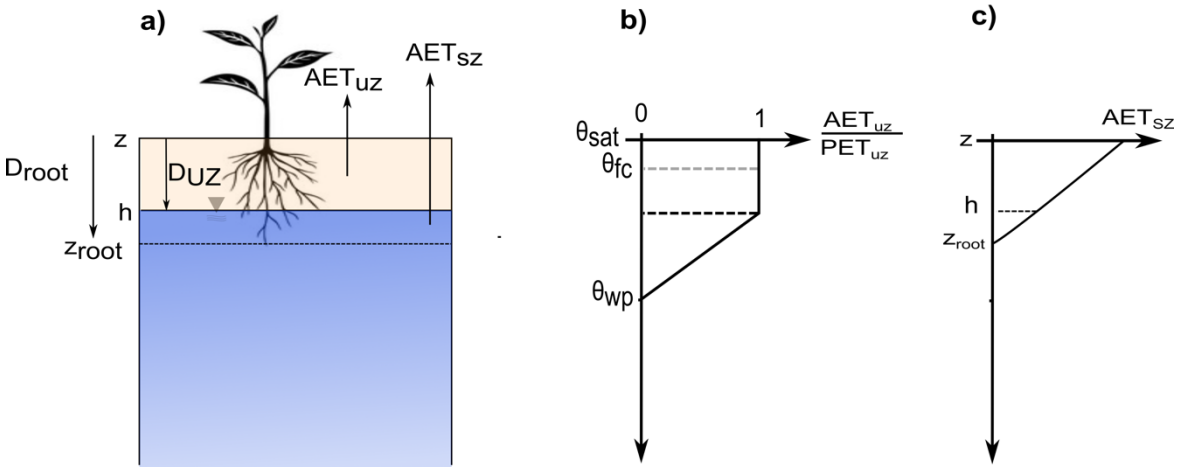

Figure 4.3: a) Schematic representation of UZ-GW interactions for shallow rooted plant functional types and evapotranspiration fluxes from the b) unsaturated and c) saturated zone.

In the case the water table rises above the rooting zone (z_{root}), DYNA-VEG assumes that plants then extract water primarily from the saturated zone, transpiring at the full potential rate until the water table drops again, at which point they switch back to satisfy their water demands with the remaining available water from the unsaturated zone. This process constitutes a major change to the original model setup of DRYP. In summary, in case the water table rises above the root zone, the amount of water taken from the groundwater is assumed to vary linearly with water table depth:

$$AET_{sz} = max\left[PET\left(\frac{h-z_{root}}{z-z_{root}}\right)\Delta t, 0\right] \quad \text{Eq. 4.1}$$

where h is the water table elevation, z_{root} is the rooting depth and z the surface elevation. In the case where the actual evapotranspiration is unable to meet PET from the groundwater, the remaining evapotranspiration is taken from the unsaturated zone, depending on the water available in the soil profile as:

$$AET_{uz} = PET - AET_{sz} \quad \text{Eq. 4.2}$$

where AET_{uz} is the actual evaporation from the unsaturated zone (Eq.4.1) and PET the potential rate.

4.2.3.2 Deep rooted plants

Within riparian zones that include groundwater-dependent vegetation, such as cottonwood or willow, the water table more dynamically interacts with the root zone, supplying water to plants and driving evapotranspiration rates. Within the DRYP model, the upper and lower boundaries of the shallow groundwater horizon for the riparian zone are determined using the hydrological concepts of capillary rise, rooting depth and extinction depth. Extinction depth in this case refers to a relative depth below the tap root up to which riparian species can extract water from the soil. Below the extinction depth, water uptake was assumed to be zero. This threshold is based on vegetation responses to observed groundwater recession rates of ~3m, at which point trees were unable to access the deepening groundwater (Williams et al. 2022b).

The concept of implementing different boundaries of an ecologically ideal shallow water depth is based on previous observations showing that groundwater dependent species show strong abiotic threshold responses to changes in water table depth (Snyder and Williams 2000; Lite and Stromberg 2005b). Multi-aged, dense cottonwood forests with consistent access to water and minimal seasonal fluctuations in water table depth (< 0.5m) showed declining productivity once water tables dropped below a certain depth. For example, previous studies in the San Pedro riparian forest reported declining plant vigor when groundwater declined below ≈ 4 – 5 m (Stromberg and Tiller 1996; Lite and Stromberg 2005b). This threshold is used here to define the optimal tap root depth (z_{tap}), below which plant vigor and water uptake start to decline.

Where a shallow water table is present, phreatophyte species predominantly develop fine roots extending into or below the capillary fringe above the shallow phreatic zone, making them sensitive to fluctuations in water table depth (Lite and Stromberg 2005a; Lite and Stromberg 2005b). The plant rooting depth (D_{root})

represents the shallow roots within the unsaturated zone, wherein the depth of the unsaturated zone (D_{uz}) is assumed to be equal to the rooting depth when the water table was below D_{root} (Figure 4.4 a). The tap depth (D_{tap}) characterizes the roots that extend into the saturated zone.

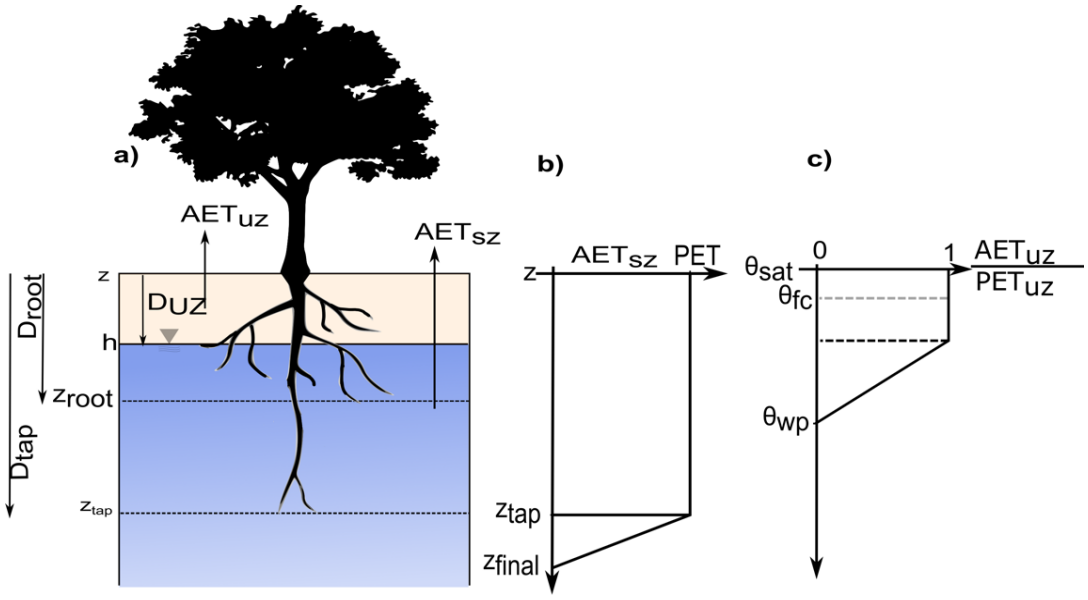

Figure 4.4: a) Schematic representation of UZ-GW interactions for deeper rooted plant functional types, where evapotranspiration in the b) saturated zone is limited by the depth of the tap root (z_{tap}) while in the c) unsaturated zone it is limited by soil water holding capacity.

In the case where the water table is shallow and well above D_{tap}, plants are assumed to transpire at the potential rate. However, when the water table declines below D_{tap}, trees may continue to access capillary water left behind by the declining water table. At this point evapotranspiration no longer occurs at the potential rate. Instead, in DYNA-VEG evapotranspiration is assumed to decline linearly with the declining water table, until the extinction depth (z_{final}) is reached. At this point, plants are no longer able to access residual water and evapotranspiration is assumed to be zero (Figure 4.4 b). In case the water table rises again above $z_{final,}$, evapotranspiration again increases linearly until it is able to reach the potential rate. In summary, the amount of water taken up by deeply rooted plants from the saturated compartment depends on the position of the water table relative to the tap root and can be expressed as:

$$AET_{sz} = \begin{cases} PET & if\ h > z_{tap} \\ PET\frac{h-z_{final}}{z_{tap}-z_{final}}, & if\ z_{final} < h < z_{tap} \\ 0, & if\ h < z_{final} \end{cases} \quad \text{Eq. 4.3}$$

where PET is the potential evapotranspiration, z_{tap} is the tap root depth, h is the water table elevation and z_{final} is the extinction depth.

In the case where the water table declines below the tap root depth, plants are assumed to make up the difference by taking additional water from the unsaturated zone to meet PET. As such, the amount of water taken from the shallow soil is estimated as the remaining AET after AET_{sz} has been taken from the saturated zone:

$$AET_{uz} = PET - AET_{sz} \quad \text{Eq. 4.4}$$

where the amount of water taken from the unsaturated compartment is limited to the depth of the unsaturated zone, with a maximum thickness of $D_{uz} = z\text{-}z_{root}$ and depending on the amount of moisture in the soil. The actual amount of evapotranspiration from the unsaturated zone is estimated through the processes described in section 2.3.3, and generally follows the FAO Soil Moisture Bucket Model by Allen et al. (1998) and was also presented in Chapter 2. In a major change from the original DRYP model, DYNA-VEG uses the tap rooting depth and the extinction depth to define the limits of the groundwater reservoir and the associated amount of plant available water within the modeling context. This allows for improved quantification of plant water uptake of groundwater dependent vegetation and its effects on the overall ecohydrological water balance.

4.2.3.3 Dryland water table dynamics

Existing ecohydrological theories of groundwater-dependent ecosystems inform the likely range of controls on climate-vegetation-soil interactions (Rodriguez-Iturbe and Perporato 2004; Caylor et al. 2006; Laio et al. 2009; Tamea et al. 2009; D'Odorico et al. 2019). In groundwater-dependent dryland ecosystems where a shallow water table inherently interacts with the shallow root zone, deep rooted plants are assumed to have near-constant access to water, as is common in riparian zones.

In such ecosystems, intense enough episodic precipitation events significantly contribute to infiltration with small amounts being intercepted by the vegetation

canopy. While the majority of water is returned to the atmosphere via evapotranspiration by plants, a small proportion of incoming rainfall percolates vertically through the unsaturated zone as diffuse recharge into the saturated zone. Excess runoff that does not infiltrate, flows into the stream. The resulting streamflow subsequently incurs transmission losses along the streambed, which are partitioned into evapotranspiration and focused recharge within DRYP.

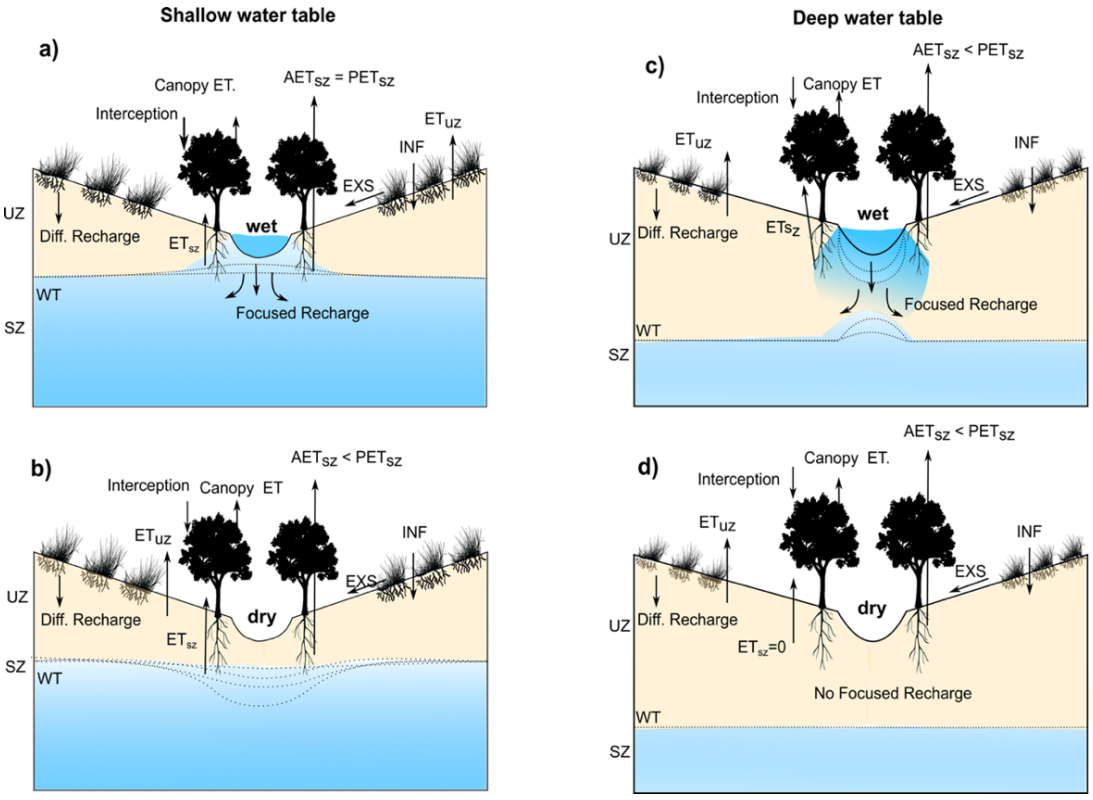

Figure 4.5: Conceptual model of interactions between the unsaturated zone and the underlying aquifer in case of a) and b) shallow and c) and d) deep groundwater tables in a dryland environment under wet (a , c) and dry (b, d) streamflow conditions.

In the case of a shallow water table depth, a fully saturated zone may develop beneath the stream, creating a continuous zone of saturation. The resulting lowered hydraulic gradient between the stream and the aquifer reduces transmission losses from the stream, producing a groundwater mound, as infiltrated water reaches the water table. This is common in ephemeral sites in SE Arizona, where groundwater levels are relatively stable even during periods of drought, thus allowing plants to

avoid the inherent limitations on precipitated water inherent in arid environments (Figure 4.5 a).

Through upward capillary fluxes, riparian vegetation accesses the groundwater reservoir, allowing plants to transpire at the maximum rate. Under more intermittent streamflow conditions, where streams only carry water for short periods, plants may experience short-term water stress despite the presence of a generally shallow water table, due to greater and more seasonally fluctuating water tables during times of reduced stream flow and reduced focused recharge (Figure 4.5 b). With receding groundwater tables, plants may start to use a greater proportion of soil water from the unsaturated zone to satisfy water demands.

When the water table is deep, the level of saturation below the stream is determined by the frequency and intensity of precipitation events, prior saturation levels and the rate of infiltration below the channel. Water infiltrating below the stream through the channel bed may be temporarily available to vegetation as it spreads and descends via gravitational drainage (Figure 4.5 c). Overall, the rate of movement through the soil depends on antecedent saturation and the hydraulic conductivity of the sediments (Singer and Michaelides 2014; Evans et al. 2018). Under such conditions, groundwater dependent vegetation is unlikely to thrive as there is no consistent access to the groundwater, with soil water from precipitation being the primary source of moisture in the unsaturated zone (Figure 4.5 d).

4.2.4 DYNA-VEG module components and governing equations

4.2.4.1 Seasonal phenology

In Chapter 3, the key processes controlling phenology are quantified and a simple phenology model is presented for different dryland plant functional groups. Hydroclimate variables such as antecedent precipitation, depth to groundwater and temperature are the key drivers of phenology, including seasonal greenness amplitude and timing. Through the presented empirical model framework, a measure of synthetic greenness can be estimated.

In addition to remotely sensed vegetation greenness, the leaf area index (LAI) constitutes a valuable vegetation metric that provides information on spatial and

temporal patterns of plant canopy structure, including seasonal and interannual variations in response to climate (Turner et al., 1999). LAI has been statistically related to numerous vegetation indices (NDVI, EVI, SAVI), due to its relation to surface reflectance, which has been explored in a number of ecohydrological studies (Turner et al. 1999; Jolly and Running 2004; Bulcock and Jewitt 2010; Glenn et al. 2011). NDVI is almost linearly related to LAI, however NDVI enters a level of saturation at which point it only increases very slowly with increasing LAI. In contrast, SAVI extends the range of LAI values over which a vegetation index is responsive, as it does not saturate as quickly as NDVI when reaching higher values of greenness, due do its internal correction for soil surface reflectance (Eq. 3.1). (Carlson and Ripley 1997; Turner et al. 1999; Glenn et al. 2011).

The strong coupling of SAVI and LAI to hydroclimate inherently includes interannual variations in vegetation dynamics, which is essential when parameterizing climate-vegetation interactions, such as canopy interception. Therefore, to achieve a realistic representation of a dynamic vegetation cover, I developed simple non-linear regression models between observed SAVI and LAI (Figure 4.6). The established models were then used with the synthetic greenness from the phenology model presented in Chapter 3 to generate synthetic LAI under variable climate forcing.

For calibration of the non-linear regression model to estimate a synthetic leaf area index, I obtained SAVI and LAI data from Sentinel 2, which is distributed at a spatial resolution of 10 m every 5 days for the period 2017 - 2020 (https://www.onda-dias.eu/cms/data/catalogue/sentinel-2/). I used the same vegetation samplings points as in Chapter 3 along the San Pedro riparian corridor and on the riparian terrace, as well as across areas of grass and shrubland at Walnut Gulch (Figure 3.1 a). Only cloudless images were manually selected from Sentinel 2, which decreased the frequency of images in some cases. Using the SNAP software, an atmospheric correction was applied using the Sen2Cor plugin from the SNAP toolbox (https://step.esa.int/main/snap-supported-plugins/sen2cor/) to convert data to surface reflectance, from which SAVI and LAI can be calculated.

Regression analysis with LAI as the dependent variable was performed to evaluate the relationship between LAI and SAVI. An exponential model was found to best represent the SAVI-LAI relationship and the correlation strength was assessed through Spearman's rank correlation. SAVI was found to explain between 67-95% of the variance in LAI, depending on vegetation type (Figure 4.6), via the equation:

$$LAI = a * e^{b*savi} \quad \text{Eq. 4.5}$$

where a and b are regression coefficients particular to a given vegetation type and *savi* represents the (synthetic) greenness forcing.

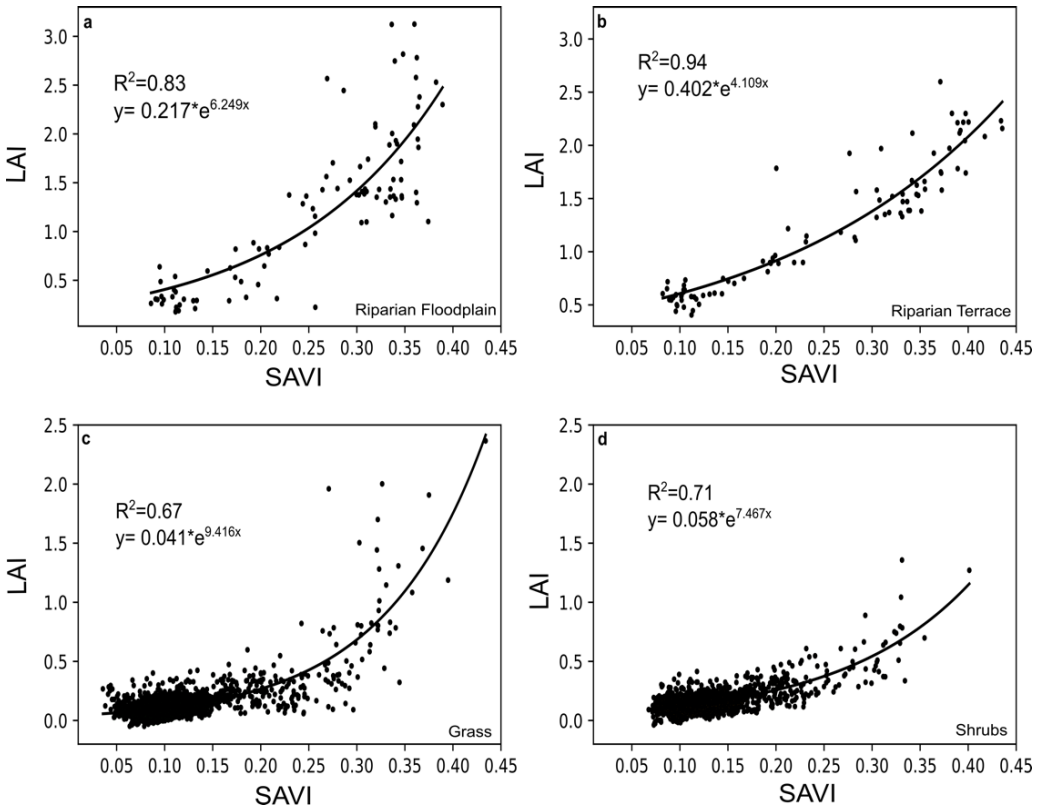

Figure 4.6: Curvilinear relationship between SAVI and LAI based on observed values from Sentinel 2 for the year 2018.

4.2.4.2 Canopy interception

The amount of precipitation reaching the ground and contributing to infiltration depends strongly on the type of vegetation and its phenological state, as well as on the precipitation rate and potential evaporative demand. Within DRYP, a new interception module has been implemented, which is coupled to the surface

module that estimated surface fluxes, such as infiltration and runoff. Based on previously used rainfall interception models, the two key components for interception estimates are meteorological – precipitation and reference evapotranspiration (ET_0), and canopy parameters - canopy storage and canopy evaporation. The most important parameters are the canopy storage capacity ($S_{cz,max}$), which is variable depending on the phenological state of the vegetation and can be estimated through the leaf area index (Vegas Galdos et al. 2012). Several statistical relationships exist between LAI and $S_{cz,max}$, with some attempts at general functions for multiple vegetation cover types. However, to get the most universal relationship that would fit different vegetation types, Vegas Galdos et al. (2012) present a general equation based on an approach by Menzel (1991) and the analysis of other published relationships between $S_{cz,max}$ and LAI. The equation was tested for six different vegetation types, including grasses, shrubs and deciduous trees. Therefore, in keeping with the parsimonious characteristics of DRYP, I follow a similar approach and estimated $S_{cz,max}$ through LAI as:

$$S_{cz,max} = f * log(1 + LAI) \quad \text{Eq. 4.6}$$

where *f* is a vegetation specific factor that varies with vegetation type; for grasses, *f* can be assumed as 1.0, for shrubs 2.6 and for deciduous trees 1.6 (Vegas Galdos et al. 2012) and LAI can be a real or synthetic input of leaf area index (from Eq. 4.5).

The water balance in the canopy is assumed to consist of incoming precipitation, which is partitioned into throughfall (P_{th}) and evaporative losses from the canopy (E_{ca}). The amount retained in the canopy – the canopy storage (S_{cz}) canbe estimated as:

$$\Delta S_{cz} = P - P_{th} - E_{ca} \quad \text{Eq. 4.7}$$

where ΔS_{cz} is the change in the canopy storage, P is the incoming precipitation, and E_{ca} is canopy evaporation.

The amount of water that can be evaporated from the canopy storage is estimated as:

$$E_{ca} = a_v \frac{S_{cz}}{S_{cz,max}} * ET_0 \quad \text{Eq. 4.8}$$

where ET_0 is the reference evapotranspiration calculated via Penman Monteith (and not to be confused with PET, which includes the crop factor k_c, see Eq. 4.11), S_{cz} is the amount of water available in the canopy, $S_{cz,max}$ is the maximum amount of water that can be stored in the canopy, and a_v is the vegetation cover factor, which ranges between 0 (no vegetation cover and 1(full canopy cover) and can vary between different plant functional groups (Kozak et al. 2007; Vegas Galdos et al. 2012).

The storage capacity of the canopy not only depends on phenology but also on the precipitation rate. During intensive rainfall events, the canopy storage capacity is significantly reduced as the leaves' capacity to store water declines with increasing precipitation. Here I assume that canopy saturation occurs exponentially as rainfall increases, until the maximum storage capacity is reached:

$$S_{cz,sat} = S_{cz,max} * \left(1 - e^{\frac{-P}{Scz,max}}\right) \quad \text{Eq. 4.9}$$

where $S_{cz,sat}$ is the canopy saturation, which affects the amount of water that can be stored in the canopy ($S_{cz,max}$) at any given time. Therefore, any excess water above $S_{cz,sat}$ will become throughfall (P_{th}) (Kozak et al. 2007). In summary, the main inputs to parameterize dynamic interception, include information regarding the state of vegetation phenology (LAI), which are used to determine the canopy storage. The main DYNA-VEG inputs for this component are rainfall and evapotranspiration and the fraction of vegetation cover.

4.2.4.3 Actual evapotranspiration by vegetation

The linear bucket soil moisture balance model incorporated in DRYP estimates potential plant evapotranspiration (PET) from the unsaturated zone through a crop coefficient (k_c), an approach originally developed to estimate plant water needs for agricultural crops (Allen et al. 1998). Recent studies have recognized the potential of using remotely sensed vegetation indices, such as NDVI or SAVI, as proxies for the crop coefficient in more natural ecosystems to improve estimates of evapotranspiration (Glenn et al., 2011; Nagler et al., 2005, 2013). The high correlation between vegetation indices, biophysical characteristics of plants, as measured by LAI and fractional vegetation cover, as well as evapotranspiration can be used as an indicator of plant water use. Based on past studies using remotely sensed

vegetation indices to estimate evapotranspiration in riparian ecosystems (Murray et al. 2009; Nagler et al. 2009; Glenn et al. 2011; Nagler et al. 2013), I estimate an artificial crop coefficient using synthetic SAVI estimates, and which can be expressed as:

$$k_c = \left(1 - \frac{VI_{max} - VI}{VI_{max} - VI_{min}}\right)^{\eta} \quad \text{Eq. 4.10}$$

where k_c can be considered a plant transpiration coefficient similar to the crop coefficient used by Allen et al. (1998) and VI is the vegetation index ranging from 0 and 1, representing bare unvegetated soil or dead senescent vegetation (VI_{min}) and fully transpiring, unstressed vegetation when greenness is at its maximum (VI_{max}), respectively (Glenn et al. 2011). The exponent η is a parameter computed by fitting the relationship between evapotranspiration and the applied vegetation index. Previous studies showed that SAVI is well suited as a proxy in drylands, due to its near-linear relationship with evapotranspiration, allowing us to set η to 1.0 (Glenn et al. 2011).

In DRYP, the potential amount of water that plants can remove without stress from the unsaturated zone through transpiration is defined as PET, which is a product between the crop coefficient and the reference evapotranspiration. The energy lost during canopy evaporation must be considered, thus potential plant evapotranspiration can be estimated as:

$$PET_{uz} = kc_{VI} * (ET_0 - ET_{ca}) \quad \text{Eq. 4.11}$$

Outside the riparian zone DRYP assumes that vegetation can transpire at the maximum rate equal to PET if there is enough water available in the unsaturated zone (see Section 4.2.3.2). With soil moisture being the chief control variable of shallowly rooting dryland vegetation dynamics, water stress is often triggered by an increasing soil moisture deficit over time, incurring water stress as soil moisture availability declines. DRYP incorporates this process through the inclusion of a parameter (*β),* that considers the available soil moisture content using the thresholds of total available water (L_{TAW}) and readily available water (L_{RAW}), which are characterized by field capacity and wilting point of the soil (Figure 4.7) (Eq. 23 in Quichimbo et al., 2021) (Egea et al. 2011; Verhoef and Egea 2014). Actual evapotranspiration from

the unsaturated zone under less than optimal conditions is then calculated using Eq. 22 of Quichimbo et al. (2021), in conjunction with the estimation of AET_{uz} (Eq. 4.2). In the riparian zone maximum evapotranspiration occurs when the water table is above the tap root depth and water uptake is not limited (see Section 4.2.3.2). Here, evapotranspiration is coupled to the water table depth, with moisture from the unsaturated zone complimenting vegetation water use in case of a lower water table (Eq. 4.3 and 4.4).

4.2.4.4 Vegetation water stress

To link plant water availability and water use, and obtain a more direct estimate of vegetation stress, DYNA-VEG adopts concepts from previous ecohydrological theory (Laio et al. 2001; Porporato et al. 2001; Rodriguez-Iturbe et al. 2001). There, the role of different plant functional groups on soil moisture dynamics and their response to water stress is used to model the stress that moisture deficits can induce in plants (Rodriguez-Iturbe et al. 2001). DRYP already uses a parameter β as an evaporation reduction coefficient for the estimation of AET for water limited conditions. However, this parameter only takes into account the available water in the soil as defined by the soil hydraulic properties (see also Figure 2.3), but not individual water stress thresholds by plants. Therefore, instead of using only soil hydraulic properties to delimit the plant available water (θ_{fc} and θ_{wp}), I assume that a reduction in evapotranspiration occurs as stomates start to close in response to a rise in hydraulic resistance within the soil at a soil moisture equal to the threshold of incipient stomatal closure (ψs^*) (Laio et al. 2001; Bréda et al. 2006) (Figure 4.7). At this point actual evapotranspiration would decline with declining soil moisture until a plant wilting point (ψs_{wp}) has been reached, at which point maximum plant water stress can be assumed.

Given that different plant functional types experience differential stress responses under the same climate and soil conditions, DYNA-VEG ultimately characterizes vegetation water stress by connecting the plant-specific information of gravimetric water potentials to relative water availability, via soil moisture. Therefore, a general form for the estimation of water stress is included after Laio et al. (2001), and which can be described as:

$$\zeta = \left[\frac{\theta s^* - \theta}{\theta s^* - s_w}\right]^{\eta} \text{ for } s_w < s(t) < s^* \qquad \text{Eq. 4.12}$$

$$z = 0 \quad \text{for } \theta > s^* \qquad \text{(no stress)}$$

$$z = 1 \quad \text{for } \theta < s_w \qquad \text{(stress)}$$

where θ is the available soil moisture within the unsaturated zone and θs^* and θs_w are the plant specific thresholds of plant water potential below which evapotranspiration is reduced and finally stopped (Figure 4.7,Table 4.1). The exponent η is a measure of nonlinearity of the effects of increasing soil moisture deficit on plant conditions and can be set to 1, assuming a linear response (Laio et al., 2001).

To obtain the individual thresholds, known plant water potentials for different plant functional types can be related to the soil matric potential of a particular soil by linking the plant specific thresholds to the current soil properties and translating them to values of relative soil moisture through Clapp and Hornberger pedo-transfer function (Clapp and Hornberger 1978) and soil-water retention curves (Laio et al. 2001). To convert matric potentials to relative soil moisture values, a simple function is used:

$$\theta_{s*} = n * (\psi s * / \psi)^{\lambda} \qquad \text{Eq. 4.13}$$

$$\theta_{swp} = n * \left(\psi_{swp} / \psi\right)^{\lambda} \qquad \text{Eq. 4.14}$$

where n is the porosity of the soil type, ψ_{s*} and ψ_{swp} are the plant matric potentials depending on the plant functional type, ψ is the maximum soil matric potential of the respective soil type and λ is the pore size distribution index. The variables related to soil hydraulic and textural properties (n, ψ and λ) vary with soil type, while the plant matric potential (a) depends on the plant functional group (Table 4.1).

In general, plant matric potential at wilting point for temperate vegetation is assumed at a value of -1.5 MPa. However, in water-limited environments values are considerably lower, with variations between different plant functional groups (Table 4.1) (Laio et al., 2001). In this context, the wilting point for grasses is generally considered to be lower than for trees, even though they experience water stress considerably earlier (Laio et al. 2001; Porporato et al. 2002; D'Odorico et al. 2019).

Plants with shallow rooting depths generally experience more frequent yet shorter periods of water stress, due to the close link to precipitation variability, compared to deeper-rooted plants that are more resistant in the presence of a shallow water table.

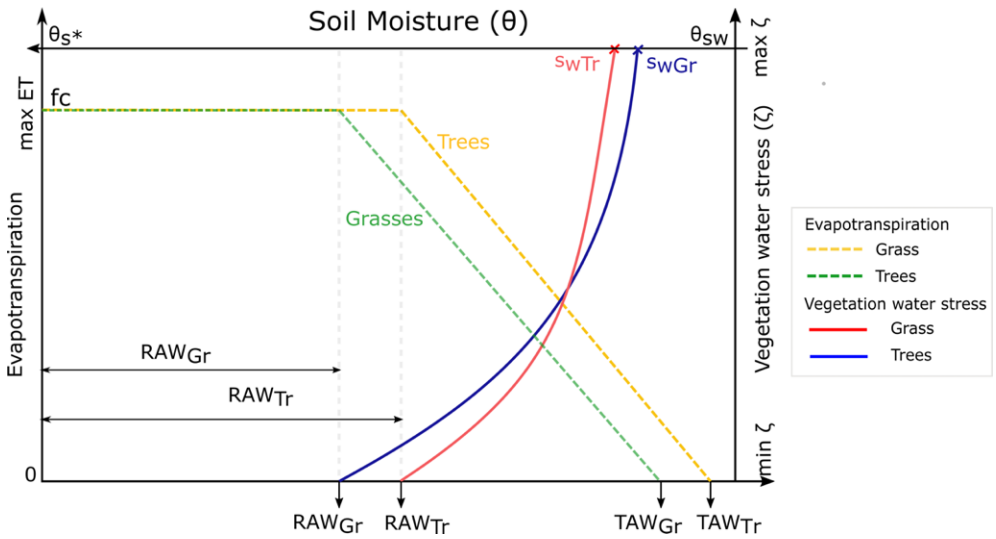

Figure 4.7: Conceptual relationships between soil moisture, evapotranspiration and vegetation water stress. Plant water potentials s and sw can be translated to relative soil moisture values through Clapp and Hornberger (Clapp and Hornberger 1978).*

Table 4.1: Plant water matric potentials for different plant functional types at incipient stomatal closure (s) and wilting point (s_{wp}) (Rodriguez-Iturbe and D'Odorico 1999; Laio et al. 2001).*

Plant Functional Group	*Plant water potential at s* (MPa)*	*Plant water potential at s_w (MPa)*
Grass	-0.025	-3.7 - -4.5
Trees	-0.05	-2.95 - -3.5

An important caveat relating to the assessment of vegetation water stress, is that it is only a proxy that assesses vegetation water stress primarily in response to soil moisture content. In the case of a shallow water table groundwater dependent vegetation, I assume that plants only experience stress, once the water table drops below the tap root depth and vegetation starts to use soil moisture to augment their water use. In that case stress starts to increase as water in the unsaturated zone is decreased by root uptake.

4.3 Integration of DYNA-VEG into DRYP

4.3.1 Synthetic model domain

Simulations were performed within DRYP using an artificial tilted-V catchment model domain (Figure 4.8), which will serve as a proof of concept of the DYNA-VEG module. The symmetrical model domain has a length and width of 2 km (20 x 20 square cells) with a cell size of 100 m, totaling 400 cells. The domain slope from upstream to downstream and the surface slope across the domain is specified as 1%, which is representative of channel gradients commonly found in dryland environments and also used for synthetic model experiments (Singer and Michaelides 2014; Quichimbo et al. 2021). The model domain is populated with three plant functional groups that reside in three spatial domains as follows i) grasses on hillslopes, ii) mesquite trees on riparian terraces and iii) and cottonwood trees on the riparian floodplain. Plant distributions in dryland environments of the Southwest generally exhibit similar configurations, determined by different biotic and abiotic factors (e.g., soil properties, available moisture, elevation) (Makings 2005; Stromberg et al. 2017). Vegetation cover and soil hydraulic characteristics are specified uniformly within each spatial domain. Rooting depths for each plant functional group, including actual rooting depth, tap rooting depth and the extinction depth are assigned for each plant functional group (Table 4.2). The extinction depth (z_{final}) defines the lower boundary of shallow groundwater below which roots are unable to obtain water and evapotranspiration from the water table ceases. Variable vegetation cover fractions (a_v) are assumed for each plant type, which is necessary to capture the sparseness of dryland vegetation. In the hillslope basal ground cover can be assumed to be between 10-15%, which is similar to values observed at the Walnut Gulch Experimental Watershed (Nearing et al. 2007). In the riparian terrace and riparian floodplain, canopy cover is estimated as 30% for terrace and 40% floodplain vegetation, which is based on a visual analysis of NAIP images of vegetation sampling points along the San Pedro Riparian Zone, used in Chapter 3.

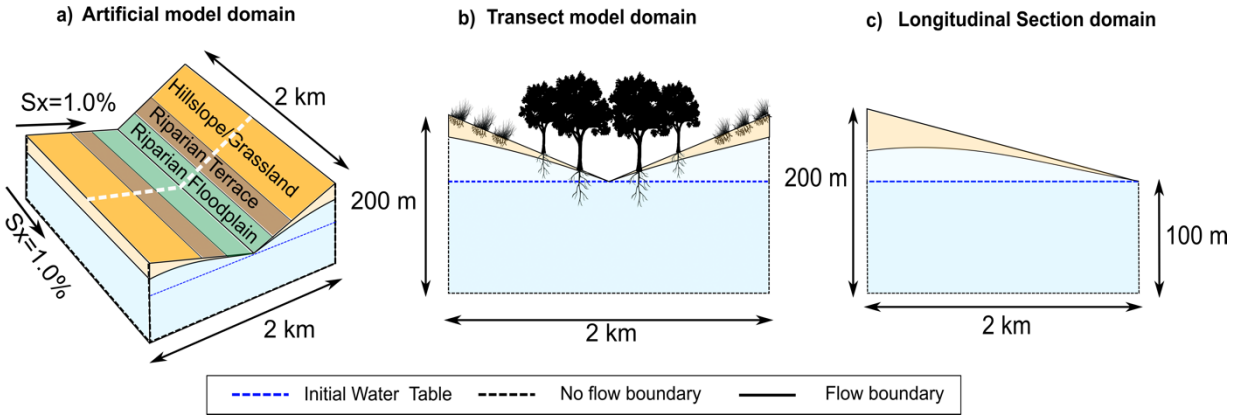

Figure 4.8: Model domain for synthetic experiments is a tilted-V catchment with flow boundary conditions and the spatial distribution of vegetation cover types specified. Baseline results are assessed across a lateral sample transects across the model domain; adapted from Quichimbo et al. (2021).

Table 4.2: Assigned rooting depth parameters, plant water potentials and cover fractions for different plant functional groups within the model domains.

Model Domain	D_{root} *[mm]*	D_{tap} *[mm]*	D_{final} *[mm]*	ψs^* *[MPa]*	ψs_w *[MPa]*	a_v [%]	*Soil Type*
Hillslope	300	300	-	-0.025	-4.0	0.10	Loamy Sand
Riparian Terrace	1500	5500	9500	-0.05	-2.95	0.30	Silt Loam
Riparian Floodplain	1500	5500	9500	-0.05	-2.95	0.40	Sandy Loam

Table 4.3: Soil hydraulic parameters for chosen texture classes with porosity (n), saturated hydraulic conductivity (K_{sat}), field capacity (θ_{fc}) and wilting point (θ_{wp}), as well as saturation suction (ψ) and pore size distribution parameter (b), based on Clapp & Hornberger (1978).

Texture	*n* *[-]*	K_{sat} *[cmh^{-1}]*	θ_{fc}	θ_{wp}	ψ *[cm]*	*b* *[-]*
Sandy Loam	0.453	10.9	0.25	0.11	21.8	0.204
Silt Loam	0.501	6.5	0.37	0.19	78.6	0.188
Loamy Sand	0.437	29.9	0.40	0.18	9	0.247

The choice of soil type was based on information from a soil survey (https://websoilsurvey.sc.egov.usda.gov/App/WebSoilSurvey.aspx) by the United States Department of Agriculture (USDA) of the San Pedro Riparian National Conservation Area. Soil types and associated hydraulic properties are differentiated between the hillslope and riparian terrace and floodplain, using a sandy loam texture in the riparian floodplain, a silt loam texture in the riparian terrace above the channel, and a loamy sand in the upland hillslope (Table 4.2). The rate of infiltration into the unsaturated zone is controlled through the saturated hydraulic conductivity (K_{sat}). The saturated zone was modelled as a homogenous and unconfined aquifer, with a hydraulic conductivity (K_{aq}) of 1 m d^{-1} and a specific yield (S_y) of 0.01, while for the channel (K_{ch}) a value of 10.9 mm/hr was chosen. These particular values of K_{ch}, K_{aq} and S_y were chosen to allow a sufficiently dynamic response of the water table to plant water uptake over shorter periods of time, and to be consistent with the original DRYP model evaluation experiments (Quichimbo et al. 2021). Flow boundary conditions were specified as no-flow on the upstream end and sides of the model as well as at the base of the model domain. A constant head boundary (chb) was implemented at the downstream end (Figure 4.8 b), which represents a discharge zone such as a perennial stream at the lower end of the model domain.

4.3.2 Baseline data and model parameters

A summary of all model parameters considered within the model is provided in Table 4.4. Initial conditions of the model were set to best capture the temporal and spatial variations within the forcing data and parameterization of the unsaturated and saturated zones. The baseline model was run on an hourly time step for all components and results summarized into daily aggregates. Simulations were forced with historical climate data over a period of 21 years, using hourly potential evapotranspiration from the hPET dataset (https://data.bris.ac.uk/data/dataset/qb8ujazzda0s2aykkv0oq0ctp), which is a multidecadal dataset at 0.1º spatial resolution over the global land area (Singer et al. 2021). The hPET data were obtained for a location in the Walnut Gulch Experimental Watershed to match the available precipitation data (31.739, -109.944). A spatially interpolated precipitation series over this time period from Walnut Gulch was used,

previously generated by Quichimbo et al. (2021), and which is based on rainfall measurements from stations within the Walnut Gulch catchment using publicly available data of rain gauges from the Southwest Watershed Research Center (SWRC) (https://www.tucson.ars.ag.gov/dap). Key input parameters and data, such as elevation, soil hydraulic properties (field capacity, wilting point, saturated hydraulic conductivity), vegetation properties (rooting depth, plant water potentials, vegetation greenness), and aquifer hydraulic properties (specific yield, aquifer thickness, saturated hydraulic conductivity) were converted into gridded raster datasets using an automated process outside the DRYP model.

4.3.3 Baseline model evaluation

The mass balance was qualitatively compared against observations from the Walnut Gulch Experimental Watershed (Quichimbo et al., 2021). The starting year of the model simulations coincides with average rainfall conditions and was used as a spin-up period to initiate the model. To reduce the influence on the initial conditions on the evaluation of the model, the first year was not included in the presented results. The main hydrologic and vegetation responses were qualitatively evaluated along a horizontal cross section (Figure 4.8a) across the center of the model domain that captures responses of each plant functional group. The fluxes in the riparian zone, including recharge and water table elevation, were evaluated along the length of the channel. Model performance was qualitatively evaluated with respect to the desired functionality of the DYNA-VEG module and conceptual models, to produce plausible outputs of dynamic surface-subsurface interactions. To compare soil moisture between the hillslope and riparian zone, volumetric soil moisture content was normalized to the porosity of each soil type. To evaluate the partitioning of incoming precipitation across the model domain, water balance contributions are presented as percentages relative to the main precipitation input. Across the model domain, the elevation of the water table was subtracted from its ground surface elevation and then presented as depth to groundwater (DTG) in meters below the surface.

Table 4.4: Summary of model parameters for the different processes overland, in the unsaturated, and saturated zone. Soil hydraulic properties, rooting depth information and crop coefficients vary spatially according to the soil and vegetation types assigned (see Table 4.2 and 4.3 .).

Parameter	*Unit*	*Description*	*Value*
	Overland Flow		
	m	Cell size	100
SAVI	-	Vegetation greenness	vegetation type
LAI	-	Leaf Area Index	vegetation type
S_{cz}	mm	Canopy storage	vegetation type
$S_{cz,sat}$	mm	Canopy saturation	vegetation type
$S_{cz,max}$	mm	Maximum canopy storage	vegetation type
a_v	-	Vegetation cover fraction	vegetation type
L_{ch}	m	Channel length	grid size
W_{ch}	m	Channel width	10
W_{rip}	m	Width of the riparian zone	160
K_{ch}	mmh^{-1}	Channel saturated hydraulic conductivity	10.9
	Unsaturated Zone		
q_{wp}	-	Water content at wilting point	soil type
q_{fc}	-	Water content at field capacity	soil type
q_{sat}	-	Saturated water content	soil type
K_{sat}	-	Saturated hydraulic conductivity	soil type
D_{root}	m	Rooting depth	vegetation type
D_{tap}	m	Tap depth	5
D_{final}	m	Extinction depth	D_{tap} + 3
k_c	-	Crop coefficient	vegetation type
	Saturated Zone		
S_y	-	Specific yield	0.01
chb	m AD	Downstream constant head groundwater flow boundary	94
K_{aq}	md^{-1}	Aquifer saturated hydraulic conductivity	1
h_b	m AD	Aquifer bottom elevation	0 at lowest point

4.3.4 Modeling of vegetation responses to altered climate forcing

In addition to baseline (historical climate) responses, the effects of altered climate forcing on hydrologic and vegetation responses are also explored. A summary of all scenarios and associated changes is presented in Table 4.5. In Scenario 1 (P_{total} (-)) annual historic precipitation is reduced by 40%, to evaluate the effects of an extreme, prolonged drought scenario on moisture availability and overall distribution of water throughout the domain. This change is considered to reflect the impacts of atmospheric conditions that might lead to a weakened monsoon (Pascale et al. 2017; Singer and Michaelides 2017). All other parameters remain unchanged, including the water table elevation. It should be noted, that since vegetation greenness is parameterized partly as a function of input precipitation (see Chapter 3), vegetation phenology also changes in this scenario (Figure 4.9).

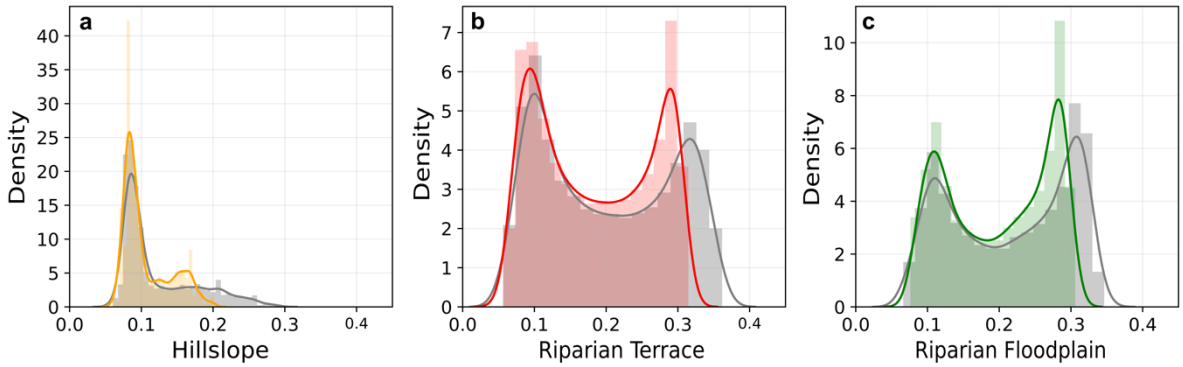

Figure 4.9: Distributions of seasonal vegetation greenness in the a)hillslope, b) riparian terrace and c) riparian floodplain. Distributions in grey and used for baseline simulations and in Scenario 2 and 3. Colored distributions are used in Scenarios 1 and 4.

Scenario 2 (PET (+)) uses historical baseline precipitation and vegetation input, and deviates only through an increased atmospheric demand, representative of a 2°C increase in air temperature, which is equivalent to an increase in PET by approximately 8%. To achieve this, spatially uniform synthetic evapotranspiration data from the stochastic potential evapotranspiration model (stoPET) was used and a 2°C temperature increase was applied to generate synthetic PET in response to temperature-based changes under future climate change. The stoPET model leverages

hPET and creates realistic timeseries of PET that capture the diurnal and seasonal variability of hPET (Singer et al. 2021; Asfaw et al. 2022).

An important caveat to the parameterization of greenness under climate change scenarios is that the phenology model presented in Chapter 3 does not account for value changes of temperature or PET, but only to step changes in the timing of the seasonal temperature distribution. Furthermore, the model in itself also does not account for changes in the energy balance, which inherently occur in response to climate change. Therefore, in the climate change simulations of Scenario 2, phenology remains unaffected by the PET changes, which potentially leads to an overestimation of the water balance in this scenario . Indeed, changes to the energy surface balance and evaporative demand would inherently affect the timing of green-up and seasonal greenness responses, however, the phenology model at this stage does not yet have this functionality.

Table 4.5: Summary of changes to climate forcing and ecosystem conditions for different climate change scenarios. NC means no change was applied to the respective forcing.

Variable	*Scenario 1* P_{total} *(-)*	*Scenario 2* *PET (+)*	*Scenario 3* *WTE (-)*	*Scenario 4* *PET (+),* P_{total}*, WTE (-)*
P	-40%	NC	NC	-40%
PET	NC	+2°C	NC	+2°C
chb	94	94	90 (-4m)	87 (-7m)

In Scenario 3 (WTE (-)) climate and vegetation forcing remain unchanged, but a deeper water table is implemented, by lowering the initial water table and constant head boundary by 4 m. This enabled the evaluation of differential vegetation responses to a lower water table in the riparian terrace and floodplain. Finally, Scenario 4 (PET (+), P_{total}, WTE (-)) assess the combined effects of multiple climate change components. It includes changes to climate forcing (P and PET) and their corresponding impact on vegetation, as well as a deeper initial water table (7 m) to evaluate the compound effects of altered climate forcing as well as hydrologic conditions on all dryland plant communities.

In all experiments, percentage changes of total flux amounts are quantified relative to the synthetic historical baseline, while distribution changes are evaluated using two-sample Kolmogorov-Smirnov testing (ks-test) to evaluate the significant differences between distributions of model outputs between altered climate forcing variables in relation to the historic baseline.

4.4 Results

4.4.1 Historical baseline

I first present results from the baseline simulations. Baseline precipitation is characterized by a high interannual variability, with a mean annual value of 235.2 mm/y. The range includes annual totals between 141.7 mm/y during a dry year with a weak monsoon between June-September (84.3 mm) and 377 mm/y in a wet year, with strong monsoon (303.8 mm). Potential evapotranspiration is characterized by a mean annual value of 1349.4 mm/y (± 77.7 mm/y) with maximum daily PET of 8.8 mmd.

4.4.1.1 Entire domain water balance

Figure 4.10 shows the total amounts over the historical simulation period and their relative percentages in relation to the incoming precipitation. Looking at the total volumes of the different components of the model domain mass balance over a period of 20 years, 93% of incoming precipitation passes through the canopy as throughfall. In the hillslope, this water becomes available for infiltration, with most of that water (89%) used as evapotranspiration in the unsaturated zone and returned to the atmosphere. Water that does not infiltrate is distributed as runoff and routed downstream, which makes up about 6% of the total precipitation. This amount is substantially reduced by transmission losses, contributing to focused recharge This amount is equal to 4 % of the incoming precipitation. Transmission losses produce focused recharge and supply moisture to the riparian unsaturated zone. Riparian evapotranspiration from the unsaturated zone (ET_{uz}) is assumed to be zero when there is a shallow water table, as the majority of water needed by deeply rooted vegetation is taken up primarily from the saturated zone (ET_{sz}). The amount of water returned to the atmosphere via evaporation from the groundwater is an amount equal to 33% of

the incoming precipitation. The amount of water leaving the model domain as surface discharge is ~1% of the total precipitation. The total cumulative change in groundwater storage for the baseline historical simulation over the simulation period due to recharge and drainage was 19.3 mm, which accounts for 0.4% of incoming precipitation.

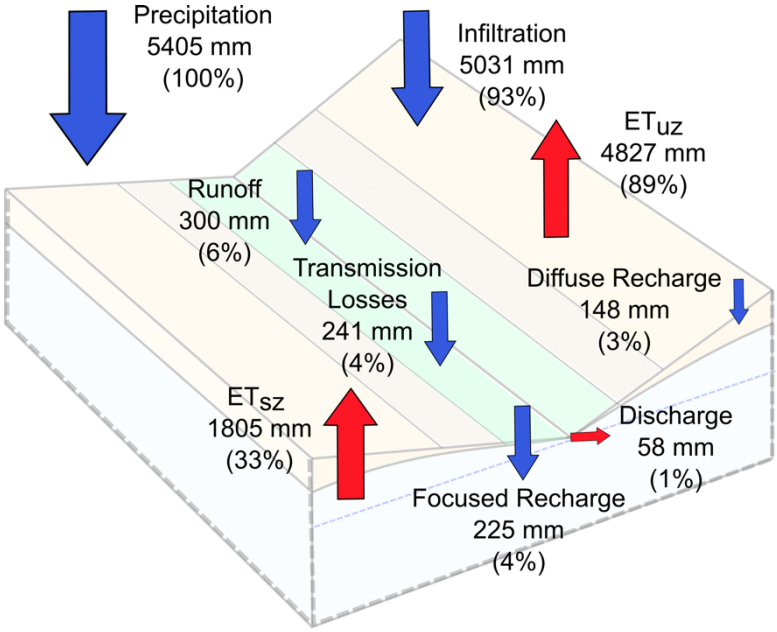

Figure 4.10: Average fluxes across the baseline model domain for the simulated period (n=21 years). Blue arrows represent inputs to the water balance, red arrows represent losses. Values are presented as totals over the simulation period, percentages are relative to the input precipitation.

In summary, the main water source to hillslope vegetation comes from infiltration, with evapotranspiration as the main outtake from the unsaturated zone. In the riparian zone, transmission losses along the stream contribute to focused recharge and moisture for evapotranspiration from the unsaturated zone. Most of the water lost from the riparian zone is by evapotranspiration from the saturated zone. These results are generally consistent with values presented for the dryland catchment in Quichimbo et al. (2021), indicating that DYNA-VEG provides realistic enhancements to DRYP through the incorporation of ecohydrology within riparian dryland environments.

4.4.1.2 Evapotranspiration from the saturated and unsaturated zone

The model is able to capture the differential daily evapotranspiration dynamics between plant functional groups for the historical baseline simulation, with respect to the conceptual water uptake defined in Chapter 4.2.3. The parameterization of phenology within DYNA-VEG produced clear seasonal signals in the riparian terrace and floodplain corresponding to growing and senescent periods (Figure 4.11 b-f), as well as seasonal variations in moisture availability, particularly in the hillslope (Figure 4.11 a). Evapotranspiration totals are presented as averages over the vegetated areas for each plant functional group.

Shallow-rooted vegetation along the hillslope primarily used the unsaturated zone to satisfy its water demands, with daily evaporation rates between 0-6 mm/d, with lower daily evaporation during drier years. Strong interannual variability were observed with total annual ET varying from 155 mm/y in drier years (t=4000) up to 344 mm/y in wetter years (t=8000) (Figure 4.11 a). As expected, based on the DYNA-VEG parameterization of phenology, ET declined to a minimum during senescent periods and in response to reduced moisture availability. The hillslope vegetation was unable to access the saturated zone, as the water table was below the specified rooting depth, thus all water is taken from the unsaturated zone.

Within the riparian terrace, plants accessed both the unsaturated and saturated zone to satisfy their water demands. Mean annual total ET ranged from 543 mm/y to 692 mm/y, with a mean daily uptake between 0-7 mm/d from the unsaturated and saturated zone. This result is consistent with water uptake by facultative phreatophyte plants, such as mesquite, that frequently access water from both the saturated zone and shallow soil moisture in cases when the water table is below their respective tap root depths (Figure 4.11 b, e). By contrast, deep rooted vegetation in the riparian floodplain primarily accesses the shallow groundwater, with daily evapotranspiration rates ranging from 0-8 mm/d and annual totals between 823 mm/y and 981 mm/y.

The modeled daily evaporation rates for the riparian floodplain are generally in good agreement with values reported in previous studies for riparian cottonwood forests, where values of up to 1100 mm/y were observed in riparian cottonwoods in California (Irmak et al. 2013; Mayes et al. 2020). No water uptake from the

unsaturated zone occurs under shallow water table conditions because uptake from the saturated zone is the first option for these groundwater-dependent trees (Figure 4.11 c, f). Overall, there is a higher interannual variability in ET_{uz} in both the hillslope and the riparian terrace, which can be attributed to the interannual variability in precipitation and associated shallow soil moisture. In contrast, ET_{sz} in the riparian terrace and floodplain show less variability, as the water table is relatively stable, with minimal seasonal fluctuations (< 0.4 m).

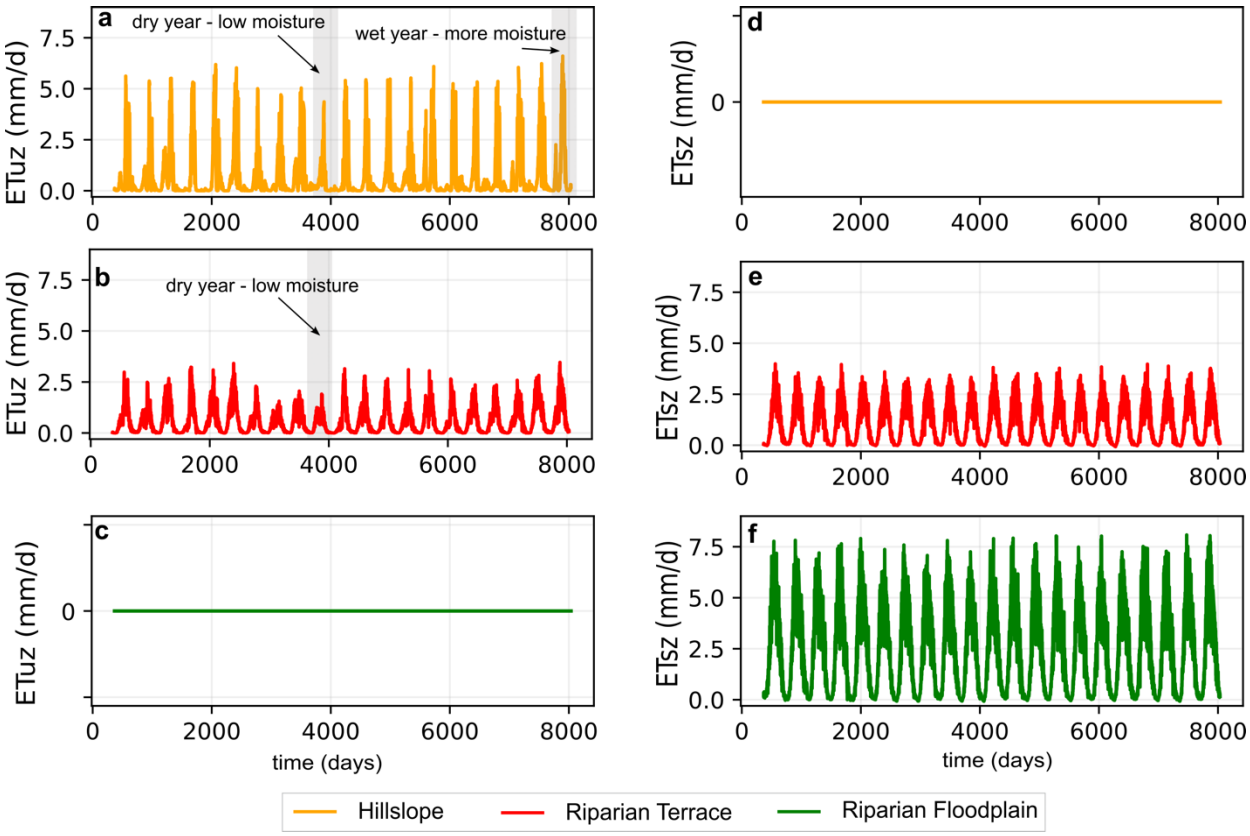

Figure 4.11: Evapotranspiration from the a-c) unsaturated and e-f) saturated zone in the hillslope (orange), riparian terrace (red) and riparian floodplain (green). No ET from the saturated occurred in the hillslope as plants primarily took water from the shallow root zone. In the riparian floodplain, water uptake primarily occurred through capillary rise from the shallow groundwater.

4.4.1.3 Shallow root zone moisture

Figure 4.12 shows the distributions of soil moisture for each plant functional group. On the hillslope, soil moisture variations were predominantly driven by precipitation variability and water uptake from shallow rooted vegetation. Over the simulation period, mean saturation was at 34%, with periods of low precipitation intensity and high evaporative demand resulting in saturation levels of < 20% (Figure 4.12 a). This translated into reduced plant water availability and lower actual evapotranspiration rates. Saturated conditions (> 95%) occurred during wetter years, which momentarily increased water availability for plants and contributed towards diffuse recharge. Due to the loamy sand texture in the hillslope water retention was generally lower than in the riparian terrace and floodplain, where higher loam and clay contents contribute to higher water holding capacities.

Within the riparian terrace, saturation levels ranged from 38% to 78%, with mean saturation of about 50%, while in the riparian floodplain mean saturation was around 75%. It should be noted that saturation in the riparian terrace may be overestimated, as only a limited amount of ET is taken from the unsaturated zone by riparian trees as parameterized here. More accurately, additional shallow rooted vegetation, such as grasses and shrubs, is often present in the understory and contributes to water uptake and AET from the shallow soil, which would generate more variability and lower overall soil moisture in these locations.

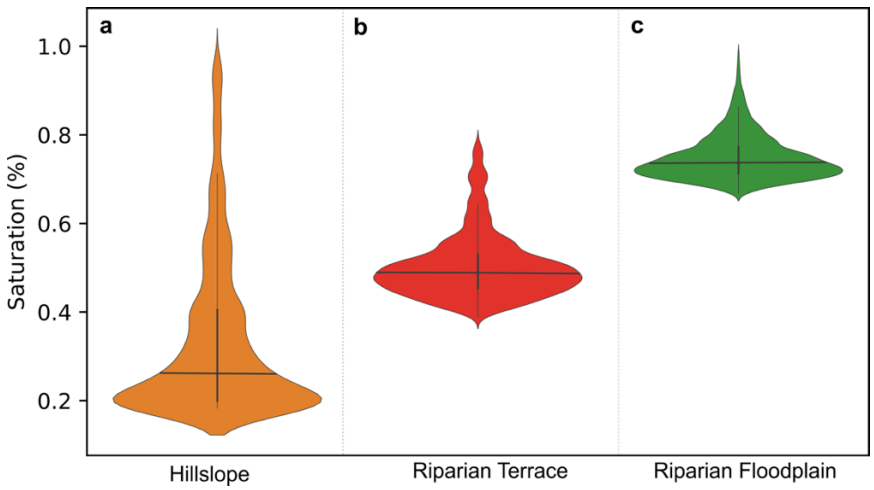

Figure 4.12: Distributions of soil saturation between areas of different vegetation cover types and soil properties across the model domain.

4.4.1.4 Water table elevation

The evolution of recharge and water table elevation across the riparian channel is shown in Figure 4.13. The distribution of recharge along the riparian channel was characterized by an accumulation of water towards the downstream end, where a constant head boundary condition was implemented (Figure 4.13 b). Recharge amounts were strongly coupled to precipitation variability with low annual totals of 77 mm/y during dry years and up to 501 mm/y in wet years. Mean DTG in the riparian channel was 3.8 m with small interannual fluctuations of up to 0.4 m. Groundwater mounding occurred beneath the riparian channel in response to focused recharge events and dissipated over time as recharge declined (Figure 4.13 f). The water table in the riparian channel was generally above the specified tap rooting depth of vegetation, thus providing consistent access to riparian vegetation, to maintain maximum evapotranspiration rates (Figure 4.11 f). In the riparian terrace mean DTG was 6.6 m, with similar small interannual variations of up 0.3 m. Here, the water table fluctuated between the specified tap root depth and the extinction depth. These fluctuations translated into a dual use of groundwater and shallow soil moisture by vegetation to satisfy water demands (Figure 4.11 b, e). In the hillslope, the water table was generally well below the shallow rooting depth of 500mm, at an average of 7.6 m and thus not accessible to shallow-rooted vegetation. The simulated variations in the water table show that DYNA-VEG generates plausible spatial and temporal changes in the water table in response to recharge contributions.

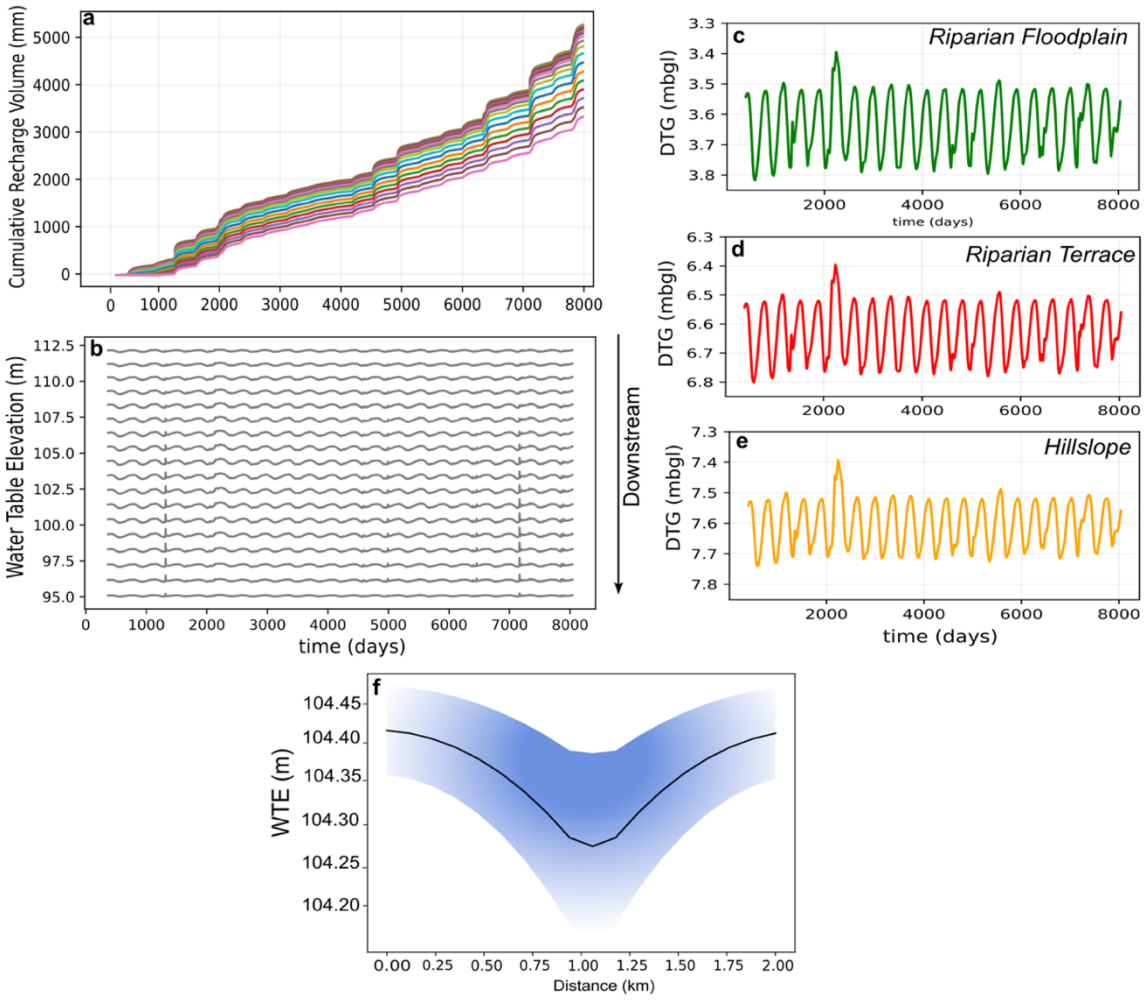

Figure 4.13: Evolution of a) recharge and b) water table elevation along the riparian channel. The specified boundary condition at the outlet controls the accumulation of recharge and shallow water table. Depth to groundwater across the horizontal transect in the c) riparian floodplain (green), d) in the riparian hillslope (red) and e) in the hillslope (orange). f) Groundwater mounding occurred beneath the riparian channel. The black line indicates the mean water table elevation across the horizontal transect, the blue shading highlights the interannual variability of water table fluctuations in response to recharge.

4.4.1.5 Vegetation water stress

Hillslope

Vegetation water stress was calculated according to Eq. 4.12. Figure 4.14 shows the evolution of water stress in the hillslope, where in wet years with consecutive months of strong monsoon precipitation, the trace of stress dissipated for longer periods due to the increasingly favorable moisture conditions during and after a rainy period. The characteristic feedback between strong monsoon precipitation and high available moisture allowed plants to transpire almost at the maximum rate during the summer growing period.

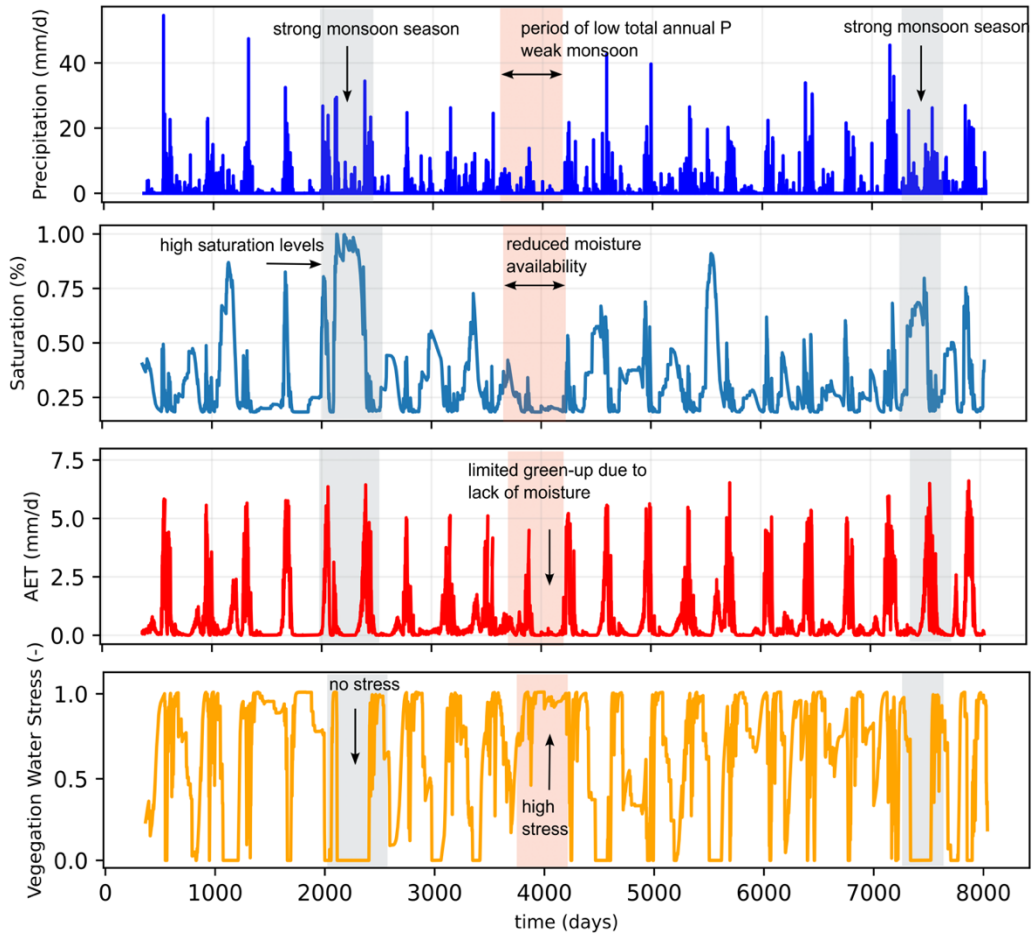

Figure 4.14: Evolution of a) precipitation, b) soil moisture, and c) evapotranspiration into d) vegetation water stress along the hillslope. Precipitation variability was the key driver of vegetation water stress for shallow rooted soil moisture dependent vegetation.

Conversely, plant transpiration rates reached minimum values during weak monsoon periods, incurring extended periods of maximum vegetation water stress, up to 40% of the time during the simulation period. Vegetation starts to brown and enter a state of senescence/dormancy, which extends until the return of favorable moisture conditions (t= 4000).

Riparian terrace and floodplain

Figure 4.15 shows the water stress response of vegetation in the riparian terrace and floodplain. The difference in soil hydraulic properties as well as depth to groundwater are the key drivers of water stress in the riparian terrace and floodplain. In the riparian terrace, vegetation experienced stress only about 20% of the time in response to seasonally varying soil moisture. However since riparian terrace trees also accessed the saturated zone to satisfy water demands, they were likely to compensate for the reduced soil moisture availability during unfavorable rainfall years (t=4000). In the riparian floodplain, due to the high saturation levels below the riparian channel and access to the shallow water table, riparian floodplain trees did not exhibit any signs of vegetation water stress.

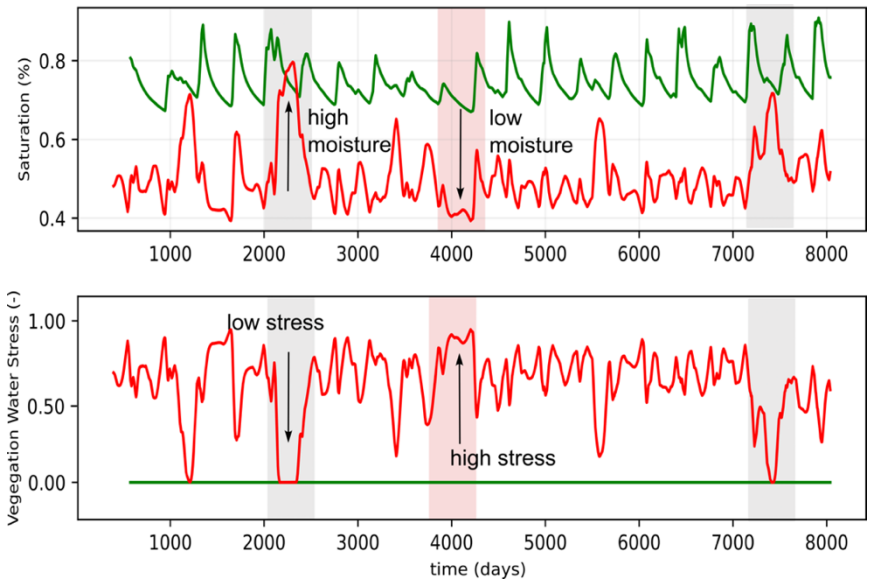

Figure 4.15: Vegetation water stress in the riparian terrace (red) and riparian floodplain (green). Due to high saturation levels below the channel and constant access to the shallow water table, riparian floodplain trees did not experience water stress. Vegetation in the riparian terrace experienced occasional moderate water stress, in response to soil moisture variability.

4.4.2 Hydrological responses to altered climate forcing

4.4.2.1 Domain water balance

The differential effects of altered climate forcing on the hydrological components of the water balance are presented in Figure 4.16 and a summary of the water balance components is presented in Table 4.6. The results show that the reduced precipitation input in Scenario 1 (P_{total} (-)) also reduced the amount of water available for infiltration by 40%. However, the amount of infiltration relative to the precipitation input remained similar, with 3% more water infiltrating as more throughfall occurred. This can be attributed to the reduced vegetation greenness associated with a lower precipitation regime, which reduced canopy capacity of plants to intercept incoming water. The amount of focused recharge was reduced to less than 1% of the incoming precipitation. Diffuse recharge remained similar, with about 2% of precipitation percolating through the soil. However, focused recharge was reduced to an amount <1% of incoming precipitation. Most notably, the amount of water returned to the atmosphere by evaporation from the unsaturated and saturated zone exceeded the incoming precipitation by approximately 40%, which highlights the existing moisture deficit between incoming precipitation and evaporative losses, common in drylands, as a result of groundwater use by deeper rooted vegetation.

Simulations of increased PET only had minimal effects on the overall water partitioning, with only minimal changes to the amounts of infiltration, excess, transmission losses and recharge. An important caveat regarding the inclusion of PET effects in the phenology model applies to this scenario, as changes to the surface energy balance would likely also affect phenology. However, such interactions are initially not accounted for in the phenology model. The lower water table in Scenario 3 (WTE (-)) did not affect the availability of water to hillslope vegetation in the shallow subsurface and the subsequent uptake by shallow-rooted vegetation. Similar to the historic baseline simulation, 96% of incoming precipitation infiltrated into the soil. Excess and transmission losses were slightly reduced to about 3 and 2 % respectively. As a result, the amount of focused recharge is < 1% as it is consistently reduced via the ET demand before it reached the deeper water table.

In Scenario 4, 96% of the infiltrated water was returned to the atmosphere via evapotranspiration, with the remaining 1% of water partitioned into excess and transmission losses. No evaporation from the saturated zone occurred, as the water table was too deep for vegetation to access.

Table 4.6: Summary of hydrological components of the water balance between climate change scenarios. Percentages are presented relative to the input precipitation.

	Baseline	*Scenario 1* P_{total} *(-)*	*Scenario 2 PET (+)*	*Scenario 3 WTE (-)*	*Scenario 4 PET(+),* P_{total}*,WTE(-)*
P total	5405 mm	2162	5405	5405	2162
Infiltration	5031 mm (93%)	2066 mm (96%)	5030 mm (93%)	5182 mm (96%)	2095 mm (97%)
Runoff	300 mm (6%)	33 mm (2%)	297 mm (6%)	149 mm (3%)	2 mm (<1%)
Transmission Losses	241 mm (4%)	31 mm 1%	240 mm (4%)	102 mm (2%)	2 mm (<1%)
Focused Recharge	225 mm (4%)	17 mm (< 1%)	224 mm (4%)	4 mm (<1%)	0 mm 0%
Diffuse Recharge	148 mm (3%)	45 mm (2%)	144 mm (3%)	62 mm (1%)	0 mm 0%
Discharge	58 mm (1%)	2 mm (< 1%)	57 mm (1%)	48 mm (<1%)	0 mm 0%
PET total	5523 mm	5523	5969	5523	5967
ET_{uz}	4827 mm (90%)	1981 mm (91%)	4821 mm (89%)	5085 mm (94%)	2083 mm (96%)
ET_{sz}	1804 mm (34%)	1956 mm (90%)	2101 mm (39%)	441 mm (8%)	0 0%

4.4.2.2 Root zone soil moisture

Looking at the propagation of altered climate forcing through the unsaturated zone in Figure 4.16, Scenario 1 (P_{total} (-)) shows a significant reduction in the amount of available water for infiltration in the hillslope (ks-stat=0.35, $p < 0.001$) (Figure 4.16 a) and riparian terrace (ks-stat=0.25, $p < 0.001$) (Figure 4.16 b). In the riparian floodplain, the reduction of transmission losses subsequently reduced the moisture in the unsaturated zone (ks-stat=0.85, $p < 0.01$) (Figure 4.16 c). Scenario 2 (PET (+)) did not significantly change saturation levels throughout the model domain (all tests had $p > 0.05$). Scenario 3 (WTE (-)) did not significantly affect the hillslope (ks-stat=0.35, p=0.23), however significant responses can be seen in the riparian terrace (ks-stat=0.58, $p < 0.001$) and the floodplain (ks-stat=0.93, $p < 0.001$) (Figure 4.16 b, c). Most notably, a significant response of soil moisture in the riparian floodplain can be seen in Scenario 4 (stat=0.99, $p < 0.001$), where saturation was reduced to a minimum due to severely reduced transmission losses and the lack of interaction with the shallow water table, illustrating the overarching effects of climate forcing and altered water table conditions on surface-subsurface interactions in riparian areas.

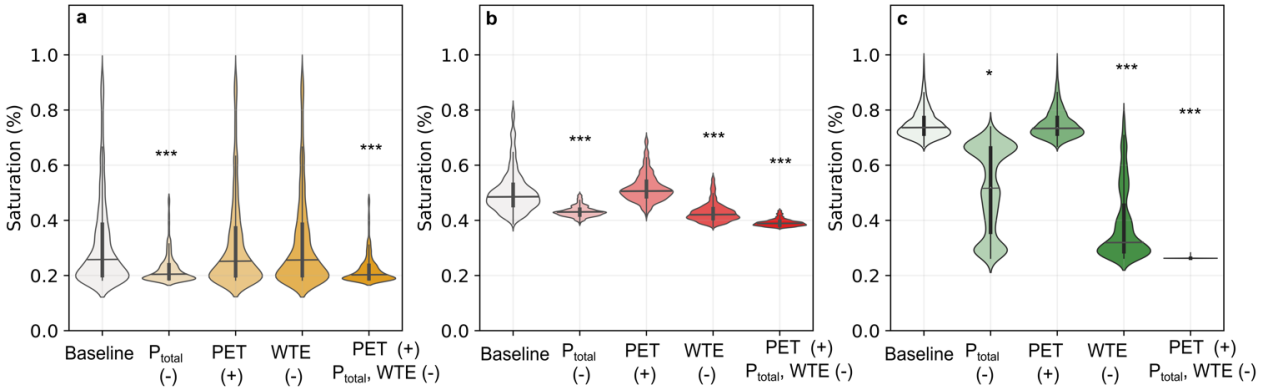

Figure 4.16: Soil saturation of the unsaturated zone in the a) hillslope, b) riparian terrace and c) riparian floodplain between the different scenarios of climate forcing. Statistical significance is indicated by an asterisk at the 0.001 (***) and 0.05 (*) level.

4.4.2.3 Evapotranspiration from the unsaturated and saturated zone

Hillslope

Actual evapotranspiration and respective contributions from the unsaturated and saturated zone are shown in Figure 4.17. Scenario 1 (P_{total} (-)) (ks-stat=0.17, $p < 0.05$) and Scenario 4 (PET (+) / P_{total}, WTE (-)) (ks-stat=0.13, $p < 0.001$) had the most significant effects in the hillslope. In both scenarios, the reduced water availability in the unsaturated zone due to a reduction in P, affected the amount of available moisture in the shallow soil. Scenario 2 (PET (+)) and Scenario 4 (WTE (-)) showed no significant differences in shallow moisture availability (ks-stat=0, p=1.0, ks-stat=0.009, p=0.87 respectively) to the historic baseline, as the increased PET and lowered water table did not significantly alter the moisture availability of hillslope vegetation. The result is consistent with observations of phenology-hydroclimate relationships observed in SE Arizona (Chapter 3), where vegetation responses are primarily driven by precipitation variability. However, a caveat to Scenario 2 applies in regard to PET-phenology interactions which may have resulted in an overestimation of moisture availability.

Riparian Terrace

In the riparian terrace, Scenario 1 (P_{total} (-)) significantly reduced the total amount of evaporation (ks-stat=0.089, $p < 0.001$). Over the simulation period, the amount of ET_{uz} significantly declined by almost 50% compared to the historic baseline, due to significantly lower moisture availability (ks-stat=0.26, $p < 0.001$). Due to the complimentary use of water from the saturated zone, total AET only declined by about 10%, compared to the historic baseline simulation. The increased evaporative demand in Scenario 2 (PET (+)) reduced peak evaporation from the unsaturated zone, which was compensated by $ET_{sz,}$ which increased by approximately 25% as plants switched to using more groundwater to account for the reduced moisture availability in the unsaturated zone (Figure 4.17 e, h). Significant reductions in AET within the riparian terrace were visible under Scenario 3 (WTE (-)) (ks-stat=0.356, $p<0.001$), and Scenario 4 (PET (+), P_{total}, WTE (-)) (ks-stat=0.47, $p<0.001$), which significantly reduced plant evapotranspiration (Figure 4.17 e, h), as a results of the lower water table.

Riparian Floodplain

In the riparian floodplain, a shallow water table within the rooting zone of riparian vegetation buffered the negative effects of the reduced precipitation in Scenario 1 and Scenario 2, thus causing no significant reductions in AET (ks-stat=0.19, p=0.28, and ks-stat=0.22, p=0.17 respectively). Only when the water table dropped below the specified extinction depth in Scenario 4, plants used the residual moisture in the subsurface to satisfy their water demands, causing a significant decline in AET (ks-stat=0.57, p <0.001), with maximum daily evaporation rates declining to 3mm/d (Figure 4.17 c, f, i).

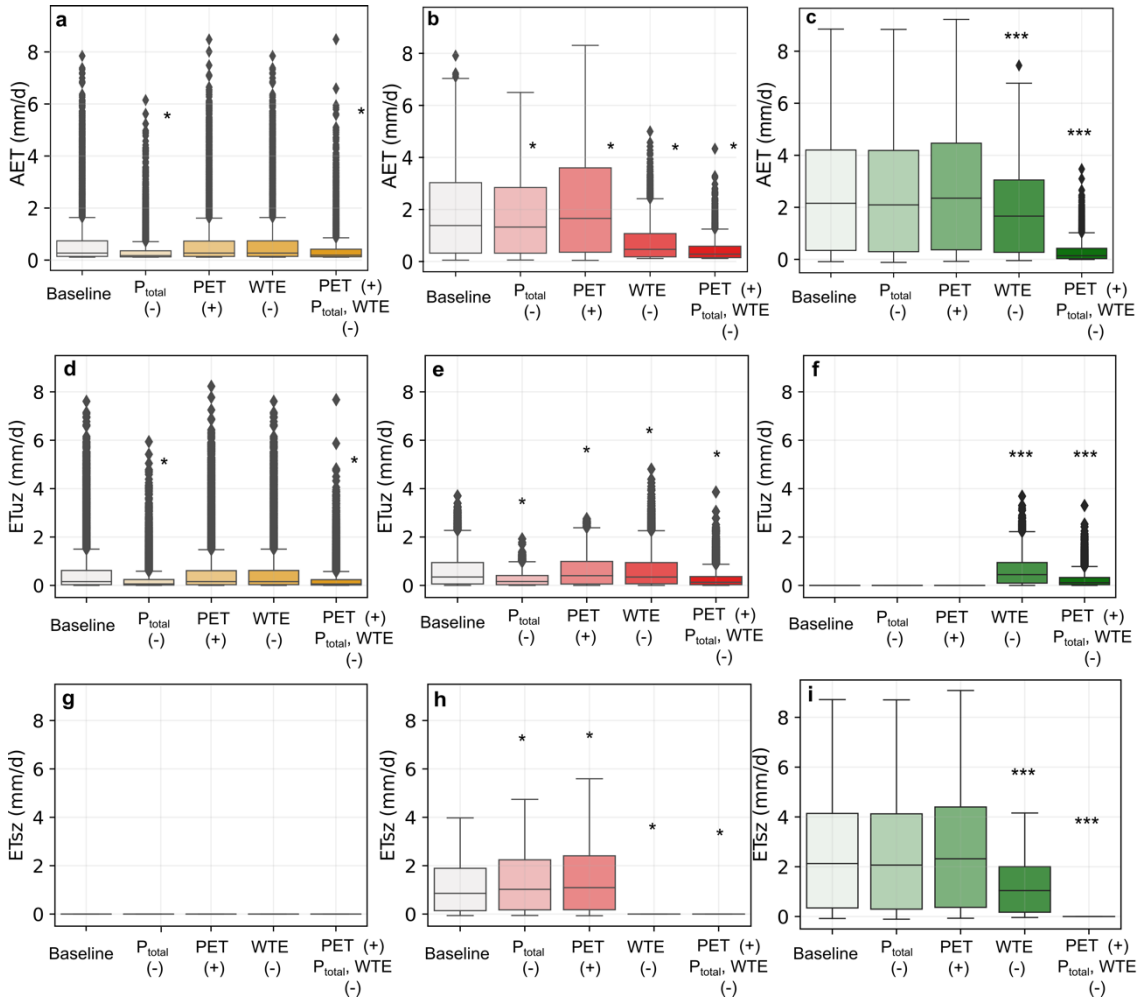

Figure 4.17: a-c) Actual evaporation, d-f) evapotranspiration from the unsaturated and g-i) from the saturated zone, for the hillslope (orange), riparian terrace (red) and riparian floodplain (green) under different climate change scenarios. Statistical significance is indicated by an asterisk at the 0.001 (***) and 0.05 (*) level.

4.4.3 Vegetation responses to altered climate forcing

4.4.3.1 Vegetation water stress

Hillslope

Figure 4.18 shows a quantification of vegetation water stress to the altered hydroclimate forcing and changes to seasonal water availability. In the hillslope most notably the Scenario 1 (P_{total} (-)) and Scenario 4 (PET (+), P_{total}, WTE (-)) incurred the most significant changes to the distribution of stress responses (ks-stat=0.36, p<0.001; ks-stat=0.28, p=0.003 respectively) (Figure 4.18 a). The reduction of incoming precipitation and available root zone moisture showed a strong negative correlation (R = -0.89, p < 0.05) with stress, resulting in a shift towards more peak stress periods, with an average value of 0.76 (higher stress) for more than 40% of the total simulation period and less than 5% of the time with no or low stress. Due to the reduced precipitation totals, stress was never completely reduced to zero, as residual soil moisture deficits remained throughout the model simulation. The results are consistent with the responses seen in soil moisture and in reduced evapotranspiration (Figure 4.16).

Conversely, scenarios of PET (+) and WTE (-) did not result in significant changes to moisture availability as to incur noticeable changes in the occurrence of stress (ks-stat=0.31, p=0.68; ks-stat=0, p=1.0 respectively). The overarching effects of reduced moisture and increased atmospheric demand were strongly correlated to the increased stress in Scenario 4 (PET (+), P_{total}, WTE (-)) (R = -0.99, p<0.05). This resulted in the strongest stress responses, where low stress levels (<0.2) only occurred 2% of the time over the entire simulation period, while plants experienced peak stress (>0.7) almost 80% of the time, due to the compound effects of low soil moisture availability and higher evaporative demand and lower precipitation.

Riparian Terrace

The responses seen in the riparian terrace (Figure 4.18 b, e), can be attributed to the variable water use of shallow soil water as well as limited use of groundwater. Due to the overall deeper position of the water table, plants generally used soil moisture in addition to groundwater. However, the reduced seasonal precipitation

input in Scenario 1 limited the amount of unsaturated zone moisture thus incurring periodical peak stress responses up to 20% of the time (>0.7) (ks-stat=0.63, p<0.001). The lower water table in Scenario 2 (PET (+)) and Scenario 4 (P_{total} (-) and PET (+)) created a greater reliance within the riparian terrace on residual root zone moisture. As soil moisture declines through plant water uptake, this resulted in peak stress up to 80% of the time, and almost permanent stress conditions in Scenario 4, as increased PET and greater soil moisture deficits further aggravated the limited water availability to these trees.

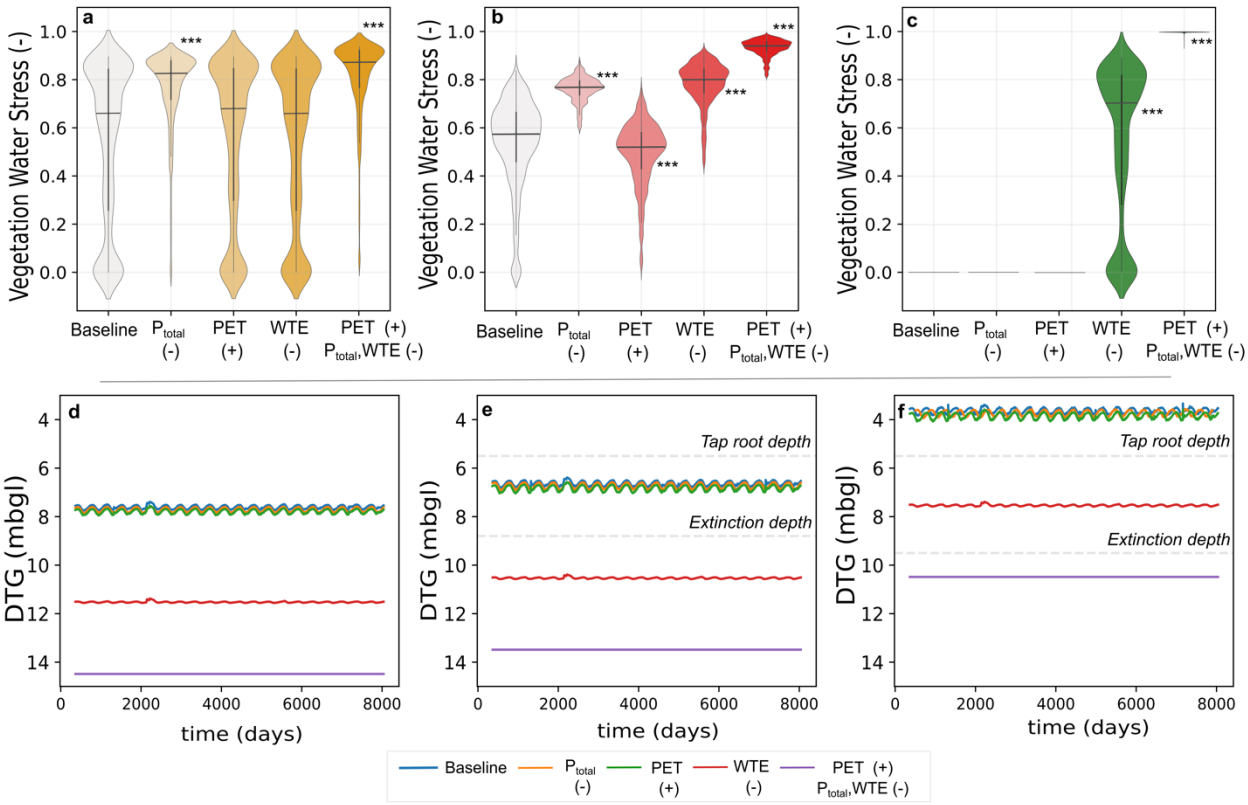

Figure 4.18: Vegetation water stress in the a) hillslope, b) riparian terrace and c) riparian hillslope under varying climate and hydrological forcing. Evolution of water levels in the d) hillslope, e) riparian terrace and f) riparian floodplain under varying hydrologic and climatic forcing. Statistical significance at the 0.001 level is denoted with an asterisk (***)

Riparian Floodplain

In the riparian floodplain it can be assumed that vegetation experiences peak stress primarily in response to varying positions of the water table. While grasses on the hillslope faced short and frequent water stress due to precipitation variability, riparian trees were generally buffered from dry periods through their consistent access to shallow water. As such, deeper rooted riparian floodplain vegetation would not be significantly impacted by the changes imposed in Scenario 4 (P_{total} (-) and PET (+)). Significant responses were observed in Scenario 2 (PET (+)) and Scenario 4 (PET (+), P_{total}, WTE (-)) (ks-stat=0.023, $p<0.001$; ks-stat=0.99, $p<0.001$ respectively) (Figure 4.18 c, f), as the water table declined to a deeper level in each scenario. In Scenario 2 (PET (+)), trees compensated for the lower water table with water from the shallow root zone, thereby moderating stress responses and resulting in only short periods of peak stress (< 40% of the time) and even brief periods of no stress (about 25% of the time). The deeper water table in Scenario 4, resulted in vegetation experiencing almost consistent stress. The results are similar to observations from previous studies of riparian vegetation, where threshold responses of reduced evapotranspiration and growth have been observed once the water table exceeded a threshold depth (Snyder and Williams 2000; Lite and Stromberg 2005a; Williams et al. 2022b).

4.5 Discussion

The baseline simulation performed with the novel DNYA-VEG module as part of the DRYP model represent a step forward towards quantifying the impacts of climate change on dryland water partitioning processes and predicting ecohydrological interactions in a changing environment. The inclusion of DYNA-VEG within this existing hydrological modeling framework inherently improves the linkages between climate, soil and vegetation, which is especially important for exploring the direct and indirect effects of climate change on natural systems. Furthermore, the synthetic experiments broadly illustrate the differential responses of plant functional groups to changes in water availability (soil moisture and groundwater) and associated evapotranspiration by vegetation. Previous studies have underscored the key role of soil water content in controlling overall ecosystem dynamics, including infiltration, runoff generation, capillary fluxes, groundwater and plant transpiration (Laio et al., 2009, Sabathier et al., 2021, Tamea et al., 2009). More specifically, the quantification of vegetation water stress revealed that each change in hydrological forcing affects the ecohydrological processes and vegetation differently. At one point reduced precipitation totals increased water stress in hillslope vegetation, but not in the riparian zone where the presence of shallow groundwater buffered such climatic changes. Conversely, a significantly deeper water table resulted in peak forest water stress as plants are unable to compensate the loss of constant access to groundwater with the sole us of shallow soil moisture. The new model framework is thus a valuable new tool to understand climate change and vegetation impacts at the appropriate temporal and spatial scales.

Model simulations of decreased precipitation totals exposed the overarching effects of vegetation-soil feedbacks in grasslands within a dryland environment on a broader scale. The interaction between precipitation variability and water holding capacity in the hillslope illustrated the high temporal variability in vegetation water stress. Similar vegetation responses were observed in previous studies from other arid and semi-arid grassland biomes (Gremer et al. 2015; Felton et al. 2020) and corroborate my simulations of soil moisture from Southern California (Chapter 2) and the phenological responses to precipitation variability I observed in SE Arizona

(Chapter 3). In general, changes to the spatial and temporal distribution of shallow root zone moisture are key factors in dryland grassland ecosystem functioning, however, with certain nuances across the landscape.

Ultimately, under a warmer and drier climate as simulated here, accounting for hydroclimatic variations across extended spatial scales is crucial to assess regional water deficits and plant drought stress. The original description of water stress after Porporato et al. (2001) already considered the influence of soil moisture dynamics on vegetation. However, the novel implementation in DYNA-VEG also takes account vegetation responses to interannual climatic fluctuations through the new phenology model (Chapter 3), an aspect previously not fully accounted for in the original framework. Incorporating this more accurate assessment of water stress into ecohydrological modeling is an important step forward in the assessment of plant survival and mortality under future climate conditions, particularly in conjunction with restoration efforts of grassland environments.

While the selection of synthetic simulations I presented here are purposefully simple and within an artificial domain, the results are still considerate of the main underlying mechanisms and key processes that define ecohydrological interactions in drylands across different spatial and temporal scales. Considering the variable soil textures across the model domain – from sandy soil in the hillslope to loamier soils in the riparian floodplain - the results highlight the importance of soil hydraulic properties on the redistribution process of precipitation moisture in the shallow soil. This ultimately determines the accumulation of potential soil water deficits and the extent of vegetation water stress responses and provides a more detailed assessment of vegetation water stress than in the simplified model simulations I presented in Chapter 2. The spatial differences in soil hydraulic properties between xeric, mesic and hydric environments mediate the impacts of rainfall events on soil moisture variability and percolation to deeper layers, creating spatially variably water stress responses. In this context, the inclusion of DYNA-VEG in DRYP improves the assessment of surface-subsurface interactions of soil moisture dependent vegetation and water partitioning processes within hillslope areas of low water holding capacity.

At the same time, in the riparian zone, the improved representation of vegetation - groundwater interactions highlight the relevant links between soil hydraulic properties, groundwater mounding, recharge, and plant water availability. Considering groundwater dependent vegetation, my model simulations show that a climate change expressed through a deeper water table and increased precipitation variability and evaporative demand would preclude the persistence of shallow groundwater access by riparian vegetation and lead to extended periods of elevated physiological stress previously unseen. On the other hand, changes to precipitation variability without a suppressed water table did not cause severe impacts on riparian vegetation, due to the persistent presence of shallow groundwater. This phenomenon is particularly prevalent in riparian zones with shallow water tables and strong streamflow-groundwater interactions, as is the case in the perennial reaches along the San Pedro River in SE Arizona. Here, the near-constant access to groundwater enabled cottonwood trees to maintain growth, as well as new seedling establishment, even during drought periods with reduced precipitation and increased atmospheric demand. Therefore, in areas with shallow water tables, it can be expected that significant changes to the water table, would lead to a significant decline in vegetation productivity and health. Significant cottonwood mortality has been observed in areas where the water table rapidly and permanently dropped by 1m (Stromberg et al., 2005). Particularly in riparian areas of the Southwest, such changes to the water table are indeed expected to continue or increase in the future, most likely inducing a train of events from declining seedling establishment to the loss of mature forests and associated habitat, as well as changes to streamflow and aquatic habitat conditions. However, if mature trees are able to continue deep root growth as water tables decline by supplementing transpiration needs with water from the shallow soil, they may be able to tolerate some water stress (Snyder et al., 2000, Lite et al., 2005).

Under such circumstances, it can be assumed that permanent exposure to drought stress would likely lead to widespread mortality as trees are unable to maintain past plant water uptake. Because of the sensitivity of riparian vegetation to groundwater fluctuations and human abstraction that leads to water table suppression across the region, the new representation of vegetation-groundwater interactions I presented here may support much needed long-term planning of terrestrial riparian ecosystem

management. In line with the overall goal of this research, the presented modeling framework explicitly integrates vegetation with surface, subsurface and groundwater processes, providing reliable estimates of surface and subsurface components of the water balance to assess vegetation water stress responses across variable spatial and temporal scales.

Within the model riparian threshold depths, such as the tap root and extinction depth, are broadly based on past observations of recession rates of several meters or water tables below an observed depth causing a decline in riparian vegetation health (Stromberg and Tiller 1996; Snyder and Williams 2000; Williams et al. 2022). However, a more definitive threshold of ecologically ideal and sustainable groundwater depths or sustainable yield is not always well defined (Rohde et al. 2021a; Saito et al. 2021). Through stochastic simulations of water table decline within a certain range, in addition to multi-year empirical-stochastic climate forcing (Singer et al. 2018), the range of tolerable or intolerable water table depths/ thresholds that would impair or enable riparian tree survival and recruitment can be explored relative to historic conditions. This is imperative for restoration and conservation plans, as historic observations alone may not be suitable management targets. Similarly, assumptions of a return to historic water table or stream flow conditions to maintain sustainable ecosystem function in the future may be flawed with respect to uncertainty regarding certain climate projections (Capon et al. 2013; Perry et al. 2015; Wilkening et al. 2019).

In that context, changes in the model parameterization of aquifer properties, channel interaction with groundwater discharge, as well as initial climate forcing suggest opportunities for future model experiments. Such experiments would further elucidate the detailed characteristics of sustainable water table thresholds that most influence riparian vegetation and water partitioning processes on a regional level. For example: a switch between a highly permeable to a less permeable aquifer (by changing hydraulic conductivity) would affect recharge and percolation rates. Changes to transmissivity and diffusivity would further affect aquifer responsiveness. At the same time, changes to soil hydraulic properties in the unsaturated zone (i.e. greater spatial variability in soil textures or less permeable soils) would affect

infiltration rates and runoff generation, which would better reflect the spatial heterogeneity of the landscape and affect the partitioning of water. The inclusion of groundwater abstraction (i.e. wells) would further affect potential recharge rates and water table fluctuations. Particularly in semi-arid areas regional water management will benefit from such simulations as future riparian habitat management plans must reconcile ecological and agricultural/urban water demands and thresholds by considering the limits and requirements of riparian vegetation water use based on a scientific understanding of water partitioning and climate change effects. Finally, investigating in more detail the effects of extreme precipitation events and PET changes on the water table dynamics, runoff generation, streamflow dynamics and recharge rates would be another key aspect crucial to future water management.

Although results from the synthetic experiments using the newly developed DYNA-VEG module serve as a proof of concepts, there are remaining uncertainties in the parameterization of vegetation, in particular the spatial distribution of plant functional groups and interactions among species. The spatial distribution of vegetation and areal coverage were kept purposely simple in the initial model simulations. However, dryland landscapes are typically far less homogenous and with considerable higher spatial variability. Therefore, questions about ecohydrological processes pertaining to specific species interactions, for example, shrub and grass understory in the riparian floodplain and terrace (the fractional pixel problem) or shifting vegetation distribution across spatial gradients and transitions in vegetation cover (e.g. vegetated to bare ground) are left to be explored. To do so, within a cell multiple vegetation types can be specified that would affect the amount of water drawn from the saturated and unsaturated zone. Also, vegetation interactions with spatially limited storm events and temporal changes to rooting depths (e.g. development of deeper roots in response to deeper water tables) can be explored through small modifications of the DYNA-VEG model framework. In detail, this could be achieved by coupling the STORM model by Singer et al. (2018) to DRYP, thus creating spatially variable precipitation scenarios of varying intensity and frequency. Together with spatially more variable vegetation distribution and soil textures across the landscape, this would generate novel insights into the effects of localized streamflow and runoff events. Such model simulations would ultimately

provide further clarification on localized ecohydrological processes and discern the role of vegetation in moderating water partitioning of local extreme events.

Future modeling work should also focus on addressing remaining questions regarding hydrological thresholds and conditions that allow for riparian seedling recruitment and habitat changes as well as shrub encroachment in channels (Seavy et al. 2009; Perry et al. 2015; Singh et al. 2021). In the case of upland dryland environments, current trends of bare ground transitions and grass-shrub conversion can be explored through DYNA-VEG, which is of particular interest in light of advancing desertification and loss of habitat in drylands (Schreiner-McGraw et al. 2020). The potential degree of vegetation cover changes, especially along riparian streams may have import implications on water partitioning processes at regional scales. Spatial and temporal climate driven changes in vegetation cover, density and species distribution could then feed-back on the expression of climate change, with either strong positive effects or detrimental negative effects, that further aggravate changes to the water cycle and aggravated the aridification of drylands.

The integration of further climate change and land-use change scenarios, as well as spatial and temporal variability in vegetation cover, aquifer and soil hydraulic properties are a next key step in expanding the modeling capabilities to further discern the impacts of coupled climate and land-use changes on vegetation water stress. From a vegetation perspective, through a refinement of spatial vegetation dynamics (e.g. vegetation cover density, species interactions & composition) multiple questions could be addressed regarding desertification, invasion of species, habitat expansion and species succession in response to climate variability (Notaro et al. 2012; Capon et al. 2013; Gremer et al. 2015; Perry et al. 2015; Peters et al. 2015). More specifically, a refinement of the phenology model using remote sensing data that includes changes in vegetation over space and time (i.e. forest-dieback, expansion of grassland, disturbance from wildfire) would add the necessary dynamism to answer such questions. Alternatively, adding a level of stochasticity to the spatial distribution of vegetation, including density and species composition, is a possibility. A more spatially explicit characterization of the vegetation dynamics would certainly further contribute to a broader understanding of the role of climate on water partitioning

processes and vegetation dynamics across dryland landscapes, with important implications for land and resource management balancing future ecosystem and human water requirements.

4.6 Conclusion

The performance and functionality of DYNA-VEG were evaluated through a range of synthetic experiments using baseline historic climate conditions. Additionally, model simulations using altered climate forcing were performed to quantify the effects of climate change and evaluate the range of climate-vegetation interactions, particularly vegetation water stress. Baseline simulation results showed overall good agreement in terms of relative contributions of the main hydrological components to the overall domain water balance. Simulations of surface and subsurface flux and storage components of the water balance, including soil moisture, evapotranspiration from the saturated and unsaturated zones, and water table elevation confirmed the functionality of DYNA-VEG, by producing reasonable behaviors of hydrologic and vegetation dynamics that are representative of dryland vegetation dynamics.

The results of modeled vegetation water stress through the DYNA-VEG modeling experiments presented above, have shown that the drivers of stress vary among vegetation types and that tracking potential water stress thresholds requires a complete understanding of the hydroclimate drivers of vegetation dynamics. While in riparian forests, climate change induced lower water tables will expose riparian vegetation to prolonged water stress, changes to precipitation regimes will be the key drivers of vegetation water stress for hillslope vegetation, due to declining soil moisture. Most importantly, the compound effects of a warmer and drier climate and lower water tables would detrimentally alter the spatial and temporal availability of water sources to riparian forests and hillslope vegetation, causing by far the most severe impact to vegetation due to dried out soils, declining recharge and lower water tables. Because the model considers these inherent climate-vegetation-soil interactions through the parameterization of phenology and climate-hydrology relationships, it paves the way for larger scale, in depth explorations of natural and anthropogenic drivers of ecohydrological dynamics. This knowledge would

fundamentally improve groundwater and ecosystem management plans in water-limited regions, leading to sustainable and adaptive solutions cognizant of the “new normal” climate conditions.

CHAPTER 5

5 Final Discussion and Conclusion

Through the research presented in this thesis, I set out to enhance the understanding of vegetation responses to water stress under historic and future climate conditions over a range of temporal and spatial scales; from local to regional and across a range of biomes and regions, from grasslands in Southern California, to riparian forests in SE Arizona. To this end, I used multiple historical climate data sets of different temporal resolutions and remote sensing information, as well as different modeling frameworks to address the main objectives defined at the beginning. The propagation of the recent multi-year drought into local soil moisture and the resulting shifts in vegetation phenology highlighted the contemporary trends of earlier drying and prolonged senescence during the recent multi-year drought in grasslands in Southern California (Chapter 2). Model simulations of soil moisture under plausible future climate change scenarios elucidated the vulnerability of grasslands to persistent soil moisture anomalies under warmer and drier climate, which would limit recovery of vegetation and further aggravate the wildfire potential throughout lowland environments (Objective 1).

The disaggregation of historical hydroclimate-phenology relationships of different plant functional groups in a dryland region of SE Arizona illustrated the differential key hydroclimate drivers of phenology in dryland vegetation. Water availability, either in the form of precipitation moisture or groundwater, is the primary growth-limiting source driving interannual greenness variability (Objective 3). The improved understanding of climate-phenology relationships led to the formulation of a simple empirical phenology model to predict future vegetation responses (Chapter 3), which led to the design of a new dynamic vegetation module, DYNA-VEG, to improve the quantification of climate-vegetation-soil interactions within dryland environments (Objective 4, Chapter 4). The integration of DYNA-VEG into the existing water partitioning model DRYP, revealed the differential sensitivities and responses to altered climate and hydrologic conditions among riparian forests and lowland vegetation. The improved parameterization of vegetation in DRYP suggests that through the new phenology routine a wide range of climate

and hydrologic conditions can be explored, including potential climate change scenarios (Chapter 5). The results from synthetic experiments highlighted the diverging sensitivities of ecohydrological processes to individual climate components and differential vegetation water stress responses (Objective 5). This novel approach improves our understanding of the effects of climate drivers on water partitioning in drylands as well as climate-vegetation-soil interactions. Such modeling approaches are crucial to providing the necessary understanding to produce actionable science for land and resource management programs in drought prone regions, such as the Southwestern USA.

5.1 Future drought stress and resource management

Looking ahead, several key challenges exist for the natural and human environment; from mitigation and adaptation to more extreme events, the protection of biodiversity and ensuring human wellbeing, to sustainable use of remaining natural resources (e.g., surface or groundwater). The accumulation of these challenges arguably requires a combination of process-based understanding and sustainable long-lasting approaches that reconcile future ecological and urban resource demands with attainable conservation and management goals under different climate adaptation strategies that consider the increasing amount of observations-based evidence.

As the true extent of climate change and its subsequent challenges to the global water cycle and natural resources and vegetation remain inexact, the need for continued monitoring and research to understand the complex interactions among global, regional, and local climate change elements that influence the physical, biological and societal processes is now more important than ever (Smith et al. 2019; Seddon et al. 2020; Cao et al. 2022). The plethora of current data provides important insights into the past, however, the velocity of current environmental change far exceeds any historic observations (IPCC 2021). Particularly on a local or regional level, evaluating the direction of possible climate shifts and vegetative and environmental thresholds can help to design and implement tailor-made climate mitigation and adaptation strategies in sensitive habitats (Capon et al. 2013; Perry et al. 2015; Dass et al. 2018; Justin and Michael 2021).

From Southern California to SE Arizona, I observed shifts in phenological behavior and seasonal greenness, which highlighted the high spatial variability of vegetation responses to drought and water limitations. Some locations appeared more buffered to the negative effects of drought and climate change than others. However, the ongoing influence of climate on vegetation was clearly present across the Southwest. Historically, coastal grasslands with higher moisture retention and riparian forests with access to shallow groundwater appeared less susceptible to drought stress than other locations. However, despite their current favorable conditions, their survival is not guaranteed, as the uneven distribution of vulnerabilities among plant functional groups and ecosystems I witnessed is not an isolated phenomenon, even within the historically dry regions throughout the Southwest USA.

Considering the differential sensitivities to precipitation regimes, moisture retention and climate forcing, certain biomes and species will be disproportionately affected by different aspects of climate. As existing imbalances will likely exacerbated by future climate change, even previously buffered areas will be driven into peak water stress and drought conditions more frequently (Garfin and Jardine 2013; Gremer et al. 2015; Gonzalez et al. 2018). The innovative modeling frameworks and climate scenario simulations I presented in this thesis, contribute to an improved understanding of the underlying differential processes of the propagation of multiyear droughts into soil moisture and vegetation responses as well as the key hydroclimate drivers on seasonal and annual vegetation dynamics. This is crucial to producing tailor-made interdisciplinary solutions that support integrated water resource management cognizant of the differential plant-water relationships and the effect of climate change .

5.2 Management of future riparian forest water stress

In riparian zones, undoubtedly the greatest threat to their future survival is the decline of groundwater levels. This is aggravated by excessive abstraction and anthropogenic alterations of natural stream flow conditions through the implementation of irreversible approaches that did not consider all ecosystem components and hydrological processes (Perry et al. 2012; Capon et al. 2013).

Historically, riparian zones were able to adapt to changes in ecosystem conditions, with many aquatic and semi-aquatic riparian species exhibiting a certain level of morphological and physical plasticity (Capon et al. 2013; Stromberg et al. 2013). However, persistent human interference throughout recent decades and the unexpected rate of environmental changes have compromised these adaptive capabilities. Evidence from deteriorated riparian zones in California and SE Arizona suggests that a return to more natural streamflow and groundwater fluctuations through the implementation of nature-based solutions and removal of hard-engineered structures could potentially again facilitate the adaptive capabilities of species and strengthen ecosystem resilience (Stromberg 2001; Richardson et al. 2007; Rohde et al. 2021b). Through the novel modeling framework I presented in Chapter 4, natural or anthropogenically driven changes to streamflow can be quantitatively evaluated, including the effects of climate on recharge, groundwater dynamics and evapotranspiration. The DRYP model has the option to include anthropogenic surface and groundwater abstraction as well as irrigation (Quichimbo et al. 2021), which is crucial when also evaluating the and human impacts on dryland ecosystem processes.

In recent years, nature-based solutions have emerged as an effective and favored tool to tackle environmental as well as societal challenges by enhancing nature (Seddon et al., 2020). The rediscovery of the benefits of a healthy natural ecosystem to overall biodiversity and human wellbeing suggests multiple feedbacks; from carbon storage, to flood control and stabilization of shorelines, to cleaner air and water, to the preservation of biodiversity and provision of recreational space (Davis and Naumann 2017; Keesstra et al. 2018; Seddon et al. 2020). Still, there remains immense unexplored potential of widely applying such wholesome approaches, that consider a process-based understanding of ecohydrological process to tackle climate mitigation and adaptation challenges in natural and urban environments throughout the Southwest. The various innovative modeling approaches I presented in this thesis, from patch scale to catchment scale, demonstrated that the impacts of vegetation changes on water yield and vice-versa can be well quantified through models of varying complexity. These approaches could be used to fully evaluate the impacts of vegetation changes such as vegetation cover transition, habitat expansion, species encroachment or climate driven changes such as increased flooding, localized storms

or streamflow alterations on water partitioning. The insights gained from such novel modeling experiments is crucial to formulate adaptation strategies that target the most sensitive species and components within an ecosystem.

One commonly debated adaptation strategies is to reverse anthropogenic alterations through conservation and reforestation of riparian habitats, including channel and floodplain restoration. The survival of riparian forest ecosystems is inevitably linked to persistent trends and threshold responses to groundwater and surface water dynamics. Through synthetic model simulations in DRYP I was able to model potential future water stress responses to deeper water tables for the first time. The results open up avenues for further scenario analyses of gradual groundwater recession (e.g., slow recession vs. rapid recession) over multiple temporal and spatial scales, which would provide an even deeper understanding about climate impacts on water partitioning processes. Similarly, modeling of future streamflow projections can help identify sites within a catchment that are most likely to need and support restoration of riparian habitat in the future. For example, a riparian site with current high stream flow and flood frequencies may seem suitable for restoration, while a lower flow area does not. However, considering projections of precipitation changes and streamflow, the suitability of certain areas might change. Including projections of potential future surface and subsurface flows at the catchment scale could thus help land managers evaluate the risks and methods to avoid potential water shortages or flood damage, given the present conditions of uncertainty of climate projections. In the same context, long-term changes to potential flood risk and low-flow periods can be evaluated and restoration efforts aimed at addressing the emerging risks by implementing sustainable groundwater thresholds, restoring connectivity of streams, or increasing flood attenuation (Lite and Stromberg 2005b; Richardson et al. 2007; Capon et al. 2013; Perry et al. 2015).

To date, one of the main challenges to restoration and conservation strategies is the lack of suitable predictive ecohydrological models that can capture the uncertainty in projected future climate, streamflow and vegetation responses. The improved parameterization of climate-vegetation interactions in DRYP now presents a useful tool for such tasks, as it not only addresses the underlying hydrological mechanisms

in drylands, such as unsaturated-saturated zone interactions, surface-groundwater interactions and vegetation-hydrology interactions, but allows for stochastic simulations within the range of projected future climate change. Indeed, individual model simulations within this thesis have shown riparian forest water stress trajectories are analogous to increased precipitation variability and declining groundwater tables. Considering for example the case where focused recharge becomes limited due to reduced precipitation; modeling streamflow dynamics and the effect of climate on surface-subsurface interactions could help determine specific proactive measures to manage aquifer recharge or increase water retention in channels and surrounding riparian terraces. Overall, the directionality between climate variability and water resource changes is well represented in DRYP and the novel DYNA-VEG module, not least through the link between hydroclimate and phenology, which provides the opportunity to explore specific key processes of the water cycle, such as evaporation and runoff, most important for watershed ecohydrological management.

Mitigation strategies such as managed aquifer recharge have been already implemented in arid areas worldwide, including California and Arizona, to mitigate recharge depleted aquifer storage and (Scanlon et al. 2016; Dahlke et al. 2018; Norman et al. 2019). While past ignorance of ecological water demand thresholds has aggravated the degradation and fragmentation of riparian zones due to regional groundwater decline, innovative predictive models such as DRYP can help identify the key hydrologic fluxes most affected by climate, in full consideration of the underlying mechanisms. Particularly in riparian forests, modeling transitions between low flow/high flow, or variable groundwater recession can help evaluate ecologically sustainable groundwater depths or managed aquifer recharge, and the potential implications on base flows, vegetation density and seedling establishment. This is of particular interest in regions such as California, where the Sustainable Groundwater Management Act (SGMA) requires groundwater basins to come up with sustainable management of their shared groundwater resource (Leahy 2016; Bedsworth et al. 2018). To do so, hydrological models must be able to capture the spatial and temporal distributions of recharge, surface-groundwater interactions, hydrogeology and

evapotranspiration (Meixner et al. 2016; Dahlke et al. 2018; Rohde et al. 2021a; Saito et al. 2021; Zhang et al. 2022).

5.3 Future drought resilience and management of grassland habitats

Considering the observations from lowland grassland ecosystems in Southern California, the combined effects of warming and drying have exposed them to frequent and prolonged water stress during the past multi-year drought. The differential effects of climate change have arguably added a new dimension to the existing land management debate, as terrain, precipitation, humidity, air temperature and soil and vegetation types interact with each other. Observations of water stress in regional ecosystems in California and throughout the Southwest, as well as in other dryland and Mediterranean ecosystems around the world, call into question the future of grassland ecosystems, as conservation goals seem irreconcilable with economic interests and benefits of current management practices and land development. My observations and model simulations of grassland and soil moisture dynamics in Southern California point towards a trend of widespread degradation and aridification of grassland habitats, due to the increasing pressure from soil moisture drying, increased evaporative demand and precipitation variability. Earlier green-up, mild winters and lack of spring precipitation historically contributed towards earlier browning of the landscape, simultaneously raising the risk for wildfire and desertification (Donovan et al., 2020). In future, significant temporal shifts in atmospheric demand and the delivery of precipitation present the most serious threat to Southern California ecosystems, as soil and vegetation dynamics are influenced by the interaction of air temperature, humidity and local soil conditions. The anticipated accelerated warming and drying trends in the region expose California ecosystems to long-term significant declines in richness and habitat as well as significant desertification and aridification of the landscape (Harrison et al., 2018, Wilson et al., 2017).

The importance of climate feedbacks is not isolated to ecological impacts alone, but extend towards urban communities, where the associated risk of extreme wildfires will increasingly affect residential areas and ecosystem and human health, as seen in recent years and again during the current 2022 fire season, which burned almost

325,000 acres of land, as of September 2022 (https://www.fire.ca.gov/incidents/). Similar to riparian forests, current land management practices of grassland biomes throughout North America need to be reconsidered and adjusted to include the emerging climate trends and threats of desertification, persistent invasion of non-native species and high-intensity wildfires, which are aggravated by changing seasonal phenological behavior and persistent warmer and drier conditions.

With these immediate threats in mind, regional analyses and projections of vegetation dynamics are an important part of management as they are often very region specific, focusing on sites that are most sensitive and likely to experience the strongest impact. Understanding the interactions between ecological and climatological elements, systematic approaches like restoration of native plant diversity have been part of many conservation efforts throughout national parks and reserves in the past as natural climate solutions are pursued more broadly throughout the U.S. to mitigate the emerging effects of climate change (Antonio et al. 2002; Pyke and Marty 2005; Barry et al. 2006; Gennet et al. 2017). However, past restoration efforts of native grasslands that relied solely on natural recruitment of native perennial plants, were frequently unsuccessful as seedlings failed to establish without the explicit reduction of exotic annual species, either grazing, mowing or prescribed fires (Antonio et al. 2002).

The diverging grassland vegetation responses I observed over regional gradients in Southern California also underscored the importance of soil hydraulic properties, which control water fluxes through the vadose zone and determine plant water availability. Previous assumptions that hydraulic properties remain static over timescales may be suspended by new studies that suggested that continental scale soil microporosity may be affected by climate change (Hirmas et al. 2018). This would reinforce existing trajectories of an intensifying global water cycle and associated hydrologic processes, with broader implications for the distribution of soil moisture and evapotranspiration. Similar to the novel parameterization of surface vegetation in DRYP, such feedbacks can and should be incorporated into regional models as it reinforces the extent of climate-related changes that can impact future vegetation dynamics beyond historic trends and patterns. Especially since high intersite

variability complicates management generalizations for grassland systems, reproducible model frameworks such as the FAO soil moisture balance model I used in this thesis, have the potential to explore the impacts of climate change driven processes, including precipitation variability, changes to evaporative demand, vegetation shifts and temporal changes soil hydraulic conductivity over extended temporal scales. Understanding how these changes can directly affect the ecosystems water holding capacities and vegetation responses is crucial to producing tailored management approaches that are based on a well-founded understanding of the underlying processes.

In addition to providing important hydrologic functions and habitat, the recent increased massive death of over 100 million trees from drought and bark beetle outbreaks (Bedsworth et al. 2018) highlighted the need for alternative carbon storage. Recent modeling experiments suggested that grassland ecosystem are potentially more resilient carbon sinks than climate vulnerable-forests, under 21st century climate change (Dass et al. 2018). The imperative to reach emission goals is inevitably coupled to lowering global carbon emissions by any means possible. Therefore, when realistic sustainable conservation and restoration goals are executed in parallel with effective management, increased biodiversity and ecosystem resilience, as well as effective natural carbon capture to reach emission goals can achieved all at once, creating an overall win-win situation that would benefit ecosystems and humans alike.

In conclusion, the effects of water stress on different plant functional groups across the Southwest have illustrated the climatic limits on water availability in water limited environments and their vulnerability to future climate changes. The diverging vegetation responses of grasslands in Southern California to drying and warming and riparian floodplain trees to changes in the water table highlights the importantce of understanding water availability gradients and ecohydrological threshold responses. As such, improved and dynamic modeling capabilities, such as DRYP and DYNA-VEG are the key to setting clear management and conservation plans for future decades.

REFERENCES

Abatzoglou, J.T. and Kolden, C.A. 2011. Climate change in Western US deserts: Potential for increased wildfire and invasive annual grasses. *Rangeland Ecology and Management* 64(5), pp. 471–478. Available at: http://dx.doi.org/10.2111/REM-D-09-00151.1.

Aghakouchak, A., Ragno, E. and Love, C. 2018. Projected Changes in Californias Precipitation Intensity-Duration-Frequency Curves. In: *California's Fourth Climate Change Assessment*. California Energy Commission, p. 32.

Allan, R.P. et al. 2020. Advances in understanding large-scale responses of the water cycle to climate change. *Annals of the New York Academy of Sciences* 1472(1), pp. 49–75. doi: 10.1111/nyas.14337.

Allen, R.G., Pereira, L.S., Raes, D. and Smith, M. 1998. *FAO Irrigation and Drainage Paper No. 56, Crop evapotranspiration (Guidelines for computing crop water requirements)*. Available at: http://www.fao.org/3/x0490e/x0490e00.htm.

Anderson, B.T., Wang, J., Salvucci, G., Gopal, S. and Islam, S. 2010. Observed trends in summertime precipitation over the southwestern United States. *Journal of Climate* 23(7), pp. 1937–1944. doi: 10.1175/2009JCLI3317.1.

Antonio, C.D., Bainbridge, S., Kennedy, C., Bartolome, J. and Reynolds, S. 2002. *Ecology and Restoration of California Grasslands with special emphasis on the influnece of fire and grazing on native grassland species*.

Anurag, H., Ng, G.H.C., Tipping, R. and Tokos, K. 2021. Modeling the impact of spatiotemporal vegetation dynamics on groundwater recharge. *Journal of Hydrology* 601(February), p. 126584. Available at: https://doi.org/10.1016/j.jhydrol.2021.126584.

Arora, V.K. 2002. Modeling vegetation as a dynamic component in soil-vegetation-atmosphere transfer schemes and hydrological models. *Reviews of Geophysics* 40(2), pp. 3-1-3–26. doi: 10.1029/2001RG000103.

Asfaw, D.T. et al. 2022. stoPET v1 . 0 : A stochastic potential evapotranspiration generator for simulation of climate change impacts. *Geoscientific Model Development (in review)* (May), pp. 1–21.

Ault, T.R., Mankin, J.S., Cook, B.I. and Smerdon, J.E. 2016. Relative impacts of mitigation, temperature, and precipitation on 21st-century megadrought risk in the American Southwest. *Science Advances* 2(10), pp. 1–9. doi: 10.1126/sciadv.1600873.

Bachelet, D., Ferschweiler, K., Sheehan, T. and Strittholt, J. 2016. Climate change effects on southern California deserts. *Journal of Arid Environments* 127, pp. 17–29. Available at: http://dx.doi.org/10.1016/j.jaridenv.2015.10.003.

Baillie, M.N., Hogan, J.F., Ekwurzel, B., Wahi, A.K. and Eastoe, C.J. 2007. Quantifying water sources to a semiarid riparian ecosystem, San Pedro River, Arizona. *Journal of Geophysical Research: Biogeosciences* 112(3), pp. 1–13. doi: 10.1029/2006JG000263.

Baird, K.J., Stromberg, J.C. and Maddock, T. 2005. Linking riparian dynamics and groundwater: An ecohydrologic approach to modeling groundwater and riparian vegetation. *Environmental Management* 36(4), pp. 551–564. doi: 10.1007/s00267-004-0181-z.

Barry, S., Larson, S. and George, M. 2006. California native grasslands: A historical perspective. *Keeping Landscapes Working: A Newsletter for Managers of Bay Area Rangelands* 3(1), pp. 3–8. Available at: http://www.cnga.org/library/GrasslandsArticleBarry2006.pdf%5Cnpapers2://publication/uuid/E4F94056-B203-4492-8562-0F715A156841.

Bedsworth, L., Cayan, D., Guido, F., Fisher, L. and Ziaja, S. 2018. California's Fourth Climate Change Assessment Statewide Summary Report. *California's Fourth Climate Change Assessment* (October), p. 133. Available at: http://www.copenhagenconsensus.com/publication/post-2015-consensus-climate-change-assessment-galianahttp://www.copenhagenconsensus.com/publication/post-2015-consensus-climate-change-assessment-galiana.

Beier, C.M., Stella, J.C., Dovčiak, M. and McNulty, S.A. 2012. Local climatic drivers of changes in phenology at a boreal-temperate ecotone in eastern North America. *Climatic Change* 115(2), pp. 399–417. doi: 10.1007/s10584-012-0455-z.

Berg, A. and Sheffield, J. 2018. Climate Change and Drought: the Soil Moisture Perspective. *Current Climate Change Reports* 4(2), pp. 180–191. doi: 10.1007/s40641-018-0095-0.

Berg, N. and Hall, A. 2015. Interannual Precipitation Extremes over California Under Climate Change. *Journal of Climate* 53(9), p. 287. doi: 10.1017/CBO9781107415324.004.

Berra, E.F. and Gaulton, R. 2021. Remote sensing of temperate and boreal forest phenology: A review of progress, challenges and opportunities in the intercomparison of in-situ and satellite phenological metrics. *Forest Ecology and Management* 480(August 2020), p. 118663. Available at: https://doi.org/10.1016/j.foreco.2020.118663.

de Beurs, K.M. and Henebry, G.M. 2010. A land surface phenology assessment of the northern polar regions using MODIS reflectance time series. *Canadian Journal of Remote Sensing* 36, pp. S87–S110. doi: 10.5589/m10-021.

Bevington, P.R. and Robinson, Keith.D. 2003. *Data Reduction and Error Analysis for the Physical Sciences. Third Edition*. Kent. A. Peterson.

Bradford, J.B., Schlaepfer, D.R., Lauenroth, W.K. and Palmquist, K.A. 2020. Robust ecological drought projections for drylands in the 21st century. *Global Change Biology* (December 2019), pp. 3906–3919. doi: 10.1111/gcb.15075.

Bréda, N., Huc, R., Granier, A. and Dreyer, E. 2006. Temperate forest trees and stands under severe drought: a review of ecophysiological responses, adaptation processes and long-term consequences. *Annals of Forest Science* 63(6), pp. 625–644. Available at: http://www.edpsciences.org/10.1051/forest:2006042.

Briggs, L.J. and Shantz, H.L. 1912. The Wilting Coefficient and Its Indirect Determination. *Botanical Gazette* 53(1), pp. 20–37.

Bulcock, H.H. and Jewitt, G.P.W. 2010. Spatial mapping of leaf area index using hyperspectral remote sensing for hydrological applications with a particular focus on canopy interception. *Hydrology and Earth System Sciences* 14(2), pp. 383–392. doi: 10.5194/hess-14-383-2010.

Burkle, L.A., Marlin, J.C. and Knight, T.M. 2013. Plant-Pollinator Interactions over 120 Years: Loss of Species, Co-Occurence, and Function. *Science* 339, pp. 1611–1615. doi: 10.1126/science.1230200.

Cao, Z., Wang, S., Luo, P., Xie, D. and Zhu, W. 2022. Watershed Ecohydrological Processes in a Changing Environment: Opportunities and Challenges. *Water (Switzerland)* 14(9). doi: 10.3390/w14091502.

Capon, S.J. et al. 2013. Riparian Ecosystems in the 21st Century: Hotspots for Climate Change Adaptation? *Ecosystems* 16(3), pp. 359–381. doi: 10.1007/s10021-013-9656-1.

Carlson, T.N. and Ripley, D.A. 1997. On the relation between NDVI, fractional vegetation cover, and leaf area index. *Remote Sensing of Environment* 62(3), pp. 241–252. doi: 10.1016/S0034-4257(97)00104-1.

Castellini, M., di Prima, S., Stewart, R., Biddoccu, M., Rahmati, M. and Alagna, V. 2022. Advances in Ecohydrology for Water Resources Optimization in Arid and Semi-Arid Areas. *Water (Switzerland)* 14(12), pp. 14–17. doi: 10.3390/w14121830.

Cayan, D.R., Das, T., Pierce, D.W., Barnett, T.P., Tyree, M. and Gershunov, A. 2010. Future dryness in the southwest US and the hydrology of the early 21st century drought. *Proceedings of the National Academy of Sciences Sciences* 107(50), pp. 21271–21276. Available at: http://www.pnas.org/content/107/50/21271.short [Accessed: 10 October 2018].

Caylor, K.K., D'Odorico, P. and Rodriguez-Iturbe, I. 2006. On the ecohydrology of structurally heterogeneous semiarid landscapes. *Water Resources Research* 42(7), pp. 1–13. doi: 10.1029/2005WR004683.

Caylor, K.K., Scanlon, T.M. and Rodriguez-Iturbe, I. 2009. Ecohydrological optimization of pattern and processes in water-limited ecosystems: A trade-off-based

hypothesis. *Water Resources Research* 45(8), pp. 1–15. doi: 10.1029/2008WR007230.

Choler, P., Sea, W., Briggs, P., Raupach, M. and Leuning, R. 2010. A simple ecohydrological model captures essentials of seasonal leaf dynamics in semi-arid tropical grasslands. *Biogeosciences* 7(3), pp. 907–920. doi: 10.5194/bg-7-907-2010.

Clapp, R.B. and Hornberger, G.M. 1978. Empirical Equations for Some Soil Hydraulic Properties. *Water Resources Research* 14(4)

Cleland, E.E., Isabelle, C. and Annette, M. 2007. Shifting Plant Phenology In Response to Global Change. *Trends in Ecology & Evolution* 22(7), pp. 357–365.

Coates, A.R., Dennison, P.E., Roberts, D.A. and Roth, K.L. 2015. Monitoring the impacts of severe drought on southern California Chaparral species using hyperspectral and thermal infrared imagery. *Remote Sensing* 7(11), pp. 14276–14291. doi: 10.3390/rs71114276.

Cole, J.E., Overpeck, J.T., Cook, E.R. and Enso, O. 2002. Multiyear La Nina events and persistent drought in the contiguous United States. 29(13), pp. 2–5.

Condon, L.E., Atchley, A.L. and Maxwell, R.M. 2020. Evapotranspiration depletes groundwater under warming over the contiguous United States. *Nature Communications* 11(1). Available at: http://dx.doi.org/10.1038/s41467-020-14688-0.

Cook, B.I., Ault, T.R. and Smerdon, J.E. 2015a. Unprecedented 21st century drought risk in the American Southwest and Central Plains. *Science Advances* 1(1), pp. 1–8. doi: 10.1126/sciadv.1400082.

Cook, B.I., Ault, T.R. and Smerdon, J.E. 2015b. Unprecedented 21st century drought risks in the American south west and central plains. *Science Advances* 1 e1400081(February), pp. 1–8.

Cook, B.I., Smerdon, J.E., Seager, R. and Coats, S. 2014. Global warming and 21stcentury drying. *Climate Dynamics* 43(9–10), pp. 2607–2627. doi: 10.1007/s00382-014-2075-y.

Cook, B.I.B.I., Ault, T.R.T.R. and Smerdon, J.E.J.E. 2015c. Unprecedented 21st century drought risks in the American south west and central plains. *Science Advances* 1(February), pp. 1–8.

Cui, T., Martz, L. and Guo, X. 2017. Grassland phenology response to drought in the Canadian prairies. *Remote Sensing* 9(12). doi: 10.3390/rs9121258.

Cuthbert, M.O. et al. 2019. Observed controls on resilience of groundwater to climate variability in sub-Saharan Africa. *Nature* 572(7768), pp. 230–234. doi: 10.1038/s41586-019-1441-7.

Cuthbert, M.O., MacKay, R. and Nimmo, J.R. 2013. Linking soil moisture balance and source-responsive models to estimate diffuse and preferential components of groundwater recharge. *Hydrology and Earth System Sciences* 17(3), pp. 1003–1019. doi: 10.5194/hess-17-1003-2013.

Dahlke, H.E. et al. 2018. Managed Aquifer Recharge as a Tool to Enhance Sustainable Groundwater Management in California: Examples From Field and Modeling Studies. *Advances in Chemical Pollution, Environmental Management and Protection* 3, pp. 215–275. doi: 10.1016/bs.apmp.2018.07.003.

Dai, A. 2011. Drought under global warming: A review. *Wiley Interdisciplinary Reviews: Climate Change* 2(1), pp. 45–65. doi: 10.1002/wcc.81.

Daly, E. and Porporato, A. 2005. A Review of Soil Moisture Dynamics : From Rainfall Infiltration to Ecosystem Response. *Environmental Engineering Science* 22(1)

Dass, P., Houlton, B.Z., Wang, Y. and Warlind, D. 2018. Grasslands may be more reliable carbon sinks than forests in California. *Environmental Research Letters* 13(7). doi: 10.1088/1748-9326/aacb39.

Davis, M. and Naumann, S. 2017. *Making the Case for Sustainable Urban Drainage Systems as a Nature-Based Solution to Urban Flooding*. doi: 10.1007/978-3-319-56091-5_8.

Dettinger, M.D. 2013. Atmospheric Rivers as Drought Busters on the U.S. West Coast. *Journal of Hydrometeorology* 14, pp. 1721–1732. doi: 10.1175/JHM-D-13-02.1.

Dettinger, M.D., Ralph, F.M., Das, T., Neiman, P.J. and Cayan, D.R. 2011. Atmospheric Rivers, Floods and the Water Resources of California. *Water* 3(2), pp. 445–478. doi: 10.3390/w3020445.

Diez, J.M. et al. 2012. Forecasting phenology: From species variability to community patterns. *Ecology Letters* 15(6), pp. 545–553. doi: 10.1111/j.1461-0248.2012.01765.x.

D'Odorico, P., Caylor, K., Okin, G.S. and Scanlon, T.M. 2007. On soil moisture-vegetation feedbacks and their possible effects on the dynamics of dryland ecosystems. *Journal of Geophysical Research: Biogeosciences* 112(4), pp. 1–10. doi: 10.1029/2006JG000379.

D'Odorico, P. and Porporato, A. 2019. *Dryland Ecohydrology*. Second Edi. Runyan Wilkinson, C. ed. Springer. doi: 10.2136/vzj2006.0053br.

D'Odorico, P., Porporato, A. and Runyan, C.W. 2019. *Dryland ecohydrology*. doi: 10.1007/978-3-030-23269-6.

Dong, C., MacDonald, G.M., Willis, K., Gillespie, T.W., Okin, G.S. and Williams, A.P. 2019. Vegetation Responses to 2012–2016 Drought in Northern and Southern California. *Geophysical Research Letters* , pp. 3810–3821. doi: 10.1029/2019GL082137.

Donovan, V.M. et al. 2020. Resilience to large, 'catastrophic' wildfires in North America's grassland biome. *Earth's Future* . doi: 10.1029/2020ef001487.

Egea, G., Verhoef, A. and Vidale, P.L. 2011. Towards an improved and more flexible representation of water stress in coupled photosynthesis-stomatal conductance models. *Agricultural and Forest Meteorology* 151(10), pp. 1370–1384. Available at: http://dx.doi.org/10.1016/j.agrformet.2011.05.019.

Evans, C.M., Dritschel, D.G. and Singer, M.B. 2018. Modeling Subsurface Hydrology in Floodplains. *Water Resources Research* 54(3), pp. 1428–1459. doi: 10.1002/2017WR020827.

Fatichi, S., Ivanov, V.Y. and Caporali, E. 2012. A mechanistic ecohydrological model to investigate complex interactions in cold and warm water-controlled environments: 1. Theoretical framework and plot-scale analysis. *Journal of Advances in Modeling Earth Systems* 4(5), pp. 1–31. doi: 10.1029/2011MS000086.

Felton, A.J., Slette, I.J., Smith, M.D. and Knapp, A.K. 2020. Precipitation amount and event size interact to reduce ecosystem functioning during dry years in a mesic grassland. *Global Change Biology* 26(2), pp. 658–668. doi: 10.1111/gcb.14789.

Fettig, C.J., Mortenson, L.A., Bulaon, B.M. and Foulk, P.B. 2019. Tree mortality following drought in the central and southern Sierra Nevada, California, U.S. *Forest Ecology and Management* 432(September 2018), pp. 164–178. Available at: https://doi.org/10.1016/j.foreco.2018.09.006.

Ganguly, S., Friedl, M.A., Tan, B., Zhang, X. and Verma, M. 2010. Land surface phenology from MODIS: Characterization of the Collection 5 global land cover dynamics product. *Remote Sensing of Environment* 114(8), pp. 1805–1816. doi: 10.1016/j.rse.2010.04.005.

Garfin, G. and Jardine, A. 2013. Assessment of Climate Change in the Southwest United States. *Assessment of Climate Change in the Southwest United States* . doi: 10.5822/978-1-61091-484-0.

Gennet, S., Spotswood, E., Hammond, M. and Bartolome, J.W. 2017. Livestock grazing supports native plants and songbirds in a California annual grassland. *PLoS ONE* 12(6), pp. 1–23. doi: 10.1371/journal.pone.0176367.

Gerten, D. 2013. A vital link: Water and vegetation in the anthropocene. *Hydrology and Earth System Sciences* 17(10), pp. 3841–3852. doi: 10.5194/hess-17-3841-2013.

Gillespie, T.W., Ostermann-kelm, S., Dong, C., Willis, K.S., Okin, G.S. and Macdonald, G.M. 2018. Monitoring changes of NDVI in protected areas of southern California. *Ecological Indicators* 88(June 2017), pp. 485–494. Available at: https://doi.org/10.1016/j.ecolind.2018.01.031.

Glenn, E.P., Neale, C.M.U., Hunsaker, D.J. and Nagler, P.L. 2011. Vegetation index-based crop coefficients to estimate evapotranspiration by remote sensing in agricultural and natural ecosystems. *Hydrological Processes* 25(26), pp. 4050–4062. doi: 10.1002/hyp.8392.

Gonzalez, P. et al. 2018. *Southwest: In Impacts, Risks and Adaptation in the United States: Fourth National Climate Assessment, Volume II*. Washington, DC, USA.

Goulden, M.L. and Bales, R.C. 2019. California forest die-off linked to multi-year deep soil drying in 2012–2015 drought. *Nature Geoscience* 12(August), pp. 632–637. Available at: http://www.nature.com/articles/s41561-019-0388-5.

Gouveia, C.M., Trigo, R.M., Beguería, S. and Vicente-Serrano, S.M. 2017. Drought impacts on vegetation activity in the Mediterranean region: An assessment using remote sensing data and multi-scale drought indicators. *Global and Planetary Change* 151, pp. 15–27. Available at: http://dx.doi.org/10.1016/j.gloplacha.2016.06.011.

Gremer, J.R., Bradford, J.B., Munson, S.M. and Duniway, M.C. 2015. Desert grassland responses to climate and soil moisture suggest divergent vulnerabilities across the southwestern United States. *Global Change Biology* 21(11), pp. 4049–4062. doi: 10.1111/gcb.13043.

Gu, Y., Hunt, E., Wardlow, B., Basara, J.B., Brown, J.F. and Verdin, J.P. 2008. Evaluation of MODIS NDVI and NDWI for vegetation drought monitoring using Oklahoma Mesonet soil moisture data. *Geophysical Research Letters* 35(22), pp. 1–5. doi: 10.1029/2008GL035772.

Hänninen, H. and Kramer, K. 2007. A framework for modelling the annual cycle of trees in boreal and temperate regions. *Silva Fennica* 41(1), pp. 167–205. doi: 10.14214/sf.313.

Harrison, S.P., LaForgia, M.L. and Latimer, A.M. 2018. Climate-driven diversity change in annual grasslands: Drought plus deluge does not equal normal. *Global Change Biology* 24(4), pp. 1782–1792. doi: 10.1111/gcb.14018.

Haynes, K.D., Baker, I.T., Denning, A.S., Stöckli, R., Schaefer, K., Lokupitiya, E.Y. and Haynes, J.M. 2019. Representing Grasslands Using Dynamic Prognostic

Phenology Based on Biological Growth Stages: 1. Implementation in the Simple Biosphere Model (SiB4). *Journal of Advances in Modeling Earth Systems* 11(12), pp. 4423–4439. doi: 10.1029/2018MS001540.

Helman, D., Lensky, I.M., Tessler, N. and Osem, Y. 2015. A phenology-based method for monitoring woody and herbaceous vegetation in mediterranean forests from NDVI time series. *Remote Sensing* 7(9), pp. 12314–12335. doi: 10.3390/rs70912314.

Hirmas, D.R., Giménez, D., Nemes, A., Kerry, R., Brunsell, N.A. and Wilson, C.J. 2018. Climate-induced changes in continental-scale soil macroporosity may intensify water cycle. *Nature* 561(7721), pp. 100–103. Available at: http://dx.doi.org/10.1038/s41586-018-0463-x.

Huang, F., Zhang, D. and Chen, X. 2019. Vegetation response to groundwater variation in arid environments: Visualization of research evolution, synthesis of response types, and estimation of groundwater threshold. *International Journal of Environmental Research and Public Health* 16(10). doi: 10.3390/ijerph16101849.

Huang, J. et al. 2017. Dryland climate change: Recent progress and challenges. *Reviews of Geophysics* 55(3), pp. 719–778. doi: 10.1002/2016RG000550.

Huang, J., Yu, H., Guan, X., Wang, G. and Guo, R. 2016. Accelerated dryland expansion under climate change. *Nature Climate Change* 6(2), pp. 166–171. doi: 10.1038/nclimate2837.

Huete, A.R. 1988. A soil-adjusted vegetation index (SAVI). *Remote Sensing of Environment* 25(3), pp. 295–309. doi: 10.1016/0034-4257(88)90106-X.

Hunsaker, D.J., Pinter, P.J. and Kimball, B.A. 2005. Wheat basal crop coefficients determined by normalized difference vegetation index. *Irrigation Science* (24), pp. 1–14. doi: 10.1007/s00271-005-0001-0.

Hunter, A.F. and Lechowicz 1992. Predicting the Timing of Budburst in Temperate Trees. *Journal of Applied Ecology* 29(3), pp. 597–604.

IPCC 2014. *Climate Change 2014: Synthesis Report. Contribution of Working Groups I, II and III to the Fifth Assessment Report of the Intergovernmental Panel on Climate Change*. doi: 10.1016/S0022-0248(00)00575-3.

IPCC 2021. *Climate Change 2021: The Physical Science Basis. Contribution of Working Group I to the Sixth Assessment Report fo the Intergovernmental Panel on Climate Change*. Masson-Delmotte, V. et al. eds. Cambride University Press, Cambridge, United Kingdom and New York, NY, USA. doi: 10.1017/9781009157896.

Irmak, S., Kabenge, I., Rudnick, D., Knezevic, S., Woodward, D. and Moravek, M. 2013. Evapotranspiration crop coefficients for mixed riparian plant community and transpiration crop coefficients for Common reed, Cottonwood and Peach-leaf willow in the Platte River Basin, Nebraska-USA. *Journal of Hydrology* 481, pp. 177–190. Available at: http://dx.doi.org/10.1016/j.jhydrol.2012.12.032.

Jenerette, G.D., Scott, R.L. and Huete, A.R. 2010. Functional differences between summer and winter season rain assessed with MODIS-derived phenology in a semi-arid region. *Journal of Vegetation Science* 21(1), pp. 16–30. doi: 10.1111/j.1654-1103.2009.01118.x.

Jia, G. et al. 2019. *Land-climate interactions. In: Climate Change and Land: an IPCC special report on climate change, desertification, land degradation, sustainable land management, food security, and greenhouse gas fluxes in terrestrial ecosystems.* Available at: https://www.ipcc.ch/srccl/ [Accessed: 14 July 2022].

Jolly, W.M., Nemani, R. and Running, S.W. 2005. A generalized, bioclimatic index to predict foliar phenology in response to climate. *Global Change Biology* 11(4), pp. 619–632. doi: 10.1111/j.1365-2486.2005.00930.x.

Jolly, W.M. and Running, S.W. 2004. Effects of precipitation and soil water potential on drought deciduous phenology in the Kalahari. *Global Change Biology* 10(3), pp. 303–308. doi: 10.1046/j.1365-2486.2003.00701.x.

Joyce, L.A., Briske, D.D., Brown, J.R., Polley, H.W., McCarl, B.A. and Bailey, D.W. 2013. Climate change and North American rangelands: Assessment of mitigation and

adaptation strategies. *Rangeland Ecology and Management* 66(5), pp. 512–528. doi: 10.2111/REM-D-12-00142.1.

Justin, C. and Michael, E. 2021. Selecting coastal California prairie species for climate-smart grassland restoration. *Grasslands* 33(1)

Keeley, J.E. and Syphard, A.D. 2016. Climate change and future fire regimes: Examples from California. *Geosciences (Switzerland)* 6(3), pp. 1–14. doi: 10.3390/geosciences6030037.

Keesstra, S., Nunes, J., Novara, A., Finger, D., Avelar, D., Kalantari, Z. and Cerdà, A. 2018. The superior effect of nature based solutions in land management for enhancing ecosystem services. *Science of the Total Environment* 610–611, pp. 997–1009. Available at: https://doi.org/10.1016/j.scitotenv.2017.08.077.

Kibler, C.L., Schmidt, E.C., Roberts, D.A., Stella, J.C., Kui, L., Lambert, A.M. and Singer, M.B. 2021. A brown wave of riparian woodland mortality following groundwater declines during the 2012-2019 California drought. *Environmental Research Letters* 16(8). doi: 10.1088/1748-9326/ac1377.

Körner, C. and Basler, D. 2010. Phenology under global warming. *Science* 327(5972), pp. 1461–1462. doi: 10.1126/science.1186473.

Kozak, J.A., Ahuja, L.R., Green, T.R. and Ma, L. 2007. Modelling crop canopy and residue rainfall interception effects on soil hydrological components for semi-arid agriculture. *Hydrological Processes* 21(2), pp. 229–241. doi: 10.1002/hyp.6235.

Laio, F., Porporato, A., Fernandez-Illescas, C.P. and Rodriguez-Iturbe, I. 2001. Plants in water-controlled ecosystems: Active role in hydrologic processes and responce to water stress II Probabilistic soil moisture dynamics. *Advances in Water Resources* 24(7), pp. 745–762. doi: 10.1016/S0309-1708(01)00007-0.

Laio, F., Tamea, S., Ridolfi, L., D'Odorico, P. and Rodriguez-Iturbe, I. 2009. Ecohydrology of groundwater-dependent ecosystems: 1. Stochastic water table dynamics. *Water Resources Research* 45(5), pp. 1–13. doi: 10.1029/2008WR007292.

Lavers, D.A., Ralph, F.M., Waliser, D.E., Gershunov, A. and Dettinger, M.D. 2015. Climate change intensification of horizontal water vapor transport in CMIP5. *Geophysical Research Letters* (42), pp. 5617–5625. doi: 10.1002/2015GL064672.

Leahy, T.C. 2016. Desperate Times Call for Sensible Measures: The Making of the California Sustainable Groundwater Management Act. *Golden Gate University Environmental Law Journal* 9(5), pp. 5–40. Available at: http://digitalcommons.law.ggu.edu/gguelj/vol9/iss1/4.

Lite, S.J., Bagstad, K.J. and Stromberg, J.C. 2005. Riparian plant species richness along laterial and longitudinal gradient of water stress and disturbance, San Pedro River, Arizona, USA. *Journal of Arid Environments* 63(4), pp. 785–813. Available at: https://doi.org/10.1016/j.jaridenv.2005.03.026.

Lite, S.J. and Stromberg, J.C. 2005a. Surface water and ground-water thresholds for maintaining Populus-Salix forests, San Pedro River, Arizona. *Biological Conservation* 125(2), pp. 153–167. doi: 10.1016/j.biocon.2005.01.020.

Lite, S.J. and Stromberg, J.C. 2005b. Surface water and ground-water thresholds for maintaining Populus-Salix forests, San Pedro River, Arizona. *Biological Conservation* 125(2), pp. 153–167. doi: 10.1016/j.biocon.2005.01.020.

Liu, S., Roberts, D.A., Chadwick, O.A. and Still, C.J. 2012. Spectral responses to plant available soil moisture in a Californian Grassland. *International Journal of Applied Earth Observation and Geoinformation* 19(1), pp. 31–44. Available at: http://dx.doi.org/10.1016/j.jag.2012.04.008.

Liu, Y., Stanturf, J. and Goodrick, S. 2010. Trends in global wildfire potential in a changing climate. *Forest Ecology and Management* 259(4), pp. 685–697. doi: 10.1016/j.foreco.2009.09.002.

Loik, M.E., Breshears, D.D., Lauenroth, W.K. and Belnap, J. 2004. A multi-scale perspective of water pulses in dryland ecosystems: Climatology and ecohydrology of the western USA. *Oecologia* 141(2), pp. 269–281. doi: 10.1007/s00442-004-1570-y.

Lu, L., Kuenzer, C., Wang, C., Guo, H. and Li, Q. 2015. Evaluation of three MODIS-derived vegetation index time series for dryland vegetation dynamics monitoring. *Remote Sensing* 7(6), pp. 7597–7614. doi: 10.3390/rs70607597.

Ma, X., Huete, A., Moran, S., Ponce-Campos, G. and Eamus, D. 2015. Abrupt shifts in phenology and vegetation productivity under climate extremes. *Journal of Geophysical Research: Biogeosciences* 120(10), pp. 2036–2052. doi: 10.1002/2015JG003144.

Makings, E. 2005. Flora of the San Pedro Riparian National Conservation Area , Cochise County , Arizona. *USDA Forest Service Proceedings* 36, pp. 92–99.

Mann, M.E. and Gleick, P.H. 2015. Climate change and California drought in the 21st century. *Proceedings of the National Academy of Sciences of the United States of America* 112(13), pp. 3858–3859. doi: 10.1073/pnas.1503667112.

Matthews, E.R. and Mazer, S.J. 2016. Historical changes in flowering phenology are governed by temperature × precipitation interactions in a widespread perennial herb in western North America. *New Phytologist* 210(1), pp. 157–167. doi: 10.1111/nph.13751.

Mayes, M., Caylor, K.K., Singer, M.B., Stella, J.C., Roberts, D. and Nagler, P. 2020. Climate sensitivity of water use by riparian woodlands at landscape scales. *Hydrological Processes* 34(25), pp. 4884–4903. doi: 10.1002/hyp.13942.

McKinnon, K.A., Poppick, A. and Simpson, I.R. 2021. Hot extremes have become drier in the United States Southwest. *Nature Climate Change* 11(July). Available at: http://dx.doi.org/10.1038/s41558-021-01076-9.

Meixner, T. et al. 2016. Implications of projected climate change for groundwater recharge in the western United States. *Journal of Hydrology* 534, pp. 124–138. Available at: http://dx.doi.org/10.1016/j.jhydrol.2015.12.027.

Memmott, J., Craze, P.G., Waser, N.M. and Price, M. v. 2007. Global warming and the disruption of plant-pollinator interactions. *Ecology Letters* 10(8), pp. 710–717. doi: 10.1111/j.1461-0248.2007.01061.x.

Menzel, A., Sparks, T.H., Estrella, N. and Roy, D.B. 2006. Altered geographic and temporal variability in phenology in response to climate change. *Global Ecology and Biogeography* 15(5), pp. 498–504. doi: 10.1111/j.1466-822X.2006.00247.x.

Montaldo, N., Rondena, R., Albertson, J.D. and Mancini, M. 2005a. Parsimonious modeling of vegetation dynamics for ecohydrologic studies of water-limited ecosystems. *Water Resources Research* 41(10), pp. 1–16. doi: 10.1029/2005WR004094.

Montaldo, N., Rondena, R., Albertson, J.D. and Mancini, M. 2005b. Parsimonious modeling of vegetation dynamics for ecohydrologic studies of water-limited ecosystems. *Water Resources Research* 41(10), pp. 1–16. doi: 10.1029/2005WR004094.

Moon, M., Seyednasrollah, B., Richardson, A.D. and Friedl, M.A. 2021. Using time series of MODIS land surface phenology to model temperature and photoperiod controls on spring greenup in North American deciduous forests. *Remote Sensing of Environment* 260(April). doi: 10.1016/j.rse.2021.112466.

Moore, G., McGuire, K., Troch, P. and Barron-Gafford, G. 2015. *Ecohydrology and the Critical Zone: Processes and Patterns Across Scales*. Elsevier B.V. Available at: http://dx.doi.org/10.1016/B978-0-444-63369-9.00008-2.

Moran, M.S., Holifield Collins, C.D., Goodrich, D.C., Qi, J., Shannon, D.T. and Olsson, A. 2008. Long-term remote sensing database, Walnut Gulch Experimental Watershed, Arizona, United States. *Water Resources Research* 44(5), pp. 1–8. doi: 10.1029/2006wr005689.

Mueller, R.C., Scudder, C.M., Marianne, E., Iii, R.T.T., Gehring, C.A. and Whitham, T.G. 2005. Differential tree mortality in response to severe drought : evidence for long-term vegetation shifts. (Ipcc 2001), pp. 1085–1093. doi: 10.1111/j.1365-2745.2005.01042.x.

Munson, S.M. and Long, A.L. 2017. Climate drives shifts in grass reproductive phenology across the western USA. *New Phytologist* 213(4), pp. 1945–1955. doi: 10.1111/nph.14327.

Murray, R.S., Nagler, P.L., Morino, K. and Glenn, E.P. 2009. An empirical algorithm for estimating agricultural and riparian evapotranspiration using MODIS enhanced vegetation index and ground measurements of ET. II. application to the lower Colorado river, U.S. *Remote Sensing* 1(4), pp. 1125–1138. doi: 10.3390/rs1041125.

Nagler, P.L., Cleverly, J., Glenn, E., Lampkin, D., Huete, A. and Wan, Z. 2005. Predicting riparian evapotranspiration from MODIS vegetation indices and meteorological data. *Remote Sensing of Environment* 94(1), pp. 17–30. doi: 10.1016/j.rse.2004.08.009.

Nagler, P.L., Glenn, E.P., Nguyen, U., Scott, R.L. and Doody, T. 2013. Estimating riparian and agricultural actual evapotranspiration by reference evapotranspiration and MODIS enhanced vegetation index. *Remote Sensing* 5(8), pp. 3849–3871. doi: 10.3390/rs5083849.

Nagler, P.L., Morino, K., Murray, R.S., Osterberg, J. and Glenn, E.P. 2009. An empirical algorithm for estimating agricultural and riparian evapotranspiration using MODIS enhanced vegetation index and ground measurements of ET. I. Description of method. *Remote Sensing* 1(4), pp. 1273–1297. doi: 10.3390/rs1041273.

NDMC 2020. United States Drought Monitor. Available at: https://droughtmonitor.unl.edu/.

Nearing, M.A., Nichols, M.H., Stone, J.J., Renard, K.G. and Simanton, J.R. 2007. Sediment yields from unit-source semiarid watersheds at Walnut Gulch. *Water Resources Research* 43(6), pp. 1–10. doi: 10.1029/2006WR005692.

Nichols, M.H., Renard, K.G. and Osborn, H.B. 2002. Precipitation changes from 1956 to 1996 on the Walnut Gulch Experimental Watershed. *Journal of the American Water Resources Association* 38(1), pp. 161–172. doi: 10.1111/j.1752-1688.2002.tb01543.x.

Norman, L.M., Callegary, J.B., Lacher, L., Wilson, N.R., Fandel, C., Forbes, B.T. and Swetnam, T. 2019. Modeling riparian restoration impacts on the hydrologic cycle at the Babacomari Ranch, SE Arizona, USA. *Water (Switzerland)* 11(2). doi: 10.3390/w11020381.

Notaro, M., Liu, Z., Gallimore, R.G., Williams, J.W., Gutzler, D.S. and Collins, S. 2010. Complex seasonal cycle of ecohydrology in the Southwest United States. *Journal of Geophysical Research: Biogeosciences* 115(4). doi: 10.1029/2010JG001382.

Notaro, M., Mauss, A. and Williams, J.W. 2012. Projected vegetation changes for the American Southwest: Combined dynamic modeling and bioclimatic-envelope approach. *Ecological Applications* 22(4), pp. 1365–1388. doi: 10.1890/11-1269.1.

Okin, G.S., Dong, C., Willis, K.S., Gillespie, T.W. and MacDonald, G.M. 2018. The Impact of Drought on Native Southern California Vegetation: Remote Sensing Analysis Using MODIS-Derived Time Series. *Journal of Geophysical Research: Biogeosciences* 123(6), pp. 1927–1939. doi: 10.1029/2018JG004485.

Orellana, F., Verma, P., Loheide, S.P. and Daly, E. 2012. Monitoring and modeling water-vegetation interactions in groundwater-dependent ecosystems. *Reviews of Geophysics* 50(3), pp. 1–24. doi: 10.1029/2011RG000383.

Pal, I., Anderson, B.T., Salvucci, G.D. and Gianotti, D.J. 2013. Shifting seasonality and increasing frequency of precipitation in wet and dry seasons across the U.S. *Geophysical Research Letters* 40(15), pp. 4030–4035. doi: 10.1002/grl.50760.

Park, C., Lee, J. and Koo, M.H. 2013. Development of a fully-distributed daily hydrologic feedback model addressing vegetation, land cover, and soil water dynamics (VELAS). *Journal of Hydrology* 493, pp. 43–56. Available at: http://dx.doi.org/10.1016/j.jhydrol.2013.04.027.

Pascale, S. et al. 2017. Weakening of the North American monsoon with global warming. *Nature Climate Change* 7(11), pp. 806–812. doi: 10.1038/nclimate3412.

Pastick, N.J., Wylie, B.K. and Wu, Z. 2018. Spatiotemporal analysis of Landsat-8 and Sentinel-2 data to support monitoring of dryland ecosystems. *Remote Sensing* 10(5), pp. 1–15. doi: 10.3390/rs10050791.

Peñuelas, J., Rutishauser, T. and Filella, I. 2009. Phenology feedbacks on climate change. *Science* 324, pp. 887–888. doi: 10.1126/science.1173004.

Perrone, D. and Rohde, M.M. 2016. Benefits and economic costs of managed aquifer recharge in California. *San Francisco Estuary and Watershed Science* 14(2), pp. 0–13. doi: 10.15447/sfews.2016v14iss2art4.

Perry, L.G., Andersen, D.C., Reynolds, L. v., Nelson, S.M. and Shafroth, P.B. 2012. Vulnerability of riparian ecosystems to elevated CO 2 and climate change in arid and

semiarid western North America. *Global Change Biology* 18(3), pp. 821–842. doi: 10.1111/j.1365-2486.2011.02588.x.

Perry, L.G., Reynolds, L. v., Beechie, T.J., Collins, M.J. and Shafroth, P.B. 2015. Incorporating climate change projections into riparian restoration planning and design. *Ecohydrology* 8(5), pp. 863–879. doi: 10.1002/eco.1645.

Peters, D.P.C., Havstad, K.M., Archer, S.R. and Sala, O.E. 2015. Beyond desertification: New paradigms for dryland landscapes. *Frontiers in Ecology and the Environment* 13(1), pp. 4–12. doi: 10.1890/140276.

Peters, D.P.C., Herrick, J.E., Monger, H.C. and Huang, H. 2010. Soil-vegetation-climate interactions in arid landscapes: Effects of the North American monsoon on grass recruitment. *Journal of Arid Environments* 74(5), pp. 618–623. Available at: http://dx.doi.org/10.1016/j.jaridenv.2009.09.015.

Petrie, M.D., Collins, S.L. and Litvak, M.E. 2015. The ecological role of small rainfall events in a desert grassland. *Ecohydrology* 8(8), pp. 1614–1622. doi: 10.1002/eco.1614.

Pettit, N.E. and Froend, R.H. 2018. How important is groundwater availability and stream perenniality to riparian and floodplain tree growth? *Hydrological Processes* 32(10), pp. 1502–1514. doi: 10.1002/hyp.11510.

Pierce, D.W., Kalansky, J.F. and Cayan, D.R. 2018. Climate, Drought, and Sea Level Rise Scenarios for the Fourth California Climate Assessment. In: *California's Fourth Climate Change Assessment*. California Energy Commission. Available at: www.climateassessment.ca.gov.

Polley, H.W., Briske, D.D., Morgan, J.A., Wolter, K., Bailey, D.W. and Brown, J.R. 2013. Climate change and North American rangelands: Trends, projections, and implications. *Rangeland Ecology and Management* 66(5), pp. 493–511. Available at: http://dx.doi.org/10.2111/REM-D-12-00068.1.

Porporato, A., D'Odorico, P., Laio, F., Ridolfi, L. and Rodriguez-Iturbe, I. 2002. Ecohydrology of water-controlled ecosystems. *Advances in Water Resources* 25(8–12), pp. 1335–1348. doi: 10.1016/S0309-1708(02)00058-1.

Porporato, A., Laio, F., Fernandez-Illescas, C.P. and Rodriguez-Iturbe, I. 2001. Plants in water-controlled ecosystems: Active role in hydrologic processes and responce to water stress III. Vegetation water stress. *Advances in Water Resources* 24(7), pp. 745–762. doi: 10.1016/S0309-1708(01)00007-0.

Porporato, A. and Yin, J. 2022. *Ecohydrology: Dynamics of life and water in the critical zone*. Cambridge University Press.

Pyke, C.R. and Marty, J. 2005. Cattle grazing mediates climate change impacts on ephemeral wetlands. *Conservation Biology* 19(5), pp. 1619–1625. doi: 10.1111/j.1523-1739.2005.00233.x.

Quichimbo, E.A., Singer, M.B. and Cuthbert, M.O. 2020. Characterizing groundwater-surface water interactions in idealized ephemeral stream systems. *Hydrological Processes* (February), pp. 1–15. doi: 10.1002/hyp.13847.

Quichimbo, E.A., Singer, M.B., Michaelides, K., Hobley, D., Rosolem, R. and Cuthbert, M. 2021. DRYP 1.0: A parsimonious hydrological model of DRYland Partitioning of the water balance. *Geoscientific Model Development Discussions* , pp. 1–34. doi: 10.5194/gmd-2021-137.

Rafferty, N.E., Diez, J.M. and Bertelsen, C.D. 2020. Changing Climate Drives Divergent and Nonlinear Shifts in Flowering Phenology across Elevations. *Current Biology* 30(3), pp. 432-441.e3. Available at: https://doi.org/10.1016/j.cub.2019.11.071.

Renard, K.G., Nichols, M.H., Woolhiser, D.A. and Osborn, H.B. 2008. A brief background on the U.S. Department of Agriculture Agricultural Research Service Walnut Gulch Experimental Watershed. *Water Resources Research* 44(5), pp. 1–11. doi: 10.1029/2006WR005691.

Renwick, K.M. et al. 2019. Modeling phenological controls on carbon dynamics in dryland sagebrush ecosystems. *Agricultural and Forest Meteorology* 274(April), pp. 85–94. Available at: https://doi.org/10.1016/j.agrformet.2019.04.003.

Reynier, W.A., Hillberg, L.E. and Kershner, J.M. 2016. Southern California Grassland Habitats: Climate Change Vulnerability Assessment Synthesis. *EcoAdapt* Version 1.

Richardson, A.D. et al. 2012. Terrestrial biosphere models need better representation of vegetation phenology: Results from the North American Carbon Program Site Synthesis. *Global Change Biology* 18(2), pp. 566–584. doi: 10.1111/j.1365-2486.2011.02562.x.

Richardson, A.D., Keenan, T.F., Migliavacca, M., Ryu, Y., Sonnentag, O. and Toomey, M. 2013. Climate change, phenology, and phenological control of vegetation feedbacks to the climate system. *Agricultural and Forest Meteorology* 169, pp. 156–173. Available at: http://dx.doi.org/10.1016/j.agrformet.2012.09.012.

Richardson, D.M. et al. 2007. Riparian vegetation degradation alien plant invasions and restoration. *Diversity and Distributions* 13, pp. 126–139.

Ridolfi, L., D'Odorico, P., Porporato, A. and Rodriguez-Iturbe, I. 2000. Duration and frequency of water stress in vegetation: An analytical model. *Water Resources Research* 36(8), pp. 2297–2307. doi: 10.1029/2000WR900104.

Rinaldo, A. and Rodriguez-Iturbe, I. 2022. Ecohydrology 2.0. *Rendiconti Lincei* 33(2), pp. 245–270. doi: 10.1007/s12210-022-01071-y.

Roberts, D., Bradley, E., Roth, K., Eckmann, T. and Still, C. 2010. Linking physical geography education and research through the development of an environmental sensing network and project-based learning. *Journal of Geoscience Education* 58(5), pp. 262–274. doi: 10.5408/1.3559887.

Rodriguez-Iturbe, I. 2000. Ecohydrology : A hydrologic perspective of climate-soil-vegetation dynamics. *Water Resources Research* 36(1), pp. 3–9.

Rodriguez-Iturbe, I., D'Odorico, P., Porporato, A. and Ridolfi, L. 1999. On the spatial and temporal links between vegetation,climate, and soil moisture. *Water Resources Research* 35(12), pp. 3709–3722.

Rodriguez-Iturbe, I. and D'Odorico, P.D. 1999. Tree-grass coexistence in savannas: The role of spatial dynamics and climate fluctuations. *Geophysical Research Letters* 26(2), pp. 247–250.

Rodriguez-Iturbe, I. and Perporato, A. 2004. *Ecohydrology of Water-Controlled Ecosystems*. Cambridge University Press.

Rodriguez-Iturbe, I., Porporato, A., Laio, F. and Ridolfi, L. 2001. Plants in water-controlled ecosystems: Active role in hydrologic processes and responce to water stress I. Scope and general outline. *Advances in Water Resources* . doi: 10.1016/S0309-1708(01)00004-5.

Rohde, M.M., Biswas, T., Housman, I.W., Campbell, L.S., Klausmeyer, K.R. and Howard, J.K. 2021a. A Machine Learning Approach to Predict Groundwater Levels in California Reveals Ecosystems at Risk. *Frontiers in Earth Science* 9(December), pp. 1–16. doi: 10.3389/feart.2021.784499.

Rohde, M.M., Stella, J.C., Roberts, D.A. and Singer, M.B. 2021b. Groundwater dependence of riparian woodlands and the disrupting effect of anthropogenically altered streamflow. *Proceedings of the National Academy of Sciences of the United States of America* 118(25), pp. 1–7. doi: 10.1073/pnas.2026453118.

Sabathier, R., Singer, M.B., Stella, J.C., Roberts, D.A. and Caylor, K.K. 2021. Vegetation responses to climatic and geologic controls on water availability in southeastern Arizona. *Environmental Research Letters* 16(6). doi: 10.1088/1748-9326/abfe8c.

Saito, L., Christian, B., Diffley, J., Richter, H., Rohde, M.M. and Morrison, S.A. 2021. Managing Groundwater to Ensure Ecosystem Function. *Groundwater* 59(3), pp. 322–333. doi: 10.1111/gwat.13089.

Samaniego, L. et al. 2018. Anthropogenic warming exacerbates European soil moisture droughts. *Nature Climate Change* 8(May). Available at: http://dx.doi.org/10.1038/s41558-018-0138-5.

Scanlon, B.R., Reedy, R.C., Faunt, C.C., Pool, D. and Uhlman, K. 2016. Enhancing drought resilience with conjunctive use and managed aquifer recharge in California and Arizona. *Environmental Research Letters* 11(3). doi: 10.1088/1748-9326/11/3/035013.

Schlaepfer, D.R. et al. 2017. Climate change reduces extent of temperate drylands and intensifies drought in deep soils. *Nature Communications* 8. doi: 10.1038/ncomms14196.

Schreiner-McGraw, A.P., Vivoni, E.R., Ajami, H., Sala, O.E., Throop, H.L. and Peters, D.P.C. 2020. Woody Plant Encroachment has a Larger Impact than Climate Change on Dryland Water Budgets. *Scientific Reports* 10(1), pp. 1–9. Available at: http://dx.doi.org/10.1038/s41598-020-65094-x.

Scott, R.L., Huxman, T.E., Barron-Gafford, G.A., Darrel Jenerette, G., Young, J.M. and Hamerlynck, E.P. 2014. When vegetation change alters ecosystem water availability. *Global Change Biology* 20(7), pp. 2198–2210. doi: 10.1111/gcb.12511.

Scott, R.L., James Shuttleworth, W., Goodrich, D.C. and Maddock, T. 2000. The water use of two dominant vegetation communities in a semiarid riparian ecosystem. *Agricultural and Forest Meteorology* 105(1–3), pp. 241–256. doi: 10.1016/S0168-1923(00)00181-7.

Seager, R., Nakamura, J. and Ting, M. 2019. Mechanisms of Seasonal Soil Moisture Drought Onset and Termination in the Southern Great Plains. *Journal of Hydrometeorology* 20, pp. 751–771. doi: 10.1175/JHM-D-18-0191.1.

Seavy, N.E. et al. 2009. Why climate change makes riparian restoration more important than ever: Recommendations for practice and research. *Ecological Restoration* 27(3), pp. 330–338. doi: 10.3368/er.27.3.330.

Seddon, N., Chausson, A., Berry, P., Girardin, C.A.J., Smith, A. and Turner, B. 2020. Understanding the value and limits of nature-based solutions to climate change and other global challenges. *Philosophical Transactions of the Royal Society B: Biological Sciences* 375(1794). doi: 10.1098/rstb.2019.0120.

Seebacher, F. and Post, E. 2015. Climate change impacts on animal migration. *Climate Change Responses* 2(1). doi: 10.1186/s40665-015-0013-9.

Sheffield, J. and Wood, E.F. 2008. Projected changes in drought occurrence under future global warming from multi-model, multi-scenario, IPCC AR4 simulations. *Climate Dynamics* 31(1), pp. 79–105. doi: 10.1007/s00382-007-0340-z.

Shellito, P.J. et al. 2016. SMAP soil moisture drying more rapid than observed in situ following rainfall events. (43), pp. 8086–8075. doi: 10.1002/2016GL069946.Received.

Singer, M.B. et al. 2021. Hourly potential evapotranspiration at 0.1° resolution for the global land surface from 1981-present. *Scientific Data* 8(1), pp. 1–13. doi: 10.1038/s41597-021-01003-9.

Singer, M.B. and Michaelides, K. 2014. How is topographic simplicity maintained in ephemeral dryland channels ? (12), pp. 1091–1094. doi: 10.1130/G36267.1.

Singer, M.B. and Michaelides, K. 2017. Deciphering the expression of climate change within the Lower Colorado River basin by stochastic simulation of convective rainfall. *Environmental Research Letters* 12(10). doi: 10.1088/1748-9326/aa8e50.

Singer, M.B., Michaelides, K. and Hobley, D.E.J. 2018. STORM 1.0: A simple, flexible, and parsimonious stochastic rainfall generator for simulating climate and climate change. *Geoscientific Model Development* 11(9), pp. 3713–3726. doi: 10.5194/gmd-11-3713-2018.

Singer, M.B., Sargeant, C.I., Piégay, H., Jérémie, R., Rob J.S., W. and Evans, C.M. 2014. Floodplain ecohydrology: Climatic, anthropogenic, and local physical controls on partitioning of water sources to riparian trees. *Water Resources Research* 50(5), pp. 4490–4513. Available at: http://doi.wiley.com/10.1002/2014WR015581.

Singh, R., Tiwari, A.K. and Singh, G.S. 2021. Managing riparian zones for river health improvement: an integrated approach. *Landscape and Ecological Engineering* 17(2), pp. 195–223. Available at: https://doi.org/10.1007/s11355-020-00436-5.

Skirvin, S. et al. 2008. Vegetation data, Walnut Gulch Experimental Watershed, Arizona, United States. *Water Resources Research* 44(5), pp. 4–9. doi: 10.1029/2006wr005724.

Small, E.E., Roesler, C.J. and Larson, K.M. 2018. Vegetation response to the 2012-2014 California drought from GPS and optical measurements. *Remote Sensing* 10(4), pp. 1–16. doi: 10.3390/rs10040630.

Smith, W.K. et al. 2019. Remote sensing of dryland ecosystem structure and function: Progress, challenges, and opportunities. *Remote Sensing of Environment* 233(July), p. 111401. Available at: https://doi.org/10.1016/j.rse.2019.111401.

Snyder, K.A. and Williams, D.G. 2000. Water sources used by riparian trees varies among stream types on the San Pedro River, Arizona. *Agricultural and Forest Meteorology* 105(1–3), pp. 227–240. doi: 10.1016/S0168-1923(00)00193-3.

Steenburgh, W.J. et al. 2013. Present Weather and Climate: Average Conditions. In: *Assessment of Climate Change in the Southwest United States: A Report Prepared for the National Climate Assessment* . Washington, DC: Island Press

Stromberg, J.C. 2001. Restoration of riparian vegetation in the south-western United States: Importance of flow regimes and fluvial dynamism. *Journal of Arid Environments* 49(1), pp. 17–34. doi: 10.1006/jare.2001.0833.

Stromberg, J.C., Bagstad, K.J., Leenhouts, J.M., Lite, S.J. and Makings, E. 2005. Effects of stream flow intermittency on riparian vegetation of a semiarid region river (San Pedro River, Arizona). *River Research and Applications* 21(8), pp. 925–938. doi: 10.1002/rra.858.

Stromberg, J.C., Lite, S.J., Rychener, T.J., Levick, L.R., Dixon, M.D. and Watts, J.M. 2006. Status of the Riparian ecosystem in the upper San Pedro River, Arizona: Application of an assessment model. *Environmental Monitoring and Assessment* 115(1–3), pp. 145–173. doi: 10.1007/s10661-006-6549-1.

Stromberg, J.C., McCluney, K.E., Dixon, M.D. and Meixner, T. 2013. Dryland Riparian Ecosystems in the American Southwest: Sensitivity and Resilience to Climatic Extremes. *Ecosystems* 16(3), pp. 411–415. doi: 10.1007/s10021-012-9606-3.

Stromberg, J.C., Setaro, D.L., Gallo, E.L., Lohse, K.A. and Meixner, T. 2017. Riparian vegetation of ephemeral streams. *Journal of Arid Environments* 138, pp. 27–37. Available at: http://dx.doi.org/10.1016/j.jaridenv.2016.12.004.

Stromberg, J.C. and Tiller, R. 1996. Effects of Groundwater Decline on Riparian Vegetation of Semiarid Regions : The San Pedro, Arizona. *Ecological Applications* 6(1), pp. 113–131.

Stromberg, J.C., Tressj, J.A., Wilkins, S.D. and Clark, S.D. 1992. *Response of velvet mesquite to groundwater decline*.

Stromberg, M.R., Crobin, J.D. and D'Antonio, C.M. 2007. *California Grasslands: Ecology and Management*. University of California Press.

Tabacchi, E., Lambs, L., Guilloy, H., Planty-Tabacchi, A.-M., Muller, E. and Decamps, H. 2000. Impacts of riparian vegetation on hydrological processes. *Hydrological Processes* 14(16–17), pp. 2959–2976. doi: 10.1002/1099-1085(200011/12)14:16/17<2977::AID-HYP130>3.0.CO;2-4.

Tamea, S., Laio, F., Ridolfi, L., D'Odorico, P. and Rodriguez-Iturbe, I. 2009. Ecohydrology of groundwater-dependent ecosystems: 2. Stochastic soil moisture dynamics. *Water Resources Research* 45(5), pp. 1–13. doi: 10.1029/2008WR007293.

Thorne, J.H., Boynton, R.M., Holguin, A.J., Stewart, J.A.E. and Bjorkman, J. 2016. *A climate change vulnerability assessment of California's terrestrial vegetation*. doi: 10.1371/journal.pone.0029507.

Tietjen, B., Jeltsch, F., Zehe, E., Classen, N., Groengroeft, A., Schiffers, K. and Oldeland, J. 2010. Effects of climate change on the coupled dynamics of water and vegetation in drylands. *Ecohydrology* 3, pp. 226–237. Available at: http://www3.interscience.wiley.com/journal/122653919/abstract.

Trenberth, K.E. 2011. Changes in precipitation with climate change. *Climate Research* 47(1–2), pp. 123–138. doi: 10.3354/cr00953.

Trenberth, K.E., Dai, A., van der Schrier, G., Jones, P.D., Barichivich, J., Briffa, K.R. and Sheffield, J. 2014. Global warming and changes in drought. *Nature Climate Change* 4(1), pp. 17–22. doi: 10.1038/nclimate2067.

Troch, P.A. et al. 2009. Climate and vegetation water use efficiency at catchment scales. *Hydrological Processes* 23(16), pp. 2409–2414. doi: 10.1002/hyp.7358.

Turner, D.P., Cohen, W.B., Kennedy, R.E., Fassnacht, K.S. and Briggs, J.M. 1999. Relationships between leaf area index and Landsat TM spectral vegetation indices across three temperate zone sites. *Remote Sensing of Environment* 70(1), pp. 52–68. doi: 10.1016/S0034-4257(99)00057-7.

Ukkola, A.M., de Kauwe, M.G., Roderick, M.L., Burrell, A., Lehmann, P. and Pitman, A.J. 2021. Annual precipitation explains variability in dryland vegetation

greenness globally but not locally. *Global Change Biology* (May), pp. 1–14. doi: 10.1111/gcb.15729.

Vegas Galdos, F., Álvarez, C., García, A. and Revilla, J.A. 2012. Estimated distributed rainfall interception using a simple conceptual model and Moderate Resolution Imaging Spectroradiometer (MODIS). *Journal of Hydrology* 468–469, pp. 213–228. Available at: http://dx.doi.org/10.1016/j.jhydrol.2012.08.043.

Verhoef, A. and Egea, G. 2014. Modeling plant transpiration under limited soil water: Comparison of different plant and soil hydraulic parameterizations and preliminary implications for their use in land surface models. *Agricultural and Forest Meteorology* 191, pp. 22–32. Available at: http://dx.doi.org/10.1016/j.agrformet.2014.02.009.

Villegas, J.C., Breshears, D.D., Zou, C.B. and Law, D.J. 2010. Ecohydrological controls of soil evaporation in deciduous drylands: How the hierarchical effects of litter, patch and vegetation mosaic cover interact with phenology and season. *Journal of Arid Environments* 74(5), pp. 595–602. doi: 10.1016/j.jaridenv.2009.09.028.

Voigt, A., Albern, N., Ceppi, P., Grise, K., Li, Y. and Medeiros, B. 2021. Clouds, radiation, and atmospheric circulation in the present-day climate and under climate change. *Wiley Interdisciplinary Reviews: Climate Change* 12(2), pp. 1–22. doi: 10.1002/wcc.694.

Walker, J.J., de Beurs, K.M. and Wynne, R.H. 2014. Dryland vegetation phenology across an elevation gradient in Arizona, USA, investigated with fused MODIS and landsat data. *Remote Sensing of Environment* 144, pp. 85–97. Available at: http://dx.doi.org/10.1016/j.rse.2014.01.007.

Walker, J.J., de Beurs, K.M., Wynne, R.H. and Gao, F. 2012. Evaluation of Landsat and MODIS data fusion products for analysis of dryland forest phenology. *Remote Sensing of Environment* 117, pp. 381–393. Available at: http://dx.doi.org/10.1016/j.rse.2011.10.014.

Wallace, C.S.A., Walker, J.J., Skirvin, S.M., Patrick-Birdwell, C., Weltzin, J.F. and Raichle, H. 2016. Mapping presence and predicting phenological status of invasive

buffelgrass in Southern Arizona using MODIS, climate and citizen science observation data. *Remote Sensing* 8(7). doi: 10.3390/rs8070524.

Wang, J., Rich, P.M. and Price, K.P. 2000. Temporal responses of NDVI to precipitation and temperature in the central Great Plains, USA. *International Journal of Remote Sensing* 24(11), pp. 2345–2364. Available at: http://citeseerx.ist.psu.edu/viewdoc/summary?doi=10.1.1.127.9664.

Wang, L., D'Odorico, P., Evans, J.P., Eldridge, D.J., McCabe, M.F., Caylor, K.K. and King, E.G. 2012. Dryland ecohydrology and climate change: Critical issues and technical advances. *Hydrology and Earth System Sciences* 16(8), pp. 2585–2603. doi: 10.5194/hess-16-2585-2012.

Wang, L., Wei, X., Bishop, K., Reeves, A.D., Ursino, N. and Winkler, R. 2018. Vegetation changes and water cycle in a changing environment. *Hydrology and Earth System Sciences* 22(3), pp. 1731–1734. doi: 10.5194/hess-22-1731-2018.

Warter, M.M., Singer, M.B., Cuthbert, M., Roberts, D., Caylor, K., Sabathier, R. and Stella, J. 2020. Onset and propagation of drought into soil moisture and vegetation responses during the 2012–2019 drought in Southern California. *Hydrology and Earth System Sciences Discussions* , pp. 1–35. doi: 10.5194/hess-2020-479.

Westerling, A.L. and Bryant, B.P. 2007. Climate change and wildfire in California. *Climatic Change* 87(1 SUPPL). doi: 10.1007/s10584-007-9363-z.

Westerling, A.L., Cayan, D.R., Brown, T.J., Hall, B.L. and Riddle, L.G. 2004. Climate, santa ana winds and autumn wildfires in southern california. *Eos* 85(31). doi: 10.1029/2004EO310001.

Westerling, A.L., Hidalgo, H.G., Cayan, D.R. and Swetnam, T.W. 2006. Warming and earlier spring increase Western U.S. forest wildfire activity. *Science* 313(5789), pp. 940–943. doi: 10.1126/science.1128834.

White, M.A. et al. 2009. Intercomparison, interpretation, and assessment of spring phenology in North America estimated from remote sensing for 1982-2006. *Global Change Biology* 15(10), pp. 2335–2359. doi: 10.1111/j.1365-2486.2009.01910.x.

Wilkening, J., Pearson-Prestera, W., Mungi, N.A. and Bhattacharyya, S. 2019. Endangered species management and climate change: When habitat conservation becomes a moving target. *Wildlife Society Bulletin* 43(1), pp. 11–20. doi: 10.1002/wsb.944.

Williams, A.P. et al. 2013. Temperature as a potent driver of regional forest drought stress and tree mortality. *Nature Climate Change* 3(3), pp. 292–297. doi: 10.1038/nclimate1693.

Williams, A.P., Cook, B.I. and Smerdon, J.E. 2022a. Rapid intensification of the emerging southwestern North American megadrought in 2020–2021. *Nature Climate Change* 12(3), pp. 232–234. doi: 10.1038/s41558-022-01290-z.

Williams, A.P., Gentine, P., Moritz, M.A., Roberts, D.A. and Abatzoglou, J.T. 2018. Effect of Reduced Summer Cloud Shading on Evaporative Demand and Wildfire in Coastal Southern California. *Geophysical Research Letters* 45(11), pp. 5653–5662. doi: 10.1029/2018GL077319.

Williams, D.G. and Scott, R.L. 2009. Vegetation-hydrology interactions: Dynamics of riparian plant water use. *Ecology and Conservation of the San Pedro River* , pp. 37–56.

Williams, J. et al. 2022b. Local groundwater decline exacerbates response of dryland riparian woodlands to climatic drought. (April), pp. 1–18. doi: 10.1111/gcb.16376.

Wolberg, G. and Alfy, I. 2002. An energy-minimization framework for monotonic cubic spline interpolation. *Journal of Computational and Applied Mathematics* 143(2), pp. 145–188. doi: 10.1016/S0377-0427(01)00506-4.

Wilson, S.D, Schlaepfer D.R, Bradford J.B, Lauenroth W.K, Duniway M.C., Hall S.A., Jamiyansharav K., Jia G., Lkhagva A., Munson S.M., Pyke D.A., and Tietjen B. 2017. Functional Groups, Biomass, and Climate Change Effects on Ecological Drought in Semiarid Grasslands. *Journal of Geophysical Research: Biogeosciences*, 123, doi: 10.1002/2017JG004173

Xin, Q., Broich, M., Zhu, P. and Gong, P. 2015. Modeling grassland spring onset across the Western United States using climate variables and MODIS-derived

phenology metrics. *Remote Sensing of Environment* 161, pp. 63–77. Available at: http://dx.doi.org/10.1016/j.rse.2015.02.003.

Zhang, R., Wu, J., Yang, Y., Peng, X., Li, C. and Zhao, Q. 2022. A method to determine optimum ecological groundwater table depth in semi-arid areas. *Ecological Indicators* 139(April), p. 108915. Available at: https://doi.org/10.1016/j.ecolind.2022.108915.

Zhang, X. et al. 2003. Monitoring vegetation phenology using MODIS. *Remote Sensing of Environment* 84(3), pp. 471–475. doi: 10.1016/S0034-4257(02)00135-9.

Zhang, X., Friedl, M.A., Schaaf, C.B. and Strahler, A.H. 2004. Climate controls on vegetation phenological patterns in northern mid- and high latitudes inferred from MODIS data. *Global Change Biology* 10(7), pp. 1133–1145. doi: 10.1111/j.1529-8817.2003.00784.x.

Zhou, S. et al. 2019. Land–atmosphere feedbacks exacerbate concurrent soil drought and atmospheric aridity. *Proceedings of the National Academy of Sciences* 116(38), pp. 18848–18853. doi: 10.1073/pnas.1904955116.

Zhu, K., Chiariello, N.R., Tobeck, T., Fukami, T. and Field, C.B. 2016. Nonlinear, interacting responses to climate limit grassland production under global change. *Proceedings of the National Academy of Sciences of the United States of America* 113(38), pp. 10589–10594. doi: 10.1073/pnas.1606734113.